A THEORY OF ABLATIVE HEAT TRANSFER AND EXPERIMENTAL VERIFICATION UNDER FLIGHT CONDITIONS

---

by

Jack William Richman

Submitted in partial fulfillment of the requirements for the degree of M. Sc. in the University of Manitoba.

ABSTRACT

This thesis presents a new theory of ablative heat transfer and its experimental verification under rocket flight conditions.

In section 1.0 the fundamental equations of continuum flow and their limitations are discussed. It is shown how these equations can be adapted for a wide range of specific vehicle geometries and coupled with an analytic linear forward finite difference method to predict ablation procession, and transient temperature distributions in composite structures. A brief discussion of the accuracy of the analytic methods is given, showing that they are practically indistinguishable from exact solutions.

To test the accuracy of the new theory and the analytic methods, section 2.0 describes a set of carefully planned inflight rocket experiments, using a varied range of simple experiment geometries. All experiments were conducted using Black Brant sounding rockets as environmental platforms, launched from the Churchill Rocket Research Range.

Section 3.0 describes a set of versatile digital computer programs

which incorporate the new theory and analytic methods, to facilitate computations for the theoretical analysis.

The results of the theoretical analysis and experimental data are compared in section 4.0. Amongst the main conclusions to be drawn from these comparisons, is that the theory and related computer programs can be used with confidence for certain vehicle geometries and flight conditions for prediction of ablation rates, and temperature distributions in composite aerospace structures. It is hoped that the theory will prove a useful "tool" for future vehicle design work.

INDEX

PAGE

FIGURE INDEX

CONTINUED

TABLE INDEX

THEORY

1.0 INTRODUCTION

During the past decade, interest has grown in the uses of ablative materials as heat shields for thermal protection of space boosters. To date, a vast amount of literature has been published on ablative materials used as heat shields, embracing experiment and theory. On reading some of the literature available on ablation, it is apparent that most writers either ignore the making of theoretical predictions needed to correlate theory with experiment, or where the theoretical results are cited, they are very poor. (For example, see references 1, 2 and 3.) It was therefore felt that the purpose of this thesis should be to delve into the theoretical aspects of ablation, and try to produce a simple theory and mathematical model for predicting reliable estimates of ablation characteristics, and then perform a set of carefully monitored flight experiments to test out the new theory.

1.1 FUNDAMENTAL EQUATIONS

Because of the sheer volume of theory required to describe the dynamics of high speed airflow over bodies coupled with ablative phenomena, it was decided to formulate the governing equations of fluid dynamics with tensor calculus, due to its compactness of notation. The general governing equations of fluid dynamics, the equation of continuity, momentum and energy taken from references 4 and 5, are

$$\frac{D\rho}{Dt} + \rho \frac{\partial u_i}{\partial x_i} = 0 \qquad 1.1.1$$

$$\rho \frac{Du_i}{Dt} - \rho F_i + \frac{\partial p}{\partial x_i} + \frac{\partial \tau_{ij}}{\partial x_j} = 0 \qquad 1.1.2$$

and

$$\rho \frac{DE}{Dt} + p \frac{\partial u_i}{\partial x_i} + \tau_{ij} \frac{\partial u_i}{\partial x_j} + \frac{\partial q_i}{\partial x_i} = 0 \qquad 1.1.3$$

respectively, together with the equation of state.

$$p = \rho R_g T \qquad 1.1.3a$$

The continuity equation 1.1.1, is the simplest of the three equations, and has the property that its form does not change under coordinate transformation. Equation 1.1.2, the momentum equation, simply expresses Newton's second law, that force

equals the rate of change of momentum, while equation 1.1.3, the energy equation, expresses the energy balance in a control volume of fluid. These equations are quite general and applicable to any type of flow as long as the assumptions for the form of the stress tensor τ_{ij} and heat vector q_i are valid. The forms of the stress tensor τ_{ij} and heat flux vector q_i will be developed in following sections.

It is through the expressions for the stress tensor τ_{ij} and the heat flux vector q_i that the momentum and energy equations depend on the form of the molecular velocity distribution function. The fundamental equations for the subsequent analysis will now be formulated; to show the limitations and restrictions applied to them.

If we let ${}_r\tau_{ij}$ and ${}_r q_i$ denote the rth order approximations to the stress tensor ${}_0\tau_{ij}^{(r)}$, and heat flux vector ${}_0 q_i^{(r)}$ respectively, we can write

$$ {}_r\tau_{ij} = \sum_{r=0}^{r} \tau_{ij}^{(r)} \qquad 1.1.4 $$

$$ {}_r q_i = \sum_{r=0}^{r} q_i^{(r)} \qquad 1.1.5 $$

where $\tau_{ij}^{(r)}$ and $q_i^{(r)}$ are the rth order corrections to ${}_r\tau_{ij}$ and ${}_r q_i$ respectively.

The first order approximation, to the molecular velocity distribution (which is a Maxwellian distribution) gives the stress tensor and heat flux vector as

$$ {}_0\tau_{ij} = \tau_{ij}^{(0)} = 0 \qquad 1.1.6 $$

$$ {}_0 q_i = q_i^{(0)} = 0 \qquad 1.1.7 $$

which together with equations 1.1.2 and 1.1.3, yield the Eulerian equations for the motion of a perfect fluid. Hence, the momentum equation becomes

$$ \rho \frac{Du_i}{Dt} - \rho F_i + \frac{\partial P}{\partial x_i} = 0 \qquad 1.1.8 $$

and the corresponding energy equation becomes

$$ \rho \frac{DE}{Dt} + P \frac{\partial u_i}{\partial x_i} = 0 \qquad 1.1.9 $$

It should be remembered that the equation of continuity remains unchanged, because of its invariance to coordinate transformation. The usefulness of these equations will become apparent in the section on stagnation point heat transfer.

The second order approximation from reference 6, to the molecular velocity distribution function gives

$$\tau_{ij} = \tau_{ij}^{(1)} = -2\mu \frac{\partial \bar{u}_i}{\partial x_j} \qquad 1.1.10$$

$$q_i = q_i^{(1)} = -K \frac{\partial T}{\partial x_i} \qquad 1.1.11$$

where μ and K are the coefficients of viscosity and thermal conductivity. These coefficients are zero for a perfect fluid, as described by equations 1.1.8 and 1.1.9. The term $\partial \bar{u}_i / \partial x_j$, is a non-divergent symmetrical tensor associated with the velocity gradient $\partial u_i / \partial x_j$. Substitution of 1.1.10 and 1.1.11 in equations 1.1.1 and 1.1.2 yields

$$\rho \frac{Du_i}{Dt} - \rho F_i + \frac{\partial P}{\partial x_i} - 2 \frac{\partial}{\partial x_j}\left(\mu \frac{\partial \bar{u}_i}{\partial x_j}\right) = 0 \qquad 1.1.12$$

which is the Navier-Stokes equation, and the corresponding energy

equation for viscous compressible flow becomes

$$\rho \frac{DE}{Dt} + p \frac{\partial u_i}{\partial x_j} - 2\mu \frac{\partial u_i}{\partial x_j} \frac{\partial \bar{u}_i}{\partial x_j} - \frac{\partial}{\partial x_i}\left(K \frac{\partial T}{\partial x_i}\right) = 0 \qquad 1.1.13$$

The third term in equation 1.1.13 is called the energy dissipation function and is the rate of doing work by the viscous stresses. The dissipation function is never negative because it always increases the internal energy of the air. Equations 1.1.1, 1.1.12, and 1.1.13 will be used extensively throughout the thesis. To use equations 1.1.12 and 1.1.13 for supersonic and hypersonic flow, it must be assumed that the air can be treated as a continuum in a shock. This can be realized if the shock is considered as a rapid, but not discontinuous, viscous change in the air. The solution of 1.1.1, 1.1.12 and 1.1.13, with the appropiate boundary conditions, will give the continuum flow around the body provided the assumptions for the form of the stresses and strains are valid and the density of the air has meaning at a point. When the mean free path of the air approaches the order of magnitude of the experiment dimensions, the equations become inadequate because density will not have a meaning at a point. Therefore, any theoretical results will be restricted to continuum flow, excluding the effects of dissociation. The continuum region is loosely characterized by the following equation.

$$L \gg \lambda \qquad 1.1.14$$

which states that the molecular mean free path λ of the air must be much less than the experiment dimensions L. For the types of experiments considered, transition between continuum and slip flow occurs at approximately 50 miles altitude where the mean free path is of the order 0.01 feet.

It will now be shown how the general equations of continuity, momentum and energy are applied to the theoretical analysis, using an adaption of the Van Driest aerodynamic heating theory from reference 8.

1.2 STAGNATION POINT HEAT TRANSFER

The purpose of this section is to present a non-linear differential equation for transient laminar and turbulent heat transfer to a two dimensional stagnation point. To do this, it is necessary to analyze the motion of the fluid in the thermal boundary layer behind the shock. In the local free stream potential flow outside the boundary layer, the viscous stresses in the air are negligible compared with the inertia stresses as shown in equation 1.1.12; whereas in the boundary layer, the viscous and inertial stresses are of the same order. The viscous stresses within the boundary layer do shearing work on the air which tends to alter the air temperature. This alteration of air temperature sets up temperature gradients and hence heat conduction through the boundary layer.

At low Mach* numbers heat transfers in the boundary layer are relatively unimportant because the internal heat transfers are of the same order as the viscous shear work which is quite small.

At high Mach* numbers, the viscous shearing work is large, and consequently heat transfer through the layers is high because of the presence of large viscous forces and inertial forces.

* Flight Mach number

The analysis of the stagnation boundary layer must take into account not only the concepts of continuity, momentum, and energy, but also density, since the density of the boundary layer varies inversely as the temperature* and the viscosity varies approximately as the 3/4 index of the temperature. This means that at high Mach numbers the compressibility effects are of the same order as viscosity changes.

As yet, the general equations are very complicated and unsolvable for a real fluid, but fortunately for stagnation point analysis in the laminar boundary layer, the general equations lend themselves well to simplification.

The non-divergent symmetrical tensor in equation 1.1.13 can be written an

$$\frac{\partial \bar{u}_i}{\partial x_j} = \frac{1}{2}\left(\frac{\partial u_i}{\partial x_j} + \frac{\partial u_j}{\partial x_i}\right) - \frac{1}{3}\frac{\partial u_k}{\partial x_k}\delta_{ij} \qquad 1.2.1$$

where δ_{ij} is a unit tensor known as the Kronecker delta. Since the flow in the boundary layer at a stagnation point is virtually incompressible, we can regard Φ as being the incompressible dissipation function, and therefore the second term on the right hand side of equation 1.2.1 vanishes since

* Boundary layer theory indicates pressure does not vary through boundary layer.

$$\nabla \bar{V} = 0 \qquad 1.2.2$$

where $\bar{V}$ is the velocity vector. Thus we can write the incompressible dissipation function using the convention of repeated subscripts from reference 6 and equation 1.2.1 as

$$\Phi = \mu\left[2\left(\frac{\partial u}{\partial x}\right)^2 + 2\left(\frac{\partial v}{\partial y}\right) + 2\left(\frac{\partial w}{\partial z}\right)^2 + \left(\frac{\partial w}{\partial y} + \frac{\partial v}{\partial z}\right)^2 + \left(\frac{\partial u}{\partial z} + \frac{\partial w}{\partial x}\right)^2 + \left(\frac{\partial v}{\partial x} + \frac{\partial u}{\partial y}\right)^2\right] \qquad 1.2.3$$

This can be further simplified in the following way. References 6 and 7 show that if an order of magnitude analysis is applied to the boundary layer at a stagnation point, and if δ is the boundary layer thickness, and the velocity u changes from zero at the body surface to U in the free stream in a length δ and, if we take U as a standard order of magnitude and δ as small, then $\partial u/\partial y$ will be $o[\delta^{-1}]$ and $\partial^2 u/\partial y^2$ will be $o[\delta^{-2}]$ in the boundary layer. Also u, $\partial u/\partial t$, $\partial u/\partial x$ and $\partial^2 u/\partial x^2$ will be of $o[1]$. Using 1.1.1, the equation of continuity for two dimensional flow becomes

$$\frac{\partial u}{\partial x} + \frac{\partial v}{\partial y} = 0 \qquad 1.2.4$$

This shows that $\partial v/\partial y$ is of $o[1]$, and since $v = 0$ when $y = 0$,

v , $\partial v/\partial t$, $\partial v/\partial x$ and $\partial^2 v/\partial x^2$ will be of $O[\delta]$ and $\partial^2 v/\partial y^2$ will be of $O[\delta^{-1}]$.

For two dimensional incompressible flow, the third, fourth and fifth terms on the right hand side of 1.2.3 vanish, and the incompressible dissipation function reduces to the approximation

$$\phi = \mu \left(\frac{\partial u}{\partial y} \right)^2 \qquad 1.2.5a$$

where ϕ is the rate of dissipation of energy per unit time per unit volume. Near the stagnation point anticipated on the model fin experiment,* the free stream velocity U in the potential flow is proportional to the distance x from the stagnation point. Thus, we can write

$$U = \beta x \qquad 1.2.5b$$

where β is the velocity gradient at the stagnation point. Just outside the boundary layer, in the potential flow region, Eulers equations of motion 1.1.8 and 1.1.9 are valid. On applying the order of magnitude analysis to 1.1.8 and using 1.2.5b, we can write

$$u \frac{\partial u}{\partial x} + v \frac{\partial u}{\partial y} = \beta^2 x + \nu \frac{\partial^2 u}{\partial y^2} \qquad 1.2.6^{\dagger}$$

* See Section 2.1 and 2.2.

† Note $\quad U \dfrac{\partial U}{\partial x} = -\dfrac{1}{\rho} \dfrac{\partial P}{\partial x} = \beta^2 x.$

where ν is the incompressible kinematic coefficient of viscosity.

The corresponding energy equation on applying the following order of magnitude analysis can be written from 1.1.13 as

$$\rho \cdot c_p \left(\frac{\partial T}{\partial t} + u\frac{\partial T}{\partial x} + v\frac{\partial T}{\partial y}\right) - \left(\frac{\partial P}{\partial t} + u\frac{\partial P}{\partial x}\right) = k\frac{\partial^2 T}{\partial y^2} + \mu\left(\frac{\partial u}{\partial y}\right)^2 \qquad 1.2.8$$

since the velocity u varies from zero at $y = 0$ to u_∞ at $y = \delta$ while the temperature T varies from T_w at the stagnation point $y = 0$ to T_∞, the free stream fluid temperature just outside the boundary layer. If u and $T_w - T_\infty$ are taken as magnitudes of standard order, then u is of $o[1]$, v is of $o[\delta]$, $\partial^2 T/\partial x^2$ is of $o[1]$, and $\partial^2 T/\partial y^2$ is of $o[\delta^{-2}]$ and $\partial^2 T/\partial x^2$ may be neglected. Also $u\,\partial T/\partial x$ is $o[1]$, $v\,\partial T/\partial y$ is $o[1]$, $u\,\partial P/\partial x$ is $o[1]$ while $v\,\partial P/\partial y$ is $o[\delta]$ and can be neglected. Equation 1.2.8 can be further simplified by assuming that the incompressible dissipation function and $u\,\partial P/\partial x$ may be neglected. These assumptions are valid, since the compressibility effect can be incorporated into the stagnation velocity gradient. Hence, the steady state equation for temperature distribution in the boundary layer for two-dimensional flow can be written as

$$u\frac{\partial T}{\partial x} + v\frac{\partial T}{\partial y} = \frac{K}{\rho c_p}\frac{\partial^2 T}{\partial y^2} \qquad 1.2.9$$

The continuity equation can be satisfied following closely the method used in reference 7 by putting

$$u = \frac{\partial \psi}{\partial y} \quad \text{and} \quad v = -\frac{\partial \psi}{\partial x} \qquad 1.2.10$$

and defining

$$\psi = (\gamma\beta)^{1/2} x \cdot f(\eta) \qquad 1.2.11$$

where

$$\eta = \left(\frac{\beta}{\gamma}\right)^{1/2} y \qquad 1.2.12$$

Hence, we may write

$$u = \beta x f'(\eta) \quad \text{and} \quad v = -(\gamma\beta)^{1/2} f(\eta) \qquad 1.2.13$$

Differentiating u and v and substituting in the momentum equation yields the differential equation

$$f'^2(\eta) - f(\eta) f''(\eta) = 1 + f'''(\eta) \qquad 1.2.14$$

If the boundary layer temperature distribution function can be represented by

$$T = T_w - (T_w - T_\infty)\,\theta(\eta) \qquad 1.2.15$$

then, using 1.2.12 and 1.2.13, 1.2.9 can be written as

$$\theta''(\eta) + Pr\, f(\eta)\, \theta'(\eta) = 0 \qquad 1.2.16$$

It is easily seen that the boundary conditions for $\theta(\eta)$, the boundary layer temperature distribution function, are that when

$$T = T_w \;, \quad \theta(\eta) = 0 \qquad 1.2.17$$

and when

$$T = T_\infty \;, \quad \theta(\eta) = 1 \qquad 1.2.18$$

Using the boundary conditions, 1.2.17, 1.2.18, equation 1.2.16 can be solved to give

$$\theta(\eta) = \alpha_1(Pr) \int_0^\eta \exp\left[-Pr \int_0^\eta f(\eta)\, d\eta\right] d\eta \qquad 1.2.19$$

where

$$\alpha_1(Pr)^{-1} = \int_0^\infty \exp\left[-Pr \int_0^\eta f(\eta)\, d\eta\right] d\eta \qquad 1.2.20$$

According to reference 7, the stagnation function $\alpha_1(Pr)$ can be closely approximated to

$$\alpha_1(Pr) = 0.57 Pr^{0.4} \qquad 1.2.21$$

From reference 8, the form of the laminar heat transfer rate is

$$q = h(T_{aw} - T_w) \qquad 1.2.22$$

where h is the laminar stagnation film heat transfer coefficient written as

$$h = \frac{f_1}{\sqrt{Rey_\infty}} \rho_\infty V_\infty C_p \qquad 1.2.22a^*$$

Now the Stanton Number C_{h_∞} can be written as

$$C_{h_\infty} = \frac{f_1}{\sqrt{Rey_\infty}} = \frac{Nu_\infty}{Pr_\infty Rey_\infty} \qquad 1.2.23$$

Hence, 1.2.22, using 1.2.22a and 1.2.23, can be written as

$$q = \frac{Nu_\infty}{Pr_\infty Rey_\infty} \rho_\infty V_\infty C_p (T_{aw} - T_w) \qquad 1.2.24$$

The solution for the heat transfer coefficient (Nusselt number) at the stagnation point can be written from 1.2.21, 1.2.22a and 1.2.23.

$$Nu_\infty = \alpha_1(Pr)\left(\frac{\beta x^2}{\nu_\infty}\right)^{1/2} \qquad 1.2.25$$

Hence we may write

* Note $f_1 = 0.57 Pr^{-0.6}$, and $Rey_\infty = \frac{Ux}{\nu_\infty}$

$$q = 0.57\,Pr^{-0.6}\,C_p\left(\beta\rho_\infty\mu_\infty\right)^{\frac{1}{2}}\left(T_{aw} - T_w\right) \qquad 1.2.26$$

Using the first law of thermodynamics, the laminar heating rate can be further expressed in linear coordinates as

$$q = \Gamma\,\frac{dT_w}{dt} \qquad 1.2.27$$

Assuming that this is valid at the flat stagnation point, equation 1.2.26 can be written as

$$\frac{dT_w}{dt} = \frac{0.57\,Pr^{-0.6}}{\Gamma}\,C_p\left(\beta\rho_\infty\mu_\infty\right)^{\frac{1}{2}}\left(T_{aw} - T_w\right) \qquad 1.2.28$$

This is a linear differential equation for which the explicit integral is not useful, but it can be integrated using numerical methods as will be shown later.

If we assume all temperatures to be measured from absolute zero, then the radiation term can be incorporated into 1.2.28, and the equation written as

$$\frac{dT_w}{dt} = \frac{0.57\,Pr^{-0.6}}{\Gamma}\,C_p\left(\beta\rho_\infty\mu_\infty\right)^{\frac{1}{2}}\left(T_{aw} - T_w\right) - \frac{\sigma\epsilon T_w^4}{\Gamma} \qquad 1.2.29$$

where σ is Boltzmann's constant, and ϵ the emissivity of the surface. Equation 1.2.29 is an exact solution for a stagnation

point on a flat plate normal to incompressible flow. It can be seen from equation 1.2.28, that the heat transfer rate is independent of x in the vicinity of the stagnation point, It is hoped to confirm this by experiment later.

It was noted earlier that β, the velocity gradient is considerably altered by the proximity of the shock at high speeds. The reason for this is that the shock alters the potential flow around the stagnation region, making the flow virtually incompressible.

It has been found from reference 9, that the form of β is dependent on Mach number in such a way that the dimensionless stagnation velocity gradient $\frac{\beta D}{V_\infty}$, decreases with increase in Mach number.

In conclusion, it is clear that for laminar supersonic flow, the temperature decreases at an increasing rate away from the stagnation point and therefore ρ_∞ and μ_∞ will likewise decrease. Consequently, heat transfer is a maximum at the stagnation point as long as laminar flow is present.

Reference 8 has suggested under certain circumstances, that flow at the stagnation point could be turbulent. This is not anticipated for the experiments* involved in this thesis because of the low Reynolds numbers expected near the stagnation point. Equation 1.2.29 can be used until ablation occurs at the stagnation point. At this time, the heat input is radically altered by mass transfer to the boundary. The next section examines this problem.

* The experiments referred to here are the fin stagnation and fin centre line experiments. These fins have blunt semi-cylindrical leading edges, which will cause the boundary layer to thicken at the stagnation point.

1.3 STAGNATION POINT HEAT TRANSFER WITH ABLATION

From the last section, it was stated that the blunt cylindrical body shape of the fin leading edge causes the boundary layer to thicken at the stagnation point. The shielding effect of the air tends to reduce the stagnation heat transfer rate, but at elevated Mach number ranges in the continuum atmosphere, the shielding effect is not sufficient to maintain desirable skin temperatures. To date several methods of controlling skin temperatures are in use such as magneto-aerodynamic techniques, refrigerating systems, insulating materials and mass transfer cooling. Perhaps, the most used and efficient technique is a combination of insulation and mass transfer cooling called ablation.

Ablation can take place in many ways depending on the type of ablator chosen. In this thesis, the theory will be restricted to subliming ablators. A "Subliming Ablator" technique is one in which heat is expended on sublimation of the body material and is an extension of the blunt nose concept, of using a thickened boundary layer to protect the nose. A Subliming Ablator is a material which, when reaching a critical temperature called the ablation temperature, turns directly from a solid into a

gas. i.e: the solid sublimes, leaving a porous char. The gas and charred material are transferred to the boundary layer, hence absorbing heat and convecting more heat parallel to the surface.

The following analysis for a subliming ablator was developed in a parallel manner to reference 11 by Roberts, who originated a theory for stagnation point ablation by melting and vaporization. Because of the nature of the intended experiment geometries, we need only consider two-dimensional flows. Consider figure 1.3.1

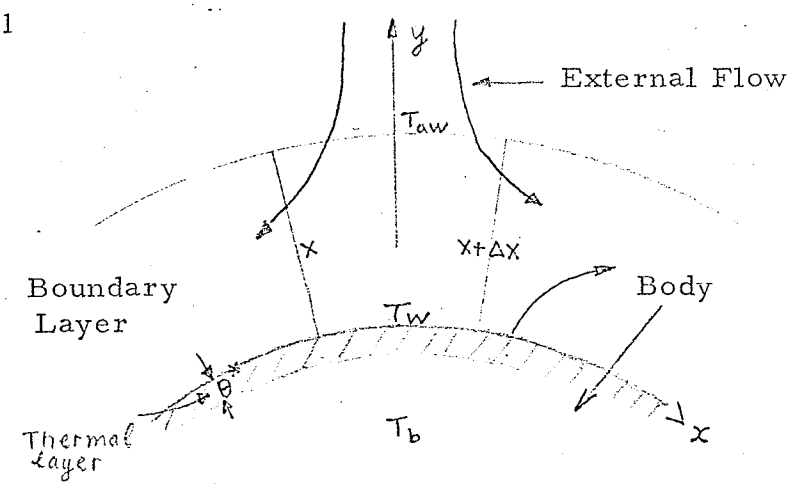

BOUNDARY LAYER MASS BALANCE DIAGRAM *

figure 1.3.1

The airflow is considered to be in the $-y$ direction. In the thin laminar boundary layer which forms in the stagnation region, the velocity, temperature and concentration of the airflow vary

* $\theta^* = \int_{-\infty}^{0} \frac{T - T_b}{T_w - T_b}\, dy$ where $T = T_b + (T_w - T_b)\, e^{y/\theta^*}$

from the external free stream values to those at the wall. It is assumed that the velocity u parallel to the wall is linear in x and that the normal component velocity v, the temperature T, and mean concentration of mass transfer material $\overline{W}$, are functions of the coordinate y, the distance normal to the wall.

Consideration of figure 1.3.1 for the wall conditions on ablation shows that the heat transfer to the wall is used as body heat and as latent heat. It will be assumed that the total aerodynamic heat flux will be committed to this process. The former statement can be written as

$$\left(k\frac{dT}{dy}\right)_w = \dot{m}\left[L + C_a\left(T_w - T_b\right)\right] \qquad 1.3.1$$

Where $\dot{m}$ is the rate of mass loss.

The mass transfer condition at the wall shows that diffusion of material away from the ablating surface and convection of material away from the ablating surface must equal the mass rate of ablation. This can be written as

$$\left(\overline{\rho}_w \overline{D}\frac{d\overline{W}}{dy}\right)_w + \overline{\rho_w v_w W_w} = \dot{m} \qquad 1.3.2$$

Where the subscript W refers to conditions at the wall.

A second condition which states there is no net transfer of air into the wall is written

$$-\left(\overline{\rho_w}\,\overline{D}\,\frac{d\overline{W}}{dy}\right)_w = (1-\overline{W}_w)\,\overline{\rho_w v_w} \qquad 1.3.3$$

The left hand term is the diffusion of air away from the surface and the right hand term represents convection of air towards the ablating surface. Elimination of the diffusion terms in equations 1.3.2 and 1.3.3 give

$$\overline{\rho_w v_w} = \dot{m} \qquad 1.3.4$$

Further examination of figure 1.3.1 shows that a simple expression for continuity of mass can be obtained. Consider the small control area of height Y and length Δx near the stagnation point, then flow of mass from the external potential flow and mass generated over the portion of ablating surface of length Δx must equal the difference between the flow at x and $x+\Delta x$. This can be expressed as

$$-\rho(Y)v(Y)\Delta x + \dot{m}\,\Delta x = \left[\int_0^Y \rho u\,dy\right]_{x+\Delta x} - \left[\int_0^Y \rho u\,dy\right]_x \qquad 1.3.5$$

Taking the limit of equation 1.3.5 and letting Δx tend to zero, we have

$$-\rho(\dot{Y})v(Y) + \dot{m} = \frac{d}{dX}\left[\int_0^Y \rho u \, dy\right] \qquad 1.3.6$$

Using the fact that flow in the stagnation region external to the boundary layer velocity varies linearly with X we can write equation 1.2.5b in the form

$$u = \beta\left(\frac{u}{U}\right)x \qquad 1.3.7$$

where $\frac{u}{U}$ is independent of x .

Differentiating 1.3.7 w.r.t. x and substituting in equation 1.3.6, equation 1.3.6 reduces to

$$-\rho(Y)v(Y) + \dot{m} = \beta\int_0^Y \rho\frac{u}{U}\, dy \qquad 1.3.8$$

Since the mass density is a function of the mass transfer, concentration and temperature, it is expedient to introduce a modified velocity component V and the transformed coordinate y as z with the relations

$$V = \frac{\rho v}{\rho_w} \qquad 1.3.9$$

$$z = \int_0^y \frac{\rho}{\rho_w}\, dy \qquad 1.3.10$$

Also, from figure 1.3.1, we can derive two more equations. The material ablated at the wall must equal the material convected from the wall, this can be written as

$$\dot{m} = \beta \bar{\rho}_w \int_0^{z_1} \overline{W} \frac{u}{\bar{u}} \, dz \qquad 1.3.11$$

The second equation is derived from the reasoning that heat flow from the external stream into the boundary layer minus the convection of heat in the boundary layer along the surface must equal the heat transfer to the surface. This can be expressed mathematically as

$$-\left(K \frac{dT}{dy}\right)_w = C_p (T_{aw} - T_w) \bar{\rho}_w \bar{V}(z_1) + \beta \bar{\rho}_w \int_0^{z_1} \bar{C}_p \, (T - T_w) \frac{u}{\bar{u}} \, dz \qquad 1.3.12$$

The quantity $\bar{V}(z_1)$ appearing in equation 1.3.12 can be eliminated by using equations 1.3.8 and 1.3.11 and the relationship

$$\bar{C}_p = \bar{C} \bar{W} + C_p (1 - \bar{W}) \qquad 1.3.13$$

where $\bar{C}_p$ is the specific heat of the air and ablated material mixture.

On elimination of $\bar{V}(z_1)$ we obtain

$$\beta \bar{\rho}_w \int_0^{z_1} \bar{C}_p (T_{aw} - T) \frac{u}{\bar{u}} \, dz = \left(K \frac{dT}{dy}\right)_w + \bar{C} (T_{aw} - T_w) \dot{m} \qquad 1.3.14$$

The rate at which a body loses mass, is determined in part by

the aerodynamic heat transfer which would prevail in the absence of ablation.

When ablation occurs, the increase in mass flow due to diffusion and convection of gaseous and solid material has the effect of thickening the boundary layer and changing the profile. This results in a reduction in the velocity, temperature and concentration gradients, reducing heat transfer to the wall, since more heat becomes convected parallel to the wall surface.

The increase in the velocity boundary layer thickness can be found by considering the mass flow parallel to the surface. The mass flow with ablation must equal the mass flow for no ablation plus the rate of mass ablated. This can be formulated as

$$\beta \bar{\rho}_w \int_0^{\delta_u} \frac{u}{\bar{u}} \, dz = \beta \rho_w \int_0^{\delta_{u,o}} \frac{u}{\bar{u}} \, dz + \dot{m} \qquad 1.3.15$$

If the assumption is made that $\bar{\rho}_w \sim \rho_w$, equation 1.3.15 can be integrated to give

$$\frac{1}{2} \delta_u = \frac{1}{2} \delta_{u,o} + \frac{\dot{m}}{\beta \bar{\rho}_w} \qquad 1.3.16$$

Since the linear profiles give, for no ablation

$$\frac{u}{U} = \frac{z}{\delta_{u,o}} \qquad 1.3.17$$

and for ablation

$$\frac{u}{U} = \frac{z}{\delta_u} \qquad 1.3.18$$

By using the equation 1.2.23 for the wall values, the rate of heat transfer to the wall when there is no ablation can be written as

$$q = \left(K\frac{dT}{dy}\right)_w = C_p(T_{aw}-T_w)(\beta\rho_w\mu_w)^{1/2}\left(\frac{Nu}{Pr\,Ra_y^{1/2}}\right)_w \qquad 1.3.19$$

Hence, 1.3.14 can be written as

$$\frac{1}{\delta_u}\int_0^{\delta_u}\left(\frac{T_{aw}-T}{T_{aw}-T_w}\right)\frac{u}{U}\,dz = \frac{1}{\delta_u}\left(\frac{\mu_w}{\bar{\rho}_w\beta}\right)^{1/2}\left[\left(\frac{Nu}{Pr\,Ra_y^{1/2}}\right)_w + \frac{\dot{m}}{(\bar{\rho}_w\mu_w\beta)^{1/2}}\right] \qquad 1.3.20$$

by use of equation 1.3.19.

Using equations 1.3.16 and 1.3.17 and the following relationships for linear profiles from reference 9.

$$\frac{T_{aw}-T}{T_{aw}-T_w} = 1 - \frac{z}{\delta_{T,o}} \qquad 1.3.21$$

and

$$\delta_{u,o}\left(\frac{\rho_w \beta}{\mu_w}\right)^{1/2} = 6\left(\frac{Nu}{Re_y^{1/2}}\right)_w \qquad 1.3.22$$

equation 1.3.20 can be reduced to the following result.

$$\left(\frac{Nu}{Pr\, Re_y^{1/2}}\right)_w = \left(\frac{Nu}{Pr\, Re_y^{1/2}}\right)_{ow} - \left(1 - \frac{Pr_w^{-0.6}}{3}\right)\frac{\dot{m}}{(\rho_w \mu_w \beta)^{1/2}} \qquad 1.3.23$$

Using equation 1.3.19 and the following relationship for two-dimensional flow

$$\left(\frac{Nu}{Re_y^{1/2}}\right)_w = 0.57\left(\frac{\rho_\infty \mu_\infty}{\rho_w \mu_w}\right)^{0.4} Pr_w^{0.4} \qquad 1.3.24$$

Again taken from reference 9, equation 1.3.23 can be written as

$$q = \left[C_a(T_w - T_b) + L + \bar{C}_p(T_{aw} - T_w)\left(1 - \frac{Pr_w^{-0.6}}{3}\right)\right]\dot{m} \qquad 1.3.25$$

If we now make the assumption that charred material is removed with the gas and transferred to the boundary layer, equation 1.3.25 can be written as

$$q = \left[C_a(T_w - T_b) + L + (\eta C_g + (1-\eta) C_c)(T_{aw} - T_w)\left(1 - \frac{Pr_w^{-0.6}}{3}\right)\right]\dot{m} \qquad 1.3.26$$

The term in parenthesis is called the effective heat of ablation

$$H_{eff} = C_a(T_w - T_b) + L + (\eta C_g + (1-\eta) C_c)(T_{aw} - T_w)\left(1 - \frac{Pr_w^{-0.6}}{3}\right) \qquad 1.3.27$$

The first term on the right hand side is the heat input required

to raise the body surface to the wall temperature, the second is the latent heat of ablation required for the material phase change, and the third and fourth are the heat blockage terms due to mass transfer of the pyrolysis gases and char material into the boundary layer, which absorb heat because their temperatures are raised from that of the body, to the effective boundary layer temperature. The symbol η represents the pyrolisis gas mass fraction.

In summary of this section, we have assumed that on ablation, the ablation surface maintains constant temperature and that the total aerodynamic heat flux is absorbed by the ablation process* and secondly, that the ablated material which consists of pyrolisis gases and char, is transferred to the boundary layer. Hence, the heat flux to the body is reduced by thickening of the boundary layer, absorption due to latent heat and transferred materials, and raising of the body to the ablation temperature.

* Ablation process is taken to include heat required to raise body temperature to the ablation temperature.

1.4 NON STAGNATION POINT HEAT TRANSFER

The purpose of this section is to present a non linear differential equation for transient laminar and turbulent heat transfer for flat surfaces and bodies of large radius such as rocket motor cases. There are a number of ways of obtaining the boundary layer equations from the general equations of continuity, momentum and energy, such as in reference 6 and 7, but none are really satisfactory from the point of view of rigour. This is due to the fact that the boundary layer equations are only approximations themselves, to the most general equations which describe the flow.

In order to see how these approximations are made, it would be best to write down the governing general equations 1.1.1, 1.1.2 and 1.1.3 again, and show how a brief order of magnitude analysis along with physical arguments can reduce the general equations to a workable form. The general equations written again are

$$\frac{D\rho}{Dt} + \rho\frac{\partial u_i}{\partial x_i} = 0 \qquad 1.4.1$$

$$\rho\frac{Du_i}{Dt} - \rho F_i + \frac{\partial P}{\partial x_i} + \frac{\partial \tau_{ij}}{\partial x_i} = 0 \qquad 1.4.2$$

and

$$\rho \frac{DE}{Dt} + p\frac{\partial u_i}{\partial x_i} + \tau_{ij}\frac{\partial u_i}{\partial x_i} + \frac{\partial q_i}{\partial x_i} = 0 \qquad 1.4.3$$

Since the equation of continuity 1.4.1 does not alter under coordinate transformation, it can be written after assuming a steady state condition, in the two dimensional form as

$$\frac{\partial}{\partial x}(\rho u) + \frac{\partial}{\partial y}(\rho v) = 0 \qquad 1.4.4$$

If the air flow is assumed to be steady state, i.e. $\frac{\partial}{\partial t} = 0$ and that body forces are zero, then applying the boundary layer approximations to equation 1.4.2, the Navier Stokes momentum equation reduces to

$$\rho u \frac{\partial u}{\partial x} + \rho v \frac{\partial u}{\partial y} = -\frac{\partial p}{\partial x} + \frac{\partial}{\partial y}\left(\mu \frac{\partial u}{\partial y}\right) \qquad 1.4.5$$

since the momentum in the y direction is zero.

If for the energy equation 1.4.3, it is assumed that the velocity and temperature gradients in the x direction are much less than in the direction y, making the corresponding viscous shear stresses and heat conduction terms in the x direction negligible.

then

$$\rho u\left[c_p\frac{\partial T}{\partial x}+\frac{\partial u}{\partial y}\right]+\rho v\left[c_p\frac{\partial T}{\partial y}+\frac{\partial}{\partial y}\left(\frac{u^2}{2}\right)\right]=\frac{\partial}{\partial y}\left(K\frac{\partial T}{\partial y}+\mu u\frac{\partial u}{\partial y}\right) \qquad 1.4.6$$

A useful form of 1.4.6 can be obtained by multiplying 1.4.5 by the velocity u in the x direction and combining with 1.4.6 to obtain

$$\rho u c_p\frac{\partial T}{\partial x}+\rho v c_p\frac{\partial T}{\partial y}=u\frac{\partial P}{\partial x}+\frac{\partial}{\partial y}\left(K\frac{\partial T}{\partial y}\right)+\mu\left(\frac{\partial u}{\partial y}\right)^2 \qquad 1.4.7$$

If zero pressure gradient is assumed and the energy dissipation function is neglected in 1.4.7, then we can write

$$u\frac{\partial T}{\partial x}+v\frac{\partial T}{\partial y}=\frac{K}{\rho c_p}\frac{\partial^2 T}{\partial y^2} \qquad 1.4.8$$

It will be noticed that 1.4.8 is identical to 1.2.9 for stagnation point heating.

The assumption of zero pressure gradient, is dependent on the pressure distribution over the body. It should be noted, however, that in the writing of the digital computer programs, the pressure distribution was included as a function of Mach number.*

* Mach number just outside boundary layer.

The method of solution of equation 1.4.8 is identical to that for the stagnation point heating. This results according to reference 7, in that the convection function $\alpha_2 (Pr)$ becomes

$$\alpha_2 (Pr) = 0.664 \, Pr_\infty^{0.33} \qquad 1.4.9$$

and the heat transfer coefficient as being

$$h = 0.5 \, Pr_\infty^{-0.66} \, C_{f\infty} \, \rho_\infty \, C_p \, V_\infty \qquad 1.4.10$$

Using 1.2.22, 1.4.9 and assuming that the simple energy equation

$$\frac{V_\infty^2}{2} = c_p \left(T_{o\infty} - T_\infty \right) \qquad 1.4.10a$$

for flow through a shock is valid, the forced convective heat transfer for supersonic flow can be written as

$$q = 0.25 \, Pr^{-0.66} \, C_{f\infty} \, \rho_\infty \, V_\infty^3 \left(\frac{T_{aw} - T_w}{T_{o\infty} - T_\infty} \right) \qquad 1.4.11$$

Equation 1.4.11 is quite general and can be applied to laminar or turbulent flows by taking into account the form of the recovery

factor.

The general equation for the recovery factor is

$$R = \frac{T_{aw} - T_\infty}{T_{o\infty} - T_\infty} \qquad 1.4.12$$

where for laminar flow

$$R = (Pr)^{1/2} \qquad 1.4.13$$

and for turbulent flow

$$R = (Pr)^{1/3} \qquad 1.4.14$$

Hence, for forced laminar flow, the laminar differential equation can be written on using 1.4.14, 1.4.13 and 1.2.27 as

$$\frac{dT_w}{dt} = \frac{1}{\Gamma}\left[\frac{Pr^{-1/6} C_{f\infty}}{2} \frac{\rho_\infty V_\infty^3}{2}\left(\frac{T_{aw} - T_\infty}{T_{aw} - T_\infty}\right) - \sigma \epsilon T_w^4\right] \qquad 1.4.15$$

where the radiation term has been included.

Similarly, the turbulent flow equations can be written using 1.4.11, 1.4.14 and the modified Reynolds Analogy for turbulent flow as

$$\frac{dT_w}{dt} = \frac{1}{r}\left[0.6\,Pr^{0.33}\,\frac{C_{f\infty}}{2}\,\rho_\infty V_\infty\left(\frac{T_{aw}-T_w}{T_{aw}-T_\infty}\right) - \sigma\epsilon T_w^4\right] \qquad 1.4.16$$

Again in the theoretical analysis, the use of this equation will be restricted to the continuum region of flight.

It will now be shown how the stagnation or non-stagnation heat fluxes can be coupled with a linear forward finite difference method for prediction of temperature distributions in composite materials.

1.5 LINEAR FORWARD FINITE DIFFERENCE METHOD

Before ablation occurs, the problem of heat transfer to the structure reduces to that of finding the transient aerodynamic heat flux q and coupling this with a linear finite difference method. To make the ablation-procession linear finite difference coupling clearer, it will be of benefit to examine the form of heat transfer before ablation starts. Consider figure 1.5.1

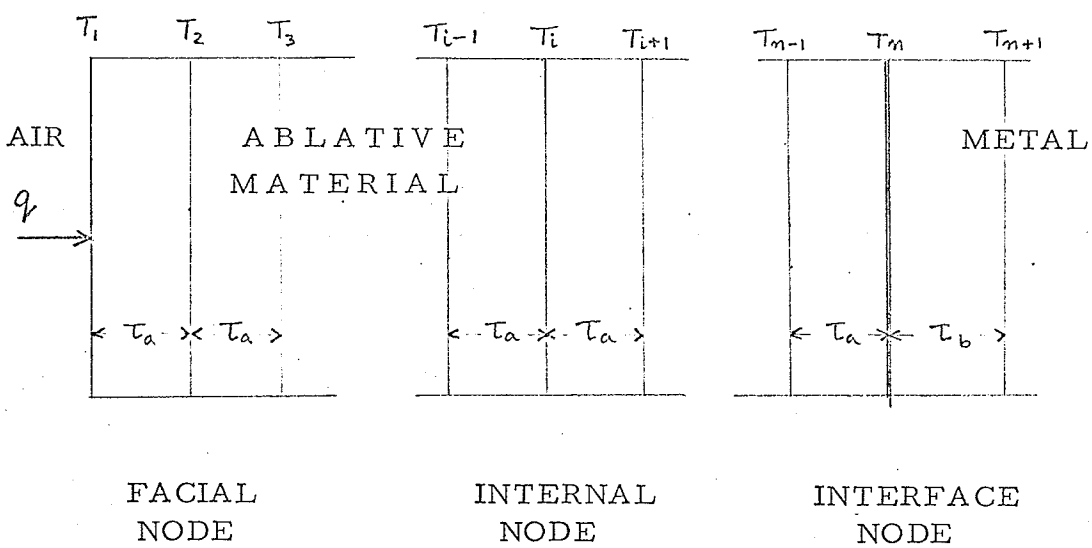

figure 1.5.1

Figure 1.5.1 illustrates a modal distribution of temperature through a section of an aerospace sandwich structure. Only two materials a and b are considered, since all the forms of the

finite difference equations can be written for the two materials.

Consider a heat balance at the facial node. The heat flux transmitted to the structure minus the heat conducted out of the first half node must equal the heat stored in the first half node. Expressing the conducted and stored heats in temperature form, the former statement can be written mathematically as

$$q - \frac{K_a}{\tau_a}(T_1 - T_2) = \frac{\rho_a C_a \tau_a}{2\Delta t}(T_1' - T) \qquad 1.5.1$$

Where T_1' is the temperature of the facial node after the heat flux q has been applied. Rearranging equation 1.5.1 and solving for T_1' we can write

$$T_1' = T_1\left(1 - \frac{2K_a\Delta t}{\tau_a^2 \rho_a C_a}\right) + T_2\left(\frac{2K_a\Delta t}{\tau_a^2 \rho_a C_a}\right) + q\left(\frac{2\Delta t}{\tau_a \rho_a C_a}\right) \qquad 1.5.2$$

A general condition for stability of any forward finite difference problem is that all coefficients be +ve . This leads to the stability criterion that

$$\left(1 - \frac{2K_a\Delta t}{\tau_a^2 \rho_a C_a}\right) \geq 0 \qquad 1.5.3$$

This means that the time interval Δt for the transient heat input must be compatible with the nodal period τ_a in material a, to satisfy the above stability criterion.

Examination of the heat balance for an internal node reveals that the heat conducted from the $(i-1)^{th}$ to i^{th} node minus the heat conducted from the ith to $(i+1)^{th}$ node must equal the heat stored in the ith nodal period. Again writing the heat balance in terms of temperature we have that

$$\frac{K_a}{\tau_a}\left(T_{i-1}-T_i\right)-\frac{K_a}{\tau_a}\left(T_i-T_{i+1}\right)=\frac{\rho_a C_a \tau_a}{\Delta t}\left(T_i'-T_i\right) \qquad 1.5.4$$

Where T_i' is the temperature of the ith node due to initial aerodynamic heat input. Rearrangement of 1.5.4 and solving for T_i' gives

$$T_i'=T_i\left(1-\frac{2K_a\Delta t}{\rho_a C_a \tau_a^2}\right)+\frac{K_a\Delta t}{\rho_a C_a \tau_a^2}\left(T_{i-1}+T_{i+1}\right) \qquad 1.5.5$$

For stability of the internal nodes we must have positive coefficients and the stability criterion becomes.

$$\left(1-\frac{2K_a\Delta t}{\rho_a C_a \tau_a^2}\right)\geqslant 0 \qquad 1.5.6$$

It should be noted here that the facial and internal stability criteria are identical.

At the interface between materials a, b the statement for the heat balance is the same as for the internal nodes except that the new material physical conditions must be accounted for. Hence, writing the heat balance in terms of the temperatures T_{n-1}, T_n and T_{n+1}, we have

$$\frac{K_a}{\tau_a}\left(T_{n-1}-T_n\right)-\frac{K_b}{\tau_b}\left(T_n-T_{n+1}\right)=\frac{\rho_a C_a \tau_a+\rho_b C_b \tau_b}{2\Delta t}\left(T_n'-T_n\right) \qquad 1.5.7$$

where T_n' is the temperature at the interface node. Rearranging 1.5.7 and solving for T_n' we have

$$T_n' = T_n\left[1-\left(\frac{K_a}{\tau_a}+\frac{K_b}{\tau_b}\right)\left(\frac{2\Delta t}{\rho_a C_a \tau_a+\rho_b C_b \tau_b}\right)\right]$$

$$+\frac{T_{n-1}}{\tau_a}\left(\frac{2K_a\Delta t}{\rho_a C_a \tau_a+\rho_b C_b \tau_b}\right)$$

$$+\frac{T_{n+1}}{\tau_b}\left(\frac{2K_b\Delta t}{\rho_a C_a \tau_a+\rho_b C_b \tau_b}\right) \qquad 1.5.8$$

Again for stability we must have positive coefficients, so the stability criterion becomes

$$\left[1-\left(\frac{K_a}{\tau_a}+\frac{K_b}{\tau_b}\right)\left(\frac{2\Delta t}{\rho_a C_a \tau_a-\rho_b C_b \tau_b}\right)\right] \geqslant 0 \qquad 1.5.9$$

It should be noted that the time interval Δt for the transient heat input should be made compatible with τ_a and τ_b the nodal thicknesses of materials a and b to satisfy the stability conditions expressed by equations 1.5.3, 1.5.6 and 1.5.9.

The foregoing equations describe a finite difference method coupled with a transient heat flux q. It will now be shown how the linear forward finite difference method can be adapted to describe the process of ablation.

1.6 COUPLING OF ABLATION PROCESSION TO LINEAR (FORWARD) FINITE DIFFERENCE PROBLEM

When ablation occurs, the facial node temperature $T_1 = T_W$ becomes equal to T_{ab} the ablation temperature. Since $T_1 = T_{ab}$ is known and will be assumed to remain constant, the next step is to find T_2 .

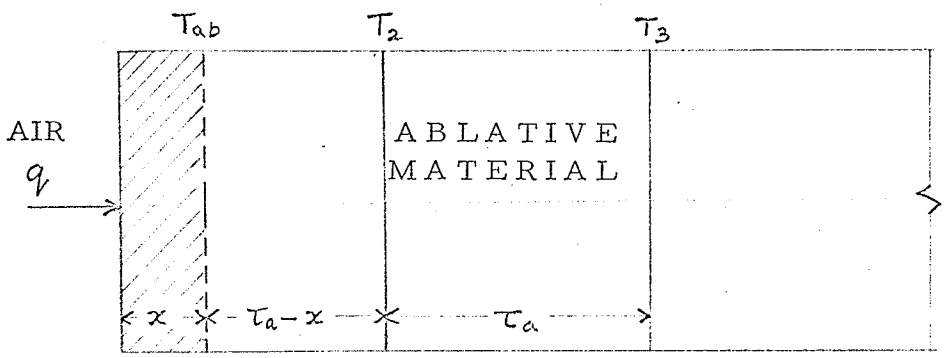

figure 1.6.1

Suppose that the heat input q ablates a depth x of the ablative material, and that ablated material is transferred into the boundary layer. Then the heat balance for the new situation from figure 1.6.1 becomes

$$\frac{K_a}{\tau_a - x}\left(T_{ab} - T_2\right) - \frac{K_a}{\tau_a}\left(T_2 - T_3\right) = \frac{\rho_a C_a \tau_a}{\Delta t}\left(T_2' - T_2\right) \qquad 1.6.1$$

on rearrangement and solving for T_2' we have

$$T_2' = T_2\left(1 - \frac{K_a \Delta t}{\rho_a C_a \tau_a (\tau_a - X)} - \frac{K_a \Delta t}{\rho_a C_a \tau_a^2}\right) + \frac{K_a \Delta t\, T_{ab}}{\rho_a C_a \tau_a (\tau_a - X)} + \frac{K_a \Delta t\, T_3}{\rho_a C_a \tau_a^2} \qquad 1.6.2$$

It should be noticed that when $X = 0$, equation 1.6.2 reverts to 1.5.5 as would be expected.

Equation 1.6.2 may be used until the stability criterion

$$\left(1 - \frac{K_a \Delta t}{\rho_a C_a \tau_a (\tau_a - X)} - \frac{K_a \Delta t}{\rho_a C_a \tau_a^2}\right) \geqslant 0 \qquad 1.6.3$$

is not satisfied. When this situation occurs it is necessary to drop the second node and write the heat balance in terms of T_{ab} , T_3 and T_4 and the new nodal distance from the original surface.

The heat balance on rearrangement for this condition would be

$$T_3' = T_3\left(1 - \frac{K_a \Delta t}{(2\tau_a - X)\rho_a C_a \tau_a} - \frac{K_a \Delta t}{\rho_a C_a \tau_a^2}\right) + \frac{T_{ab} K_a \Delta t}{(2\tau_a - X)\rho_a C_a \tau_a} + \frac{T_4 K_a \Delta t}{\rho_a C_a \tau_a^2} \qquad 1.6.4$$

When the $(n-1)^{th}$ node is dropped due to ablation procession the nodal distance in the equation becomes

$$(n-1)\tau_a \qquad 1.6.5$$

and the stability condition for the nth node would be

$$\left(1 - \frac{K_a \Delta t}{\left[\left(\sum_{1}^{n=i-1} \tau_{a_i}\right) - X\right]\rho_a C_a \tau_a} - \frac{K_a \Delta t}{\rho_a C_a \tau_a^2}\right) \geqslant 0 \, . \qquad 1.6.6$$

This and the previous equations are all that are necessary for

computing the temperature distributions in a two material structure, when ablation occurs. It can be seen that the ablation process, on assuming constant surface ablation temperature, can be represented by a simple series expression with the stability criterion of equation 1.6.6.

The next section discusses the accuracy of the "Ablation Procession-Finite Difference Method".

1.7 ACCURACY OF ABLATION PROCESSION-FINITE DIFFERENCE METHOD

Some knowledge of the accuracy of ablation procession finite difference method can be obtained from reference 21, a recent paper on a finite difference method with ablation (September 1967). This paper compares a forward finite difference process similar to that described in this section, with exact solutions for a steady state problem. It should be remembered that in this thesis all problems are transient. The analytical solution is indistinguishable from the exact solution provided the following condition is observed

$$\beta \leq 0.25 \qquad 1.6.7$$

2β corresponds to the term

$$\left\{ \frac{K_a \Delta t}{\left[\left(\sum_{n=1}^{n=i-1} \tau_{a_i}\right) - x\right] \rho_a c_a \tau_a} + \frac{K_a \Delta t}{\rho_a c_a \tau_a^2} \right\} \qquad 1.6.8$$

in equation 1.6.6. In all digital computations for this thesis the value of 1.6.8 was always less than 0.25, corresponding to 1.6.7, showing that not only is the stability criterion of equation 1.6.6 satisfied, but that the analytic solutions are indistinguishable from exact solutions. This accounts for the extraordinary correlation between experiment and theory recorded in section 4.0. It is suggested that differences which do occur are due to inaccuracies in other data inputs, such as trajectory parameters and

the Van Driest Aerodynamic heating theory (reference 8), adapted for this thesis and described in sections 1.2 and 1.4.

It should be noted that when the recession distance x in 1.6.8 is zero, corresponding to the no ablation case described in section 1.5, that the stability criterion of equation 1.5.3 is preserved and

$$\beta = \frac{K_a \Delta t}{\tau_a^2 \rho_a C_a} \leq 0.25 \qquad 1.6.9$$

showing that the analytic solution is "exact".* This concludes the discussion of accuracy of the analytic solution.

The next section describes a set of carefully planned experiments to test the theory cited in previous sections.

* This was subsequently proved by taking several values of $\beta \leq 0.25$, and computing temperature distributions in the ablative material with the ablation program described in section 3.2.

EXPERIMENTS

2.0 EXPERIMENTS

The following sections describe a set of carefully designed in flight ablative heat transfer experiments, to probe a wide range of inflight vehicle heating conditions.

The design and geometry of the experiments was dictated by several anticipated inflight conditions and tailored to suit theoretical considerations. It was endeavoured to avoid any undesirable aerodynamic effects and to duplicate as near as possible, the conditions and assumptions made in the theoretical analysis.

A second objective to verifying the ablative theory in Section 1 was to compare the relative merits of thin ablative coverings, of Armstrong Insulcork 2275 and Avcoat II as thermal protection systems for booster vehicles during the ascent boost phase. The experimental results obtained are indicative of the ablative material performances only for the geometries and inflight conditions experienced, and may not be indicative of other geometries or flight conditions.

Although the results obtained from the inflight experiments will only be compared with the theoretical analysis for the continuum flight region, they are valid for a much wider range of flight conditions. Experimental results were obtained for continuum, slip, intermediate, free molecular and deep space heating conditions, and could be used to indicate thermal conditions in real space.

Perhaps at some future date the data in the slip, intermediate, and free molecular regions can be analysed theoretically, but as stated before, the experimental results will only be given and compared with theory over the continuum flight regime.

It should be noted that all dimensions on diagrams in the following sections have the units of inches, unless otherwise stated.

2.1 FIN STAGNATION EXPERIMENT

The fin stagnation experiment was designed specifically to gather transient temperature history data at the interface between an ablative coating and a stainless steel substructure over a wide range of temperature and flight conditions.

Two identically constructed fins were produced, one covered with Armstrong Insulcork 2275 and the other with Avcoat II. By exposing the ablative fins to similar flight conditions, it was hoped to compare the relative merits of Insulcork and Avcoat as aerospace thermal protection systems. The fin design and geometry were dictated by the facts that it was necessary that the fins would not adversely affect the platform vehicle aerodynamic characteristics and performance, and yet ensure true stagnation conditions to enable a good comparison with the developed ablative theory. True stagnation conditions were realized by producing a fin with no sweepback to minimise crossflow and non linear boundary layer effects. The thermocouple sensor locations were placed to eliminate influence from fin body interference and fin tip vortex effects. Employment of the afore mentioned philosophy led to the following fin design and fabrication designated type "A".

The type "A" fins were machined from a solid block of A.I.S.I.

321 heat resistant stainless steel to the dimensions shown in figure 2.1.1. The fin blanks were drilled with a 0.078 inch diameter drill at an angle of 45°, 0.20 inches from the leading outer edge, and countersunk to a depth of 0.50 inches from the opposite end of the hole. Using the same diameter drill, holes were drilled from the fin root chord along the centre line until the 45° holes were met. The fin leading edges were then bevelled to a radius of 0.125 inches to form an unswept semi-cylindrical stagnation surface. The fins were then welded to baseplates made of the same material having diameters of 2.38 inches and thicknesses of 0.24 inches as shown in figure 2.1.2 and 2.1.3 to facilitate securing of the fin blades on the rocket igniter housing mounting. To effect thermocouple installations, a fifth hole of 0.1695 inches in diameter was drilled in the centre of each base plate to accept the Chromel - Alumel thermocouples. The thermocouple installation was effected by pushing the thermocouples through the base plate hole into the centre line hole, and bending the thermocouple wire through 135° into the 45° hole. The thermocouple heads were then brought coincident with the fin surfaces, and welded into place. Welds were finished flush to the contours of the fin leading edges, the thermocouples themselves being held in place by small plugs, tack welded into the 45° holes and finished flush at the fin trailing edges. The completed type "A"

fin substructure is shown in figure 2.1.2.

The GG-20-CT Chromel-Alumel thermocouples used in the experiment were chosen for their accuracy through the experimental temperature ranges anticipated. Their accuracy is guaranteed to within $\pm$ 0.75% through the temperature range 50 - 1800° F which corresponds to $\pm$ 4° F or $\pm$ 0.89 millivolts e.m.f.

The thermocouples consist of Chromel-P, a heat resistant nickel chromium alloy containing 90% nickel and 10% chromium. This alloy has a temperature e.m.f. relationship that is positive to almost every known metal or alloy. Alumel alloy was used as a negative wire in the thermocouple assembly. Fabrication of the thermocouples was accomplished by twisting the wires together before welding. It was felt that although the "twist" type is known to have slower response characteristics to temperature fluctuations than "butt" type welds, it had the advantage of greater reliability in the sense that it held the wires in place and reinforced the weld. Even with a slower response than the "butt" type thermocouple, its accuracy as stated above, was more than sufficient for this type of experiment.

The final process in the fabrication of the complete fins was the

bonding of Insulcork 2275 and Avcoat II to the metal substructures, the bonding technique for each ablative material is identical and so only the technique for the bonding of Insulcork 2275 will be described in detail.

The application of Insulcork 2275 to the metal substructure is quite straightforward. Pieces of Insulcork 0.050 inch thick were cut slightly oversize to those dimensions shown in figure 2.1.1. The fin surfaces were then cleaned to free them from grease contamination and mill scale, and the precut Insulcork smeared with Insulcork J.1156-E-30 epoxy adhesive were applied to the clean fin surface and held in place with masking tape. The pressures required during bonding are not critical for a good bond, the minimum being that necessary for good contact. To ensure complete removal of air bubbles from the bonded surfaces, a vacuum bagging technique was employed. The bagging technique consisted of enclosing the fin in a polythene bag and then evacuating the air from the bag, hence removing any trapped air bubbles. Tests made by the Armstrong Insulcork Company on simple lap joints have indicated that film thickness from 0.005 to 0.010 inches do not vary significantly in strength. Curing of the J.1156-E-30 adhesive enabled handling after eight hours and high strength within twenty-four hours. When a good bond had been established, any voids due to cork mismatching

were filled with trowable mastic Armstrong Insulcork KN-5A ablation compound. Its cork content makes it relatively light in weight, and its curing performance is similar to that of the J.1156-E-30 adhesive. The final cleaning operation of the fin involved sanding the fin surface, rough edges and protrusions, to a smooth finish, being careful to maintain the 0.050" thickness of ablative Insulcork. The maintenance of correct thickness was ensured by checking the ablative layer periodicly with an Ultrasonic Densometer.

The Avcoat II covered fin was fabricated in exactly the same manner as for the Insulcork 2275, the only difference being that the bonding agent and filler material used in the fabrication was liquid Avcoat II.

The completed fins were then mounted on the vehicle igniter housing at the Churchill Rocket Range and connected to the rocket telemetry system. Description of the whole telemetry package for temperature data transmission would be unnecessary and complicated, therefore, only a brief description is given of the general functions concerned with temperature relay.

A block diagram of the necessary components in the telemetry

package for temperature relay is shown in figure 2.1.4. The sensor thermocouples at the fin blade-ablation material interface convert the temperature, to voltage anologs. The voltage analog is fed as a signal input to a 30 channel, 10 r.p.s. commutator which sequentially samples the output from a group of pickups measuring vehicle performance. The modulation input to the subcarrier oscillator in turn supplies the frequency modulated transmitter with the combined signal output which is fed to the quadraloop antennae for transmission.

The ground receiving station contains a F.M. receiver, the output of which feeds, both a tape recorder, and a bank of discriminators, one for each subcarrier used. The discriminators which contain filters to separate the subcarrier oscillator frequencies convert the frequency analogs to voltage analogs which are recorded on a multiple channel oscillograph recorder, and on paper records.

A similar type of telemetry system as the one just described was used for all experiments generating in-flight data.

The vehicle used to produce the experiment environmental condition was the Black Brant IV-07, launched from the Fort Churchill Rocket Range. The vehicle performance was excellent giving a good smooth

flight, performing closely to theoretical prediction, Figure 2.1.5 shows a diagram of the Black Brant IV vehicle and the experiment located on the second stage igniter housing.

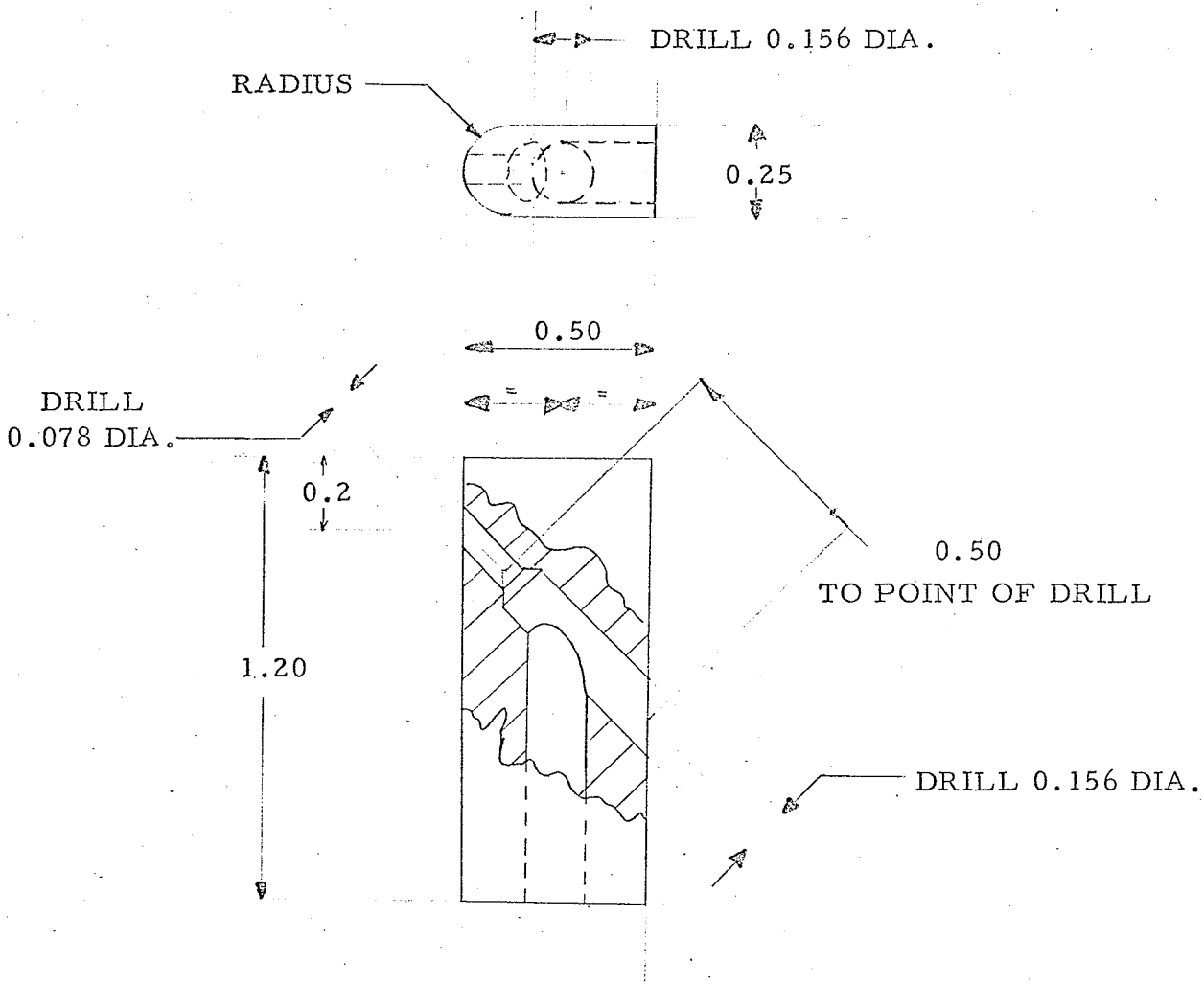

SECTION AND PLAN VIEW OF TYPE A FIN

figure 2.1.1

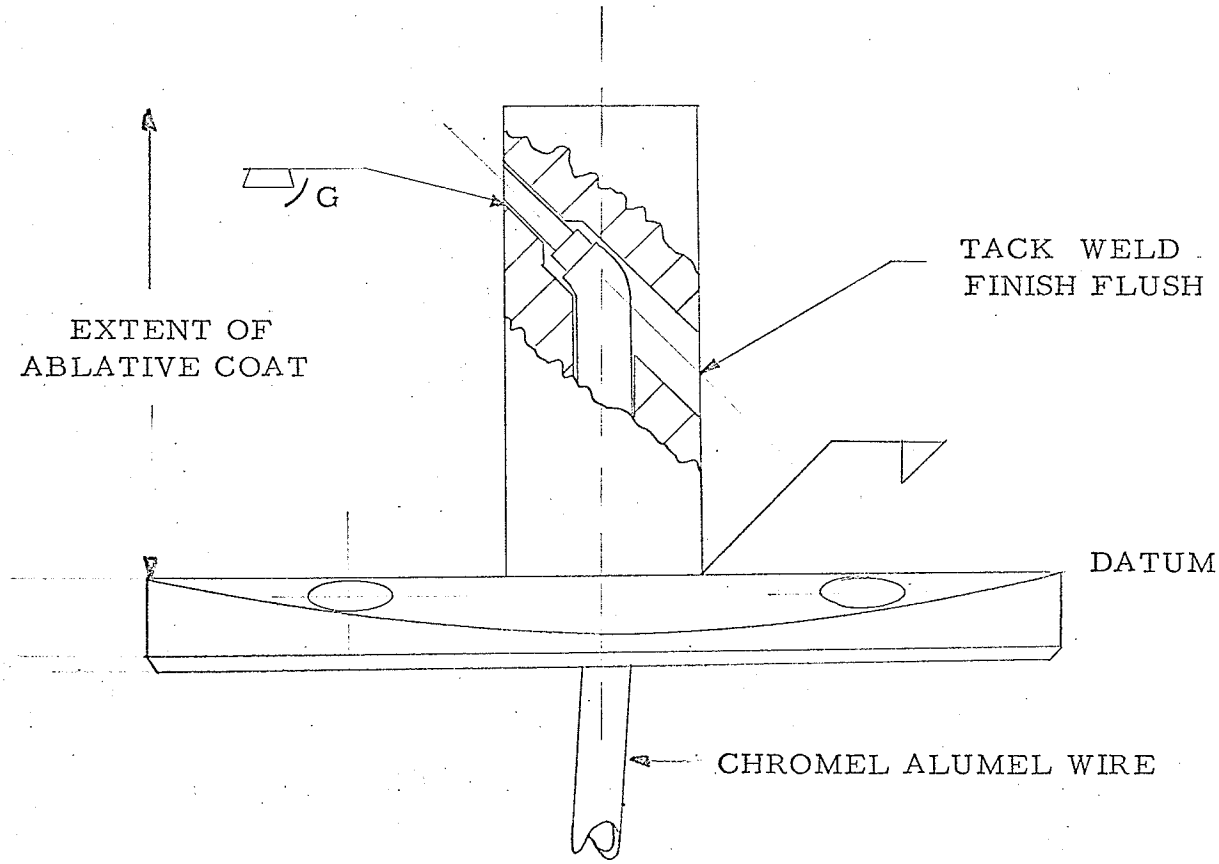

PLAN VIEW TYPE A FIN

figure 2.1.2

SECTION AND PLAN VIEW OF BASE PLATE

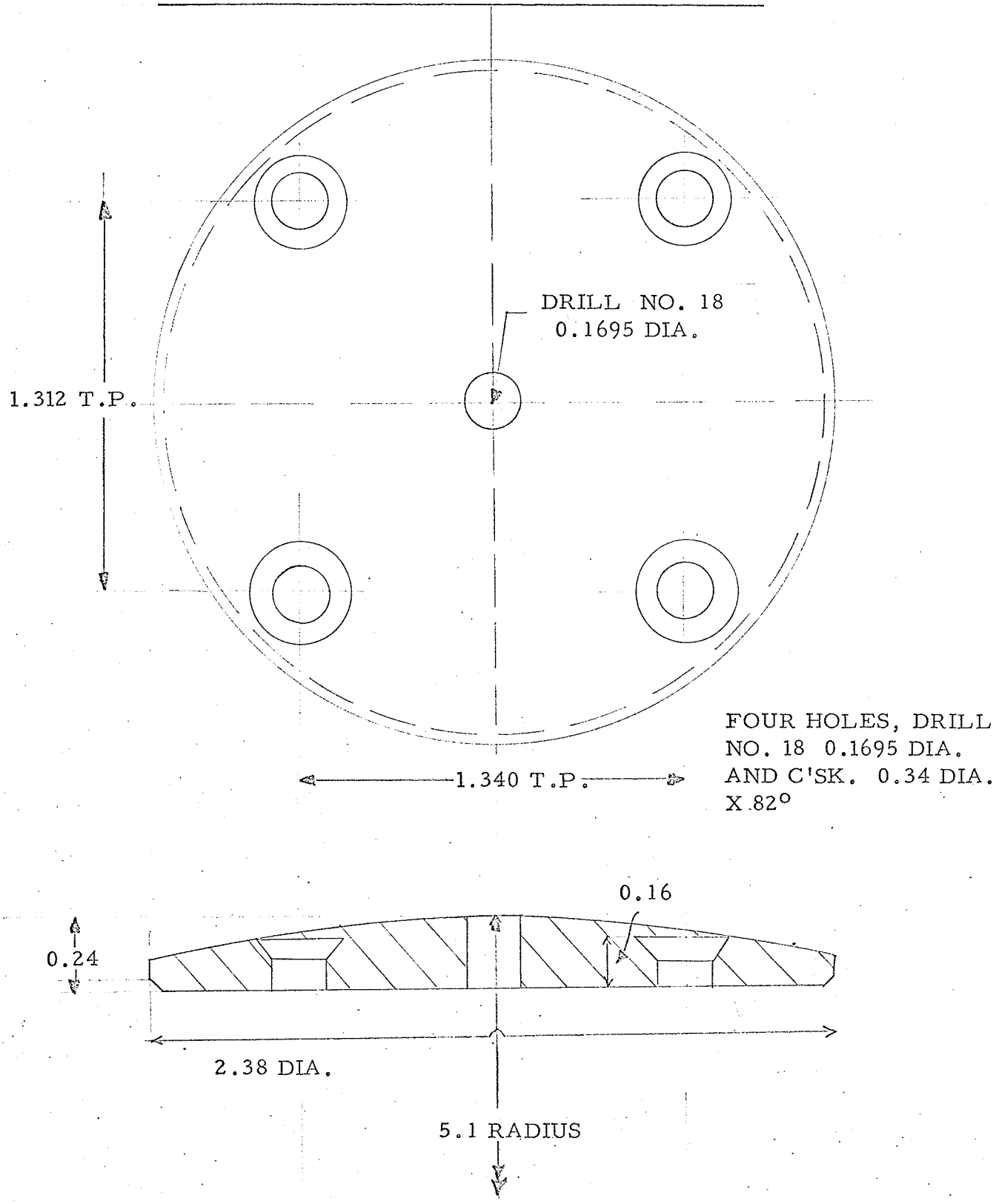

figure 2.1.3

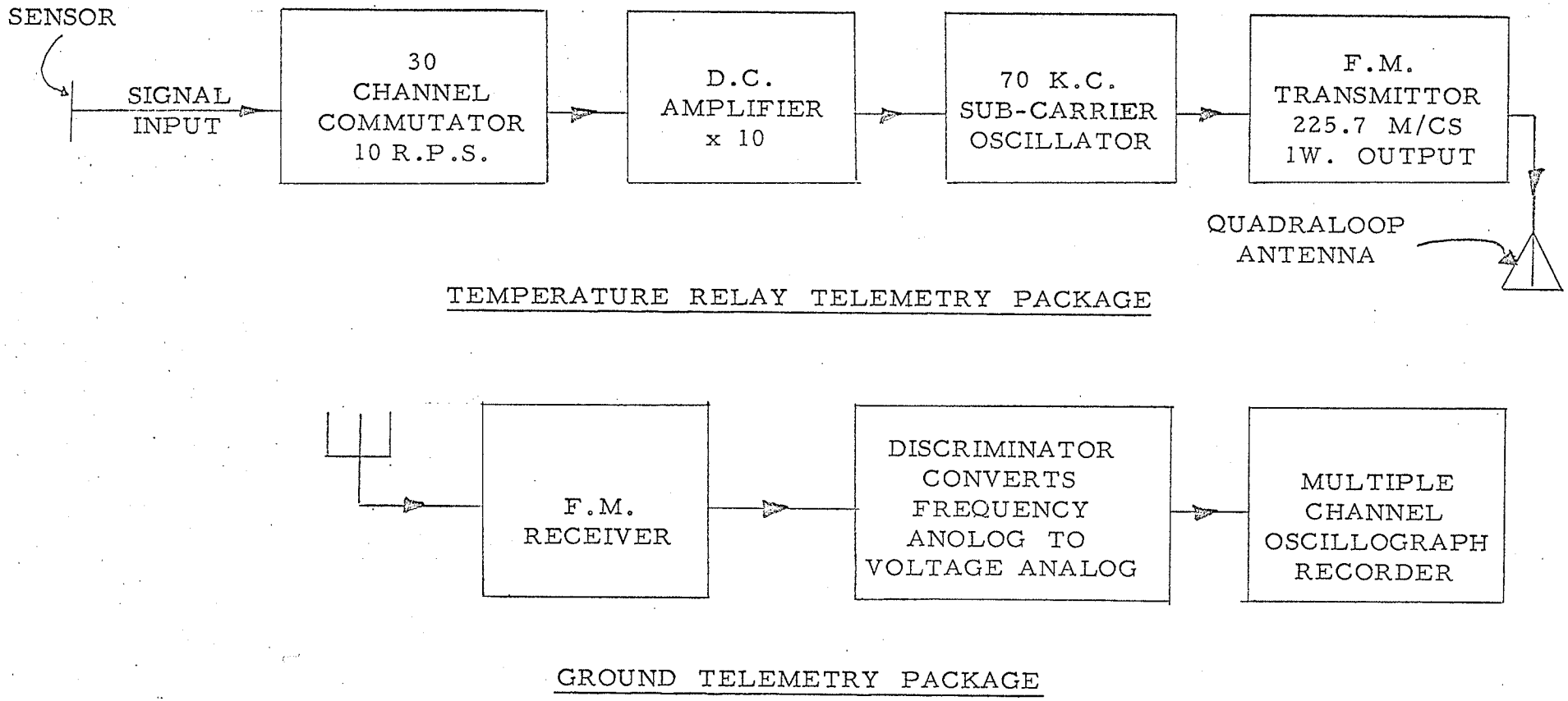
SENSOR
SIGNAL INPUT
30 CHANNEL COMMUTATOR 10 R.P.S.
D.C. AMPLIFIER x 10
70 K.C. SUB-CARRIER OSCILLATOR
F.M. TRANSMITTOR 225.7 M/CS 1W. OUTPUT
QUADRALOOP ANTENNA
TEMPERATURE RELAY TELEMETRY PACKAGE
F.M. RECEIVER
DISCRIMINATOR CONVERTS FREQUENCY ANOLOG TO VOLTAGE ANALOG
MULTIPLE CHANNEL OSCILLOGRAPH RECORDER
GROUND TELEMETRY PACKAGE

figure 2.1.4

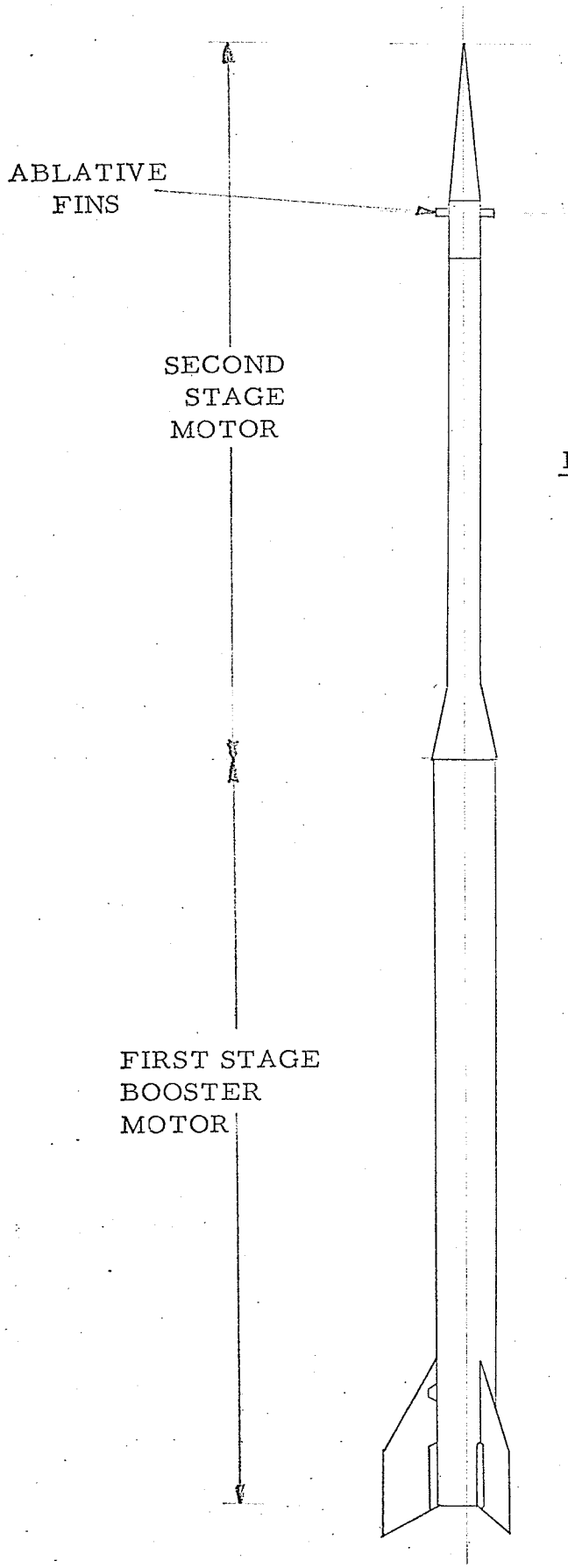

LOCATION OF ABLATIVE FINS

ON BB IV

0-7 AND 0-8

figure 2.1.5

2.2 FIN CENTER LINE EXPERIMENT

The fin center line experiment was designed to obtain a transient temperature history at the interface between an ablative coating and the stainless steel substructure at the center line of the fins.

The design philosophy and range of data of this experiment are identical to those mentioned in the fin stagnation heat transfer experiment. The center line experiment differs only in the construction of the fin blanks, and data received; identical materials and thermocouples were used throughout. With this experiment, it was hoped to show that the temperatures near the stagnation point are independent of the curvilinear coordinate x.

This second fin design, designated type "B", was fabricated in a similar manner to the type "A" fin, the only difference being that instead of a 45° hole being drilled, a vertical hole* 0.125 inches in diameter was drilled 0.20 inches in from the fin root tip along the fin center line. A wide slitting saw was then used to cut along the fin center line from the root tip as far as the vertical hole. Installation of the Chromel-Alumel thermocouples was effected in the same manner as for the type "A" fin, the finishing operations being identical. The final fin blade substructure is shown in figure 2.2.1 and 2.2.2.

* Normal to fin center line 0.20 inches in from fin root tip.

The experiment was mounted on the Black Brant IV-08 igniter housing as shown in figure 2.1.5 and fired from Fort Churchill Rocket Range, Manitoba, just six hours after launch of Black Brant IV-07.

Comparison of experimental results, and the theoretical analysis, are given in subsection 4.2.

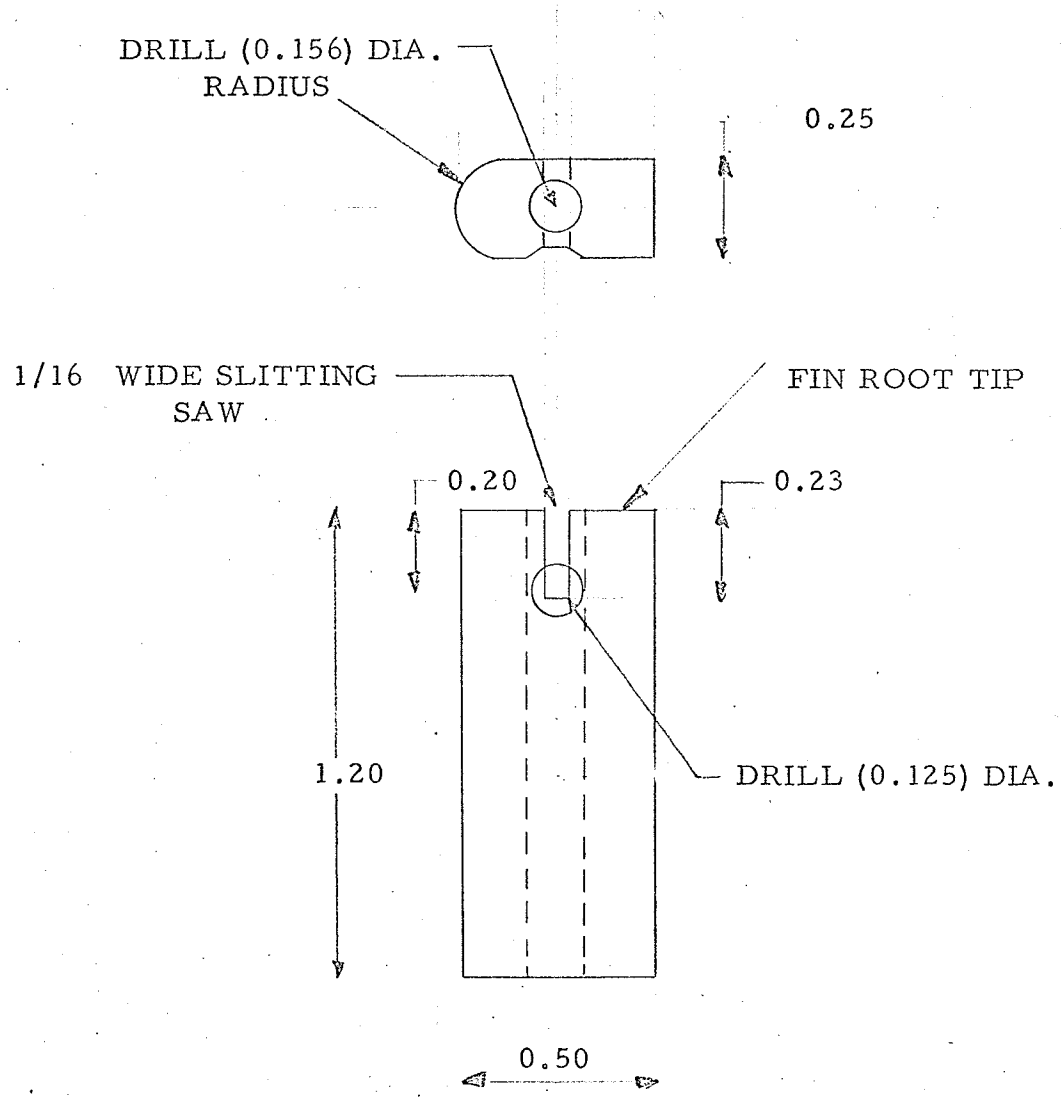

figure 2.2.1

SECTION AND PLAN VIEW

TYPE B FIN

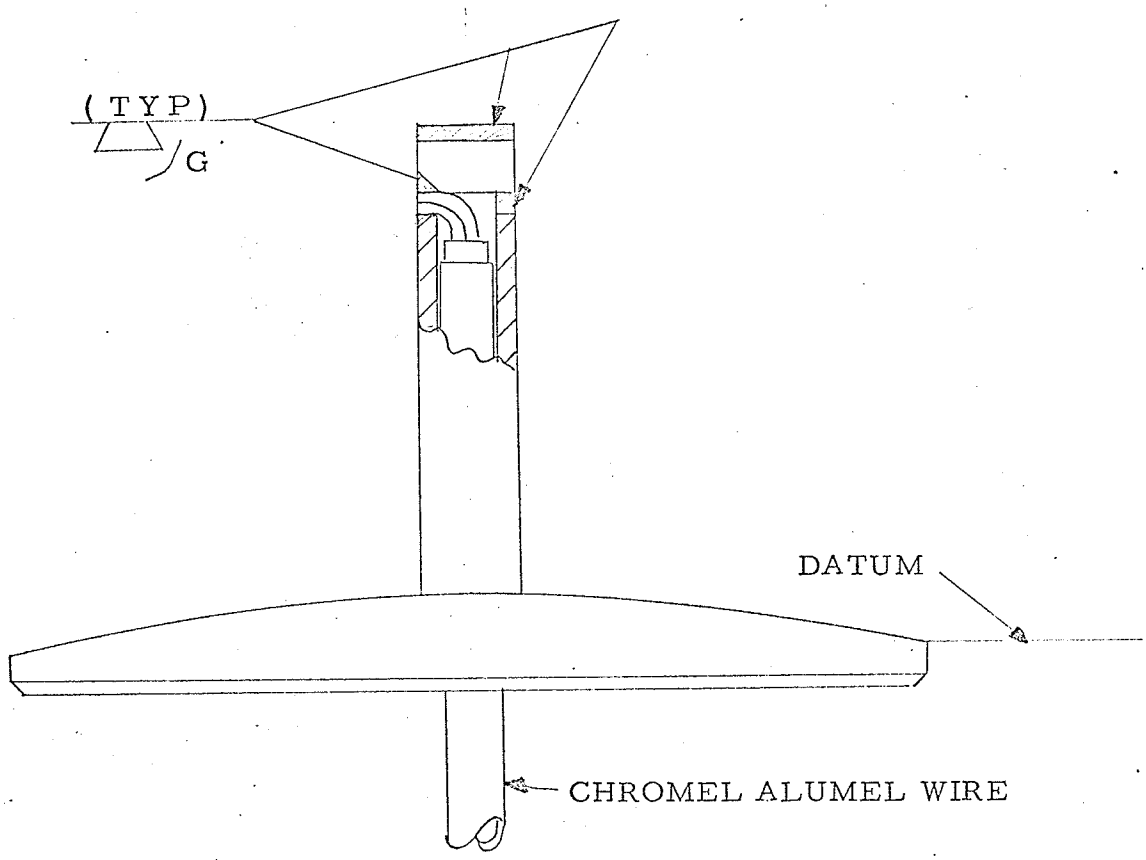

SIDE VIEW TYPE B FIN

figure 2.2.2

2.3 ABLATIVE PANEL EXPERIMENT

The design of the second phase of the experimental work was dictated in part by the results of the fin stagnation and center line experiments. It was thought that in the fin experiments that a combination of the high aerodynamic shear forces and heat transfer processes in the boundary layer, separated the Insulcork from the fin substructure prematurely in the initial stages of the flight. Therefore, in the second phase, to protect both the Insulcork and Avcoat from the bulk of the aerodynamic shear forces, ablative panels were constructed to the dimensions shown in figure 2.3.1.

The base and upper template of the ablative panel holders were made from 0.043 inch and 0.050 inch thick MIL-S-6721 T.I. stainless steel sheet, respectively. The base and template were then radiused to 8.60 inches which was the local radius of the Black Brant VA nose cone at Station 76 inches from the nose tip. The template was spotwelded to the base and 0.1695 inch diameter holes drilled and countersunk to 0.335 inch in diameter to accept ANS07C832-14 screws for installation to the vehicle nose-cone. Finally the leading edge was champfered to 30° to eliminate flow separation and reduce severe stagnation point heating.

Four such holders were made, two containing Insulcork 2275,

0.050 inch thick ablative material recessed into the template, and two containing 0.050 inch thick Avcoat sheet. These panels were then mounted on a Black Brant VA cone, the two Insulcork panels at 200° and 78° and the two Avcoat panels at 168° and 47° on the vehicle nose cone circumference.

The four panels were to be flown without telemetry on a Black Brant VA vehicle with a recoverable nose cone. On recovery, the ablative panels were to be examined to ascertain the depth of thermal degradation. The average thicknesses of material degraded were then to be compared with the thermal degradation values obtained from the theoretical analysis.

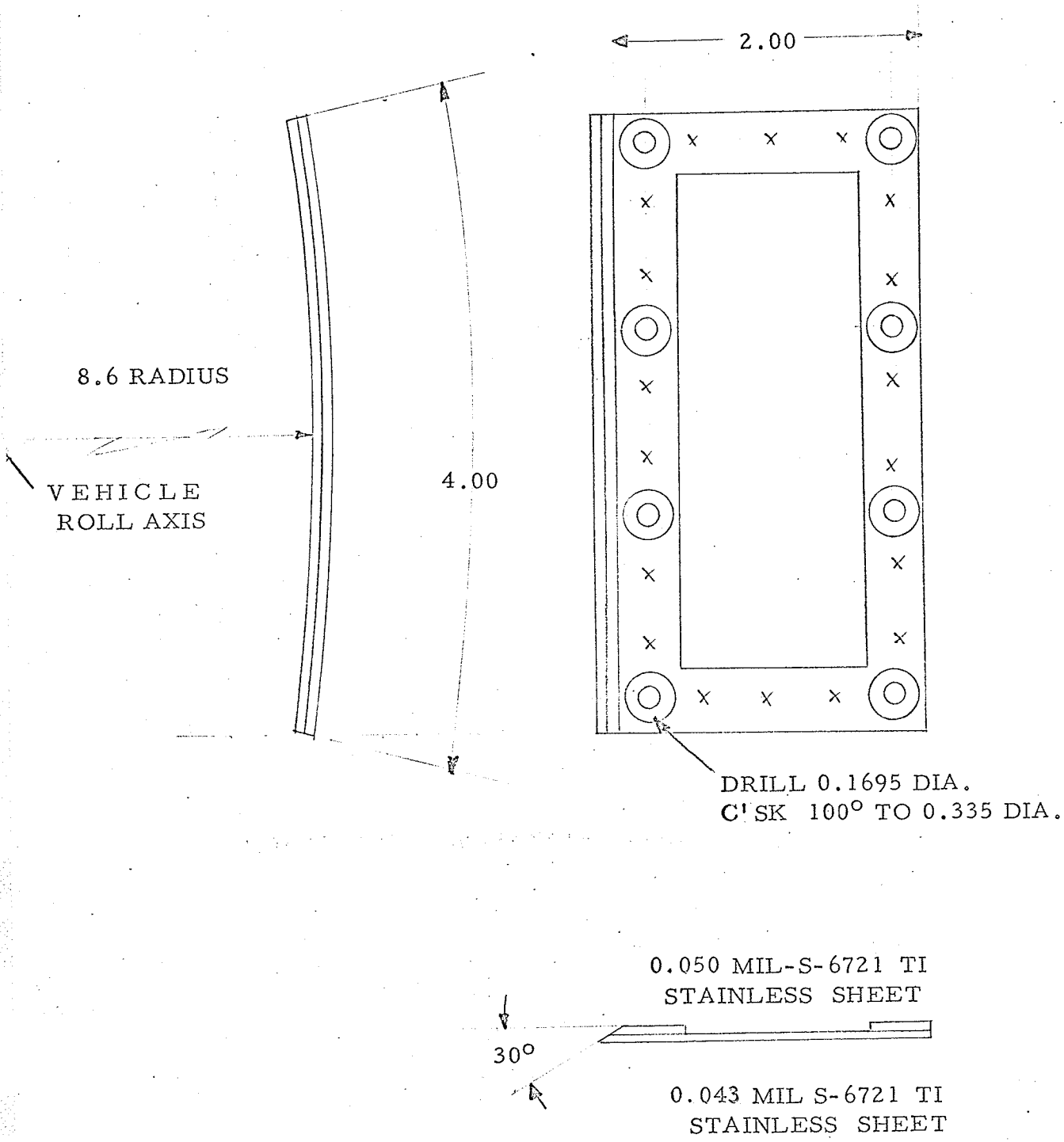

figure 2.3.1

SPECIMEN HOLDER

2.4 FIN PLANFORM EXPERIMENT

In view of the successes of the first two experiments, a third was devised to illustrate how the theoretical analysis could be used in a real design case, and at the same time, obtain experimental information of a practical nature.

The need arose to extend the flight envelope environment of the Black Brant VA vehicle. This involved extensive redesign of the Avcoat fin insulation, to ensure adequate thermal protection from anticipated higher heating rates. The computer program indicated that the fin insulation be increased in thickness from 0.060 inches to 0.09 inches for adequate thermal protection. Based on the computer results, fins were made with the increased insulation thickness, with the intention of firing them on the final Black Brant VA-AFF-119/120 development flights.

It was decided to embed thermocouples at the fin Avcoat-metal interface in several identical locations on each side of the fin, with the following objectives in mind. To obtain a temperature map over the fin platform area; to indicate where thermal insulation was most needed; to determine whether greater heating rates are obtained on the one side of the fin which rotates in the direction of the rolling vehicle; and lastly, to analyse the experimental results using the ablative theory.

It was decided not to fly any more Insulcork experiments in view of the results of the fin stagnation and center line experiments. The general layout of the fin planform experiment is shown in figure 2.4.1. Five GG-20-CT Chromel-Alumel thermocouples were installed at the fin Avcoat metal interface and the thermocouple leads gathered to a common point at the fin base. Because of the cost, and difficulty of installing telemetry in the vehicle aft end, the thermocouple leads were run up the whole length of the motor case to the forward end igniter housing joint, where they were connected to the vehicle telemetry system, similar to that described in experiments 2.1 and 2.2. The thermocouple leads on the motor case were protected from the high speed boundary layer shear forces by a stainless steel channel bonded to the motor case with Armstrong J.E. 1156-E-30 epoxy bonding material, as shown in figures 2.4.1 and 2.4.2.

It was imperative that for complete success of the experiment the stainless steel protective trough would remain fastened to the motor case during flight. To ensure complete telemetry results, a separate experiment was made to test the bonding of the stainless steel trough to the motor case, but this will not be described here as details are available in reference 20.

A detailed layout of the thermocouple locations is shown in figure 2.4.1. In all, there were ten thermocouples, five situated on each side of the fin in mirror locations.

To install the thermocouples, channels were gouged in the 0.090 inch Avcoat sheet, where the thermocouple wires are located in figure 2.4.1. Figures 2.4.3 and 2.4.4 show the installation of the thermocouples at the Avcoat-metal interface. Ideally, the thermocouples should be welded flush into the aluminium metal substructure, but this was not practical since it would have entailed weakening of the fin honeycomb sandwich substructure. Instead, the thermocouple ends were wrapped flat as shown in figure 2.4.3 and silver soldered as dimensioned. A 0.125 inch diameter self tapping screw fastened the thermocouple head to the aluminium face. The thermocouple heads were 0.060 inches thick when screwed to the fin metal face. After installation of the thermocouples, the troughs were filled in with liquid Avcoat and allowed to cure, then the fin surfaces were finished flush to 0.090 inches in thickness.

The result of installing the thermocouples in this manner will be

that the experimental temperatures recorded will be between that of the back face of the Avcoat and that of the aluminium surface and not the Avcoat-aluminium interface as would be ideally desired. It is hoped in the theoretical analysis, to indicate therefore, only the general transient temperature trends.

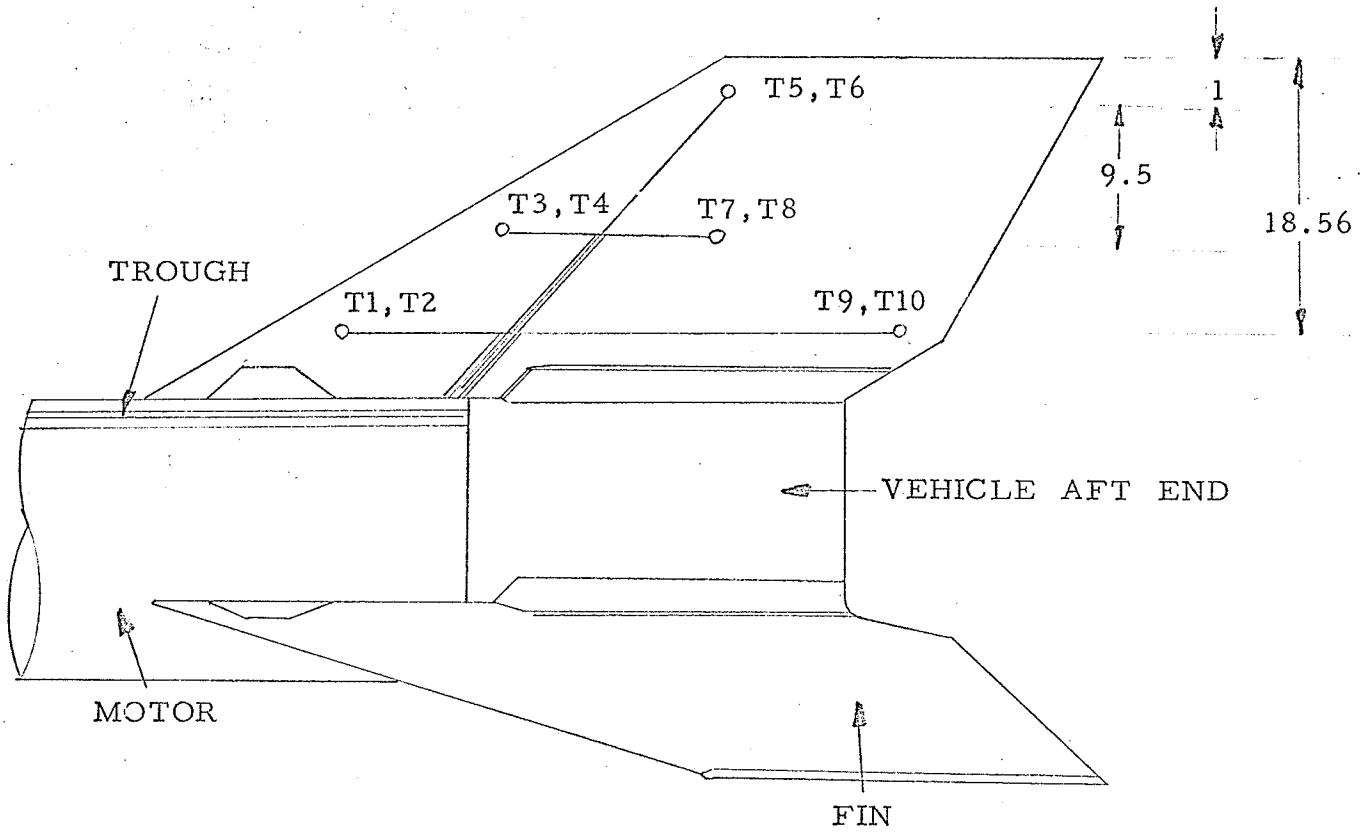
T5,T6
1
9.5
18.56
T3,T4
T7,T8
TROUGH
T1,T2
T9,T10
VEHICLE AFT END
MOTOR
FIN

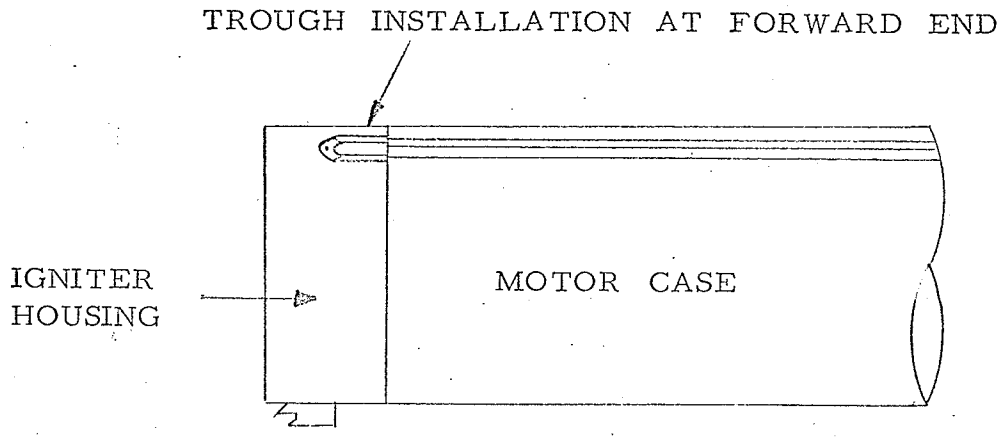
TROUGH INSTALLATION AT FORWARD END
IGNITER
HOUSING
MOTOR CASE

figure 2.4.1

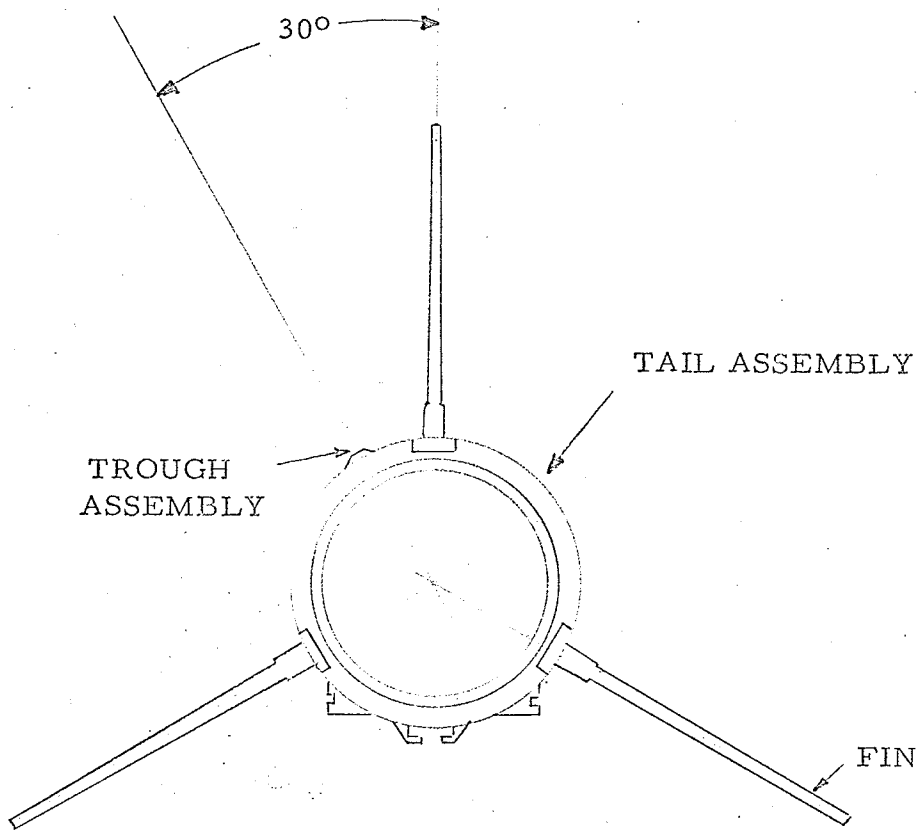

figure 2.4.2

VIEW ALONG VEHICLE ROLL AXIS

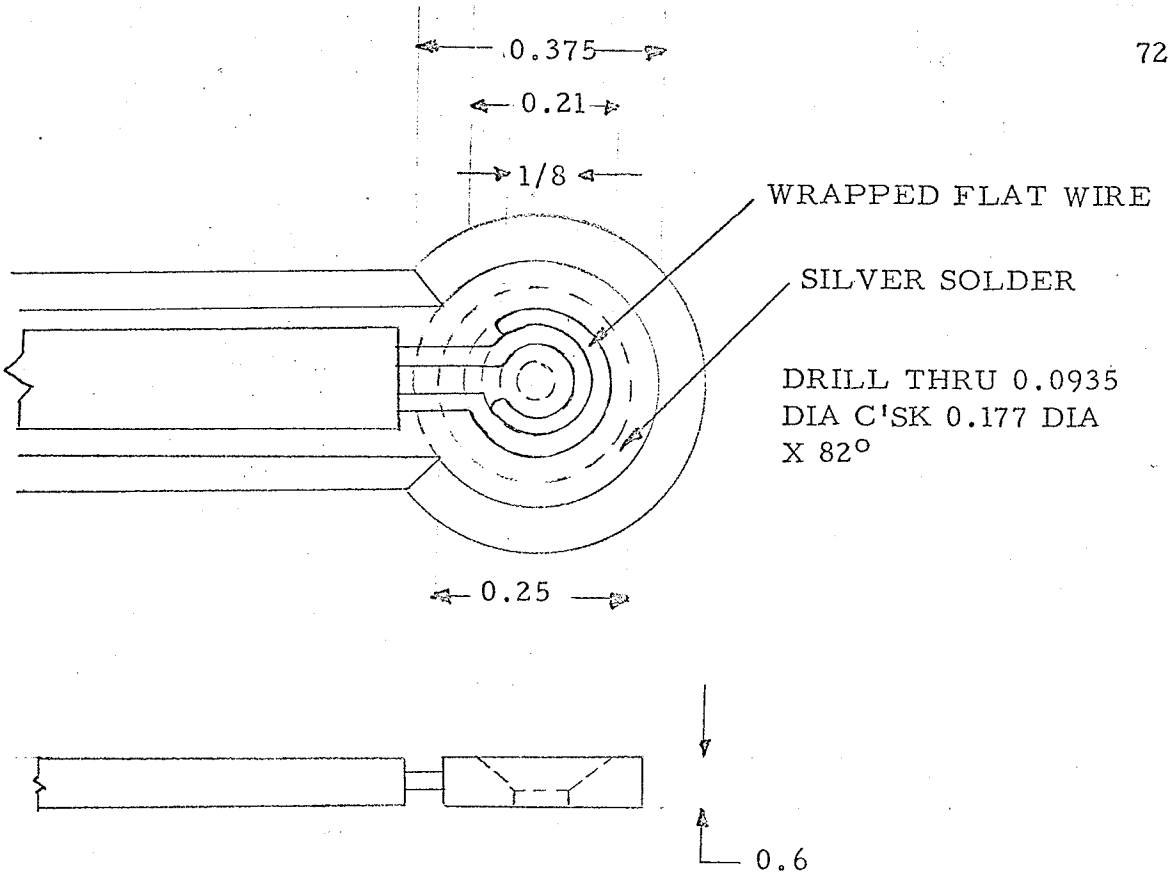

PLAN OF THERMOCOUPLE

figure 2.4.3

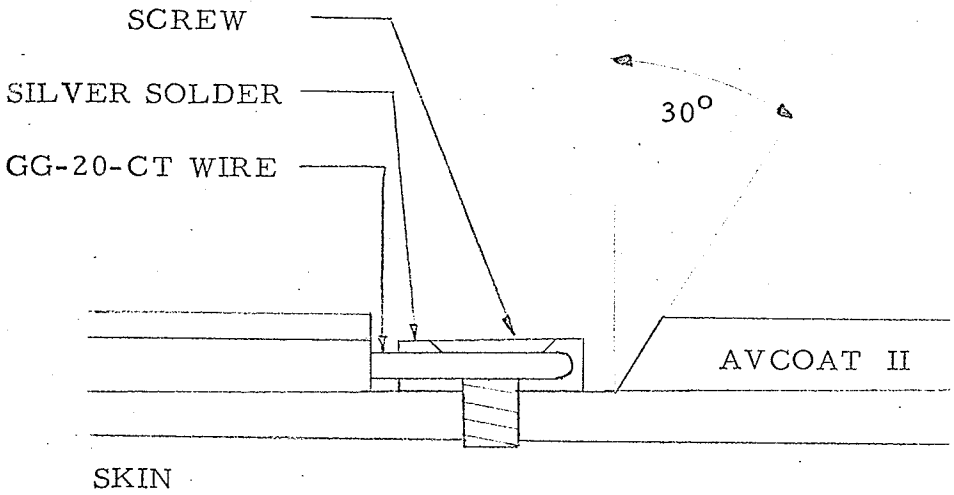

SECTION VIEW OF THERMOCOUPLE INSTALLATION

figure 2.4.4

COMPUTER PROGRAMS

3.0 COMPUTER PROGRAMS

Initially to reduce the amount of computational work involved in the theoretical analysis, a universal computer program was envisaged which would handle the whole of the analysis for many types of body geometries and conditions.

Unfortunately this attractive idea proved impractical due to one main reason - cost. Because of the diversification of problems, a large part of such a program would remain redundant, increasing computational time and absorbing unecessarily large amounts of core storage space.

It was therefore decided to write two programs which could be used alone, or in conjunction after some suitable program "tailoring".

A third program was adapted from the I.B.M. program library to reduce the amount of work involved in computer inputs to the two main programs, and reduce their complexity.

A description of these programs, their limitations and usefulness, will be given in the following sections.

3.1 STAGNATION POINT HEAT TRANSFER COMPUTER PROGRAM

This program is the simplest of the three programs to be described. It was written to be used alone, or in conjunction with the Ablative Heat Transfer Program described in the next section.

Basically this computer program is a programming of the two dimensional stagnation point heat transfer theory contained in section 1.2 and gives the solution to the first order, first degree, non linear differential equation 1.2.27 written as

$$q = \Gamma \frac{dT_w}{dt} = 0.57 Pr^{-0.6} C_p \left(\beta \mu_\infty \rho_\infty\right)^{1/2} \left(T_{aw} - T_w\right) - \sigma \epsilon T_w^4 \qquad 3.1.1$$

That is it will give the transient stagnation heat input q or stagnation wall temperature T_w, as a function of vehicle flight time.

Initially, details of the vehicle performance, and ambient atmosphere conditions are programmed into the computer in the form of polynomial coefficients, along with details of the experiment geometry. The computer then proceeds to evaluate the variable coefficients in equation 3.1.1, and then solves the equation using the second order Runge Kutte method of numerical integration, to give the temperature of the stagnation point as a function of time.

The limitations of the program are those of the theory described

in 1.2, these are that the program should only be used to obtain theoretical results in the continuum flight regime, for supersonic and near hypersonic flow conditions. The program however, is more flexible than the two-dimensional theory in section 1.2 since it can handle three dimensional problems by simply inserting $0.76Pr^{-0.6}$, in place of $0.57Pr^{-0.6}$ in equation 3.1.1. It can also be used for swept two dimensional geometries (such as a swept rocket fin) by insertion of a reduction factor $F(\Lambda, M)$ in equation 3.1.1 to give the form

$$\Gamma \frac{dT_w}{dt} = 0.57 Pr^{-0.6} C_p \; F(\Lambda, M) \left(\beta \mu_\infty \rho_\infty\right)^{1/2} (T_{aw} - T_w) - \sigma \epsilon T_w^4 \qquad 3.1.2$$

Although the program will not be used in the two latter forms, the opportunity was taken to reveal its flexibility.

The program was written in Fortran IV language for an I.B.M. 360 computer. A program print-out and symbol listing follows.

STAGNATION POINT HEAT TRANSFER PROGRAM

```
      DOUBLE PRECISION A(7),B(7),C(7),D(7),U(7),Y(7),Z(7),YY(7),ZZ(7),AA
     1 (7),BB(7)
      DOUBLE PRECISION VY,DA,DAL,D2,DS
      WRITE(3,100)
  100 FORMAT(1H1,41HFIN STAGNATION WALL TEMPERATURE PROGRAM)
      WRITE(3,101)
  101 FORMAT(1H1,110H          TIME            MACH NO.          DENSITY
     1   VELOCITY        AMB.TEMP        WALL TEMP        ADIAB.TEMP)
      READ(1,1) Y
      READ(1,1) Z
      READ(1,1) YY
      READ(1,1) ZZ
      READ(1,1) AA
      READ(1,1) BB
      READ(1,1) A
      READ(1,1) B
      READ(1,1) C
      READ(1,1) D
      READ(1,1) U
      READ(1,2) TW,TBO,T,H
      READ(1,2) S,X,DD,TL,AAAA
    2 FORMAT(6F13.8)
    1 FORMAT(5F16.8)
    7 IF(T-TBO)11,11,12
   11 EM=.0
      V=.0
      T1=T
```

```
      DO 104 N=1,7
      VEL=Y(N)*T1**(7-N)
      FMACH=Z(N)*T1**(7-N)
      V=V&VEL
104   EM=EM&FMACH
      GO TO 14
 12   EM=.0
      V=.0
      T1=T
      DO 105 N=1,7
      VEL=YY(N)*T1**(7-N)
      FMACH=ZZ(N)*T1**(7-N)
      V=V&VEL
105   EM=EM&FMACH
 14   DA=.0
      TA=.0
      DO 106 N=1,7
      DAL=AA(N)*T1**(7-N)
      TAL=BB(N)*T1**(7-N)
      DA=DA&DAL
106   TA=TA&TAL
      DA=DA/10000.
      D06N=1,2
      VY=3.73E-7*(TW/519.)**.5*(1.&.505*(TW/519.))/(1.505)
      TAW=TA*(1.&.17*EM**2)
      IF(EM-1.)20,20,21
 20   EM2=EM
      D2=DA
      GO TO 50
```

```
 21  EM2=((1.&.2*EM**2)/(1.4*EM**2-.2)**.5
     D2=DA*(((1.&1.4*EM**2)*(1.&.2*EM2**2))/((1.&1.4*EM2**2)*(1.&.2*EM*
    1 *2)))
 50  DS=D2*(1.&.2*EM2**2)**2.5
     TR=TW/100.
     P=.0
     SG=.0
     GF=.0
     F=.0
     VGF=.0
     DO 103 N=1,7
     PL=A(N)*TR**(7-N)
     SGL=B(N)*TR**(7-N)
     GFL=C(N)*TR**(7-N)
     FL=D(N)*EM**(7-N)
     VGFL=U(N)*EM**(7-N)
     P=P&PL
     SG=SG&SGL
     GF=GF&GFL
     F=F&FL
103  VGF=VGF&VGFL
     G=S*X*GF
     VG=(V/DD)*VGF
     DIFF=(AAAA*P**(-.6)*32.2*SG*F)*SQRT(VG*DS*VY)*(TAW-TW)/G-4.3E-13*T
    1 W**4/G
     GO TO (4,5),N
  4  AKI=H*DIFF
     TWO=TW
     TW=TWO&AKI
```

```
 6  CONTINUE
 5  AK2=H*DIFF
    TW=TWO&(AKI&AK2)*.5
    WRITE(3,10) T,EM,DA,V,TA,TW,TAW
    T=T&H
10  FORMAT (7F16.6)
    IF(T-TL)7,7,8
 8  STOP
    END
```

FORTRAN SYMBOLS	MEANING
SG	Specific heat of air at constant pressure
GF	Specific heat of skin
G	Heat absorption capacity of skin
EM2	Local Mach Number just outside boundary layer
EM	Free stream Mach Number
P	Prandtl Number
TAW	Adiabatic Wall Temperature
TW	Wall Temperature
X	Thickness of skin
T	Total Time
H	Time Interval
V	Free stream velocity
S	Specific weight of skin material
VG	Stagnation velocity gradient
D	Diameter
TL	Total Time Limit
TA	Ambient Temperature
DA	Ambient Density
DIFF	dT_W/dt
VY	Local free stream viscosity
F	Fin Sweep-back Factor

FORTRAN SYMBOLS	MEANING
DS	Stagnation Density
D2	Local free stream density
AP, BP, CP	Prandtl number Polynomial Coefficients
AGF, BGF	Polynomial Coefficients of specific heat of skin material
AG, BG, CG	Polynomial Coefficients of specific heat of air
AF, RF	Polynomial Coefficients of Sweep-back factor
AV, RV	Polynomial Coefficients of $\beta D/V_\infty$

3.2 ABLATION HEAT TRANSFER COMPUTER PROGRAM

The ablation heat transfer program is by far the most sophisticated and complex computer program in this section, incorporating theory from sections 1.1, 1.2, 1.3, 1.4 and 1.5. It is universal in the sense that it can do the job of the first two programs in 3.1 and 3.2 as well as the ablation problem, and finite difference methods for prediction of temperature distributions through materials. For instance, if the program is used to solve a stagnation problem, the stagnation heat input from 3.1 can be coupled with the ablation heat transfer program, similarly if a non-stagnation point is analysed a non-stagnation point heat input is used with the ablation heat transfer program.

In the form presented in this section the program is set up for a non-stagnation point problem. In the operation of the program, information on vehicle performance, ambient air conditions, and experiment geometry are fed into the computer, which then computes the free stream conditions and type of air flow, laminar or turbulent. It then computes the skin friction coefficient, and hence the heat transfer coefficient, to obtain a heat input to the body, by the Runge-Kutte numerical integration method. If the material is not at the ablation temperature, it proceeds with the finite difference

method to determine the temperature through the material or composite materials. If the surface reaches its ablation temperature the program switches to the ablation procession - finite difference coupling routine, to predict the temperature distribution through composite materials.

This program was used to analyse the fin-centre line, panel, and fin plan form experiments, in 2.2, 2.3 and 2.4 respectively. Its limitations are of course, those of the theory as cited in section 1.1, 1.2. 1.3, 1.4 and 1.5. The advantage of this program is that it is capable of yielding far more information than the first two programs, and can do more varied and complex problems.

ABLATION HEAT TRANSFER COMPUTER PROGRAM

```
      DISK OPERATING SYSTEM/360  FORTRAN   360N-FO-451  21

      DIMENSION T(4),TT(4),DNB(4),SD(4),SQ(4),CQ(4),R(4),RR(4)
      DOUBLE PRECISION A(7),B(7),C(7),D(7),Q(7),S(7),U(7),Y(7),ZZ(7),AA(
     17),BB(7),CC(7)
      DOUBLE PRECISION REFF,VISF,DE,DEL,DF
      WRITE(3,1111)
 1111 FORMAT(1H1/1HO,106H          TIME          TAW        T(1)          T(2)
     1         T(3)          INT.FACE     TT(2)         TT(3)       TT(4))
      WRITE(3,2222)
 2222 FORMAT(89H             TF             VF                DF
     1 TA                   DE             V)
      WRITE(3,2121)
 2121 FORMAT(60H       CFFL       CFFT          TBL            TB
     1  AHH)
      WRITE(3,1212)
 1212 FORMAT(92H           REFF                ST1                      ST2
     1              ST3                    Q1)
      READ(1,82) A
      READ(1,82) B
      READ(1,82) C
      READ(1,82) D
      READ(1,82) Q
      READ(1,82) S
      READ(1,82) U
      READ(1,82) Y
      READ(1,82) ZZ
```

```
      READ(1,82) AA
      READ(1,82) BB
      READ(1,82) CC
      READ(1,81) AL,DX1,DX2,T1,RHO2
      READ(1,12) TIN,AHC,TIP,TAB,M1,N1
      READ(1,81) TRIAL,TBO,H,ANN
      DO 56 I=1,M1
 56   READ(1,81) T(I)
      DO 57 I=1,N1
 57   READ(1,81) TT(I)
 81   FORMAT(6F13.7)
 82   FORMAT (5F16.8)
 12   FORMAT(4F13.7,2I3)
 36   IF(T1-TBO)50,50,51
 50   EM=0
      V=0
      DO 101 N=1,7
      VEL=A(N)*T1**(7-N)
      FMACH=B(N)*T1**(7-N)
      V=V&VEL
101   EM=EM&FMACH
      GO TO 54
 51   V=.0
      EM=.0
      DO 102 N=1,7
      VEL=C(N)*T1**(7-N)
      FMACH=D(N)*T1**(7-N)
      V=V&VEL
102   EM=EM&FMACH
```

```
   54  DE=.0
       TA=.0
       DO 103 N=1,7
       DEL=S(N)*T1**(7-N)
       TAL=Q(N)*T1**(7-N)
       DE=DEL&DE
  103  TA=TA&TAL
       DE=DE/10000.
       IF(EM-1.)43,43,44
   43  VF=V
       DF=DE
       TF=TA
       GO TO 45
   44  PR=.0
       DO 1007 N=1,7
 1007  PR=BB(N)*EM**(7-N)&PR
       VR=(1.-(PR**(.286)-1.)/(.2*EM**2.))**.5
       TR=1.&.2*EM**2.*(1.-VR**2.)
       DR=TR**2.5
       VF=V*VR
       TF=TA*TR
       DF=DE*DR
   45  VISF=3.73E-7*(TF/519.)**.5*(1.&.505*(TF/519.))/1.505
       TAW=TF*(1.&.17*EM**2.)
       M=M1
       AM=M&2
       T(M&1)=TT(1)
```

```
      DO 9 I=1,N1
      R(I)=T(I)/100.
    9 RR(I)=TT(I)/100.
      P=.0
      DO 63 N=1,7
   63 P=CC(N)*R(1)**(7-N)&P
      DO 61 J=1,N1
      SD(J)=U(1)*R(J)**6.&U(2)*R(J)**5.&U(3)*R(J)**4.&U(4)*R(J)**3.&U(5)
     1 *R(J)**2.&U(6)*R(J)&U(7)
      DNB(J)=Y(1)*R(J)**6.&Y(2)*R(J)**5.&Y(3)*R(J)**4.&Y(4)*R(J)**3.&Y(5
     1)*R(J)**2.&Y(6)*R(J)&Y(7)
      SQ(J)=ZZ(1)*RR(J)**6.&ZZ(2)*RR(J)**4.&ZZ(4)*RR(J)*
     1*3.&ZZ(5)*RR(J)**2.&ZZ(6)*RR(J)&ZZ(7)
   61 CQ(J)=AA(1)*RR(J)**6.&AA(2)*RR(J)**5.&AA(3)*RR(J)**4.&AA(4)*RR(J)*
     1*3.&AA(5)*RR(J)**2.&AA(6)*RR(J)&AA(7)
      REFF=DF*VF*AL/VISF
      DT1=H
   24 ST1=2.*DNB(1)*DT1/(RHO1*SD(1)*DX1**2.)
      ST2-2.*DNB(1)*DT1/((DX1*RHO1*SD(1)&DX2*RHO2*SQ(1))*DX1)&2.*CQ(1)*D
     1T1/((DX1*RHO1*SD(1)&DX2*RHO2*SQ(1))*DX2)
      ST3=2.*CQ(1)*DT1/(RHO2*SQ(1)*DX2**2.(&2.*DT1**2.*AHC/(RHO2*SQ(1)*D
     1X2)
      IF (ST1-1.)25,25,26
   26 DT1=DT1-0.01
      GO TO 24
   25 IF(ST2-1.)27,27,28
   28 DT1=DT1-.01
      GO TO 24
```

```
   27  IF(ST3-1.)29,29,32
   32  DT1=DT1-.01
       GO TO 24
   29  H=DT1
       CONTINUE
       IF(AL-.33)1122,1122,1133
 1122  IF(REFF-5.E&5)1,1,2
 1133  IF(REFF-7.E&6)1,1,2
    1  CFFL=.664/(REFF)**.5
       AHH=.25*P**(-.166)*DF*CFFL*VF**3./(778.*(TAW-TF))
       GO TO 66
    2  TB=.242*ATAN((TAW/TF-1.)**.5)/(TAW/TF-1.)**.5
       CFFT=.002
       L=1
   18  TBL=CFFT**.5*(ALOG10(CFFT)&.41-.76*ALOG10(TAW/TF)&DLOG10(REFF))
       IF(ABS(TB-TBL)-.002)49,49,8
    8  IF(L-5)10,10,49
   10  IF(TBL-TB)13,13,14
   13  GO TO(15,16,17,17,17),L
   15  CFFT=CFFT&.001
       L=L&1
       GO TO 18
   16  CFFT=CFFT&.0005
       L=L&1
       GO TO 18
   17  CFFT=CFFT&.0001
       L=L&1
       GO TO 18
   14  GO TO (19,20,21,21,21),L
   19  CFFT=CFFT-.001
       L=L&1
```

```
      GO TO 18
   20 CFFT=CFFT-.0005
      L=L&1
      GO TO 18
   21 CFFT=CFFT-.0001
      L=L&1
      GO TO 18
   49 AHH=.3*P**.333*CFFT*DF*VF**3./(778.*(TAW-TF))
   66 Q1=AHH*(TAW-T(1))-4.3E-13*(T(1)**4.-TF**4.)
      T(1)=T(1)*(1.-2.*DNB(1)*H/(RHO1*SD(1)*DX1**2.))&T(2)*2.*DNB(1)*H/(
     1RH01*SD(1)*DX1**2.)&Q1*2.*H/(RHO1*SD(1)*DX1)
 1117 FORMAT(5F20.8)
   11 FORMAT(5F13.8)
      M=M1
      N=N1
      I=2
      IF(TAB-T(1))72,73,73
   72 IF(TIN-1.)58,59,58
   59 J=2
      GO TO 60
   58 J=TIN
      IF (J-(M&2))60,68,68
   60 HE=SD(J)*(TAB-T(J))&1000.&.155*(TAW-TAB)
      XX=TIP
      XX=Q1*H/(HE*RHO1)&XX
      DD=XX/DX1&1.
      ANN=1.
   85 IF(ANN-DD)83,83,84
   83 ANN=ANN&1.
      GO TO 85
```

```
 84   AM1=M
      WRITE(3,76) Q1,XX,DD,ANN
 76   FORMAT(7F16.8)
      IF(AM-ANN)86,86,88
 86   DX1=DX2
      RHO1=RHO2
      DO 1008 N=1,7
      U(N)=ZZ(N)
1008  Y(N)=AA(N)
      T(1)=TAB
      ANN=AM&1
 68   TT(1)=T(1)
      GO TO 108
 88   XX1=XX-(ANN-2.)*DX1
      NN=ANN
      IF(NN-(M&1))1001,1002,1001
1002  NN=M
1001  XB=DNB(NN)*H/(RHO1*SD(NN)*DX1*(DX1-XX1))&DNB(NN)*H/(RHO1*SD(NN)*DX
     11*DX1)
      IF(1.-XB)94,96,96
 64   IF(ANN-AM1)97,97,98
 98   DO 92I=1,M
 92   T(I)=TAB
      GO TO 108
 97   NNN=ANN&1.
      NN=ANN-1.
      DO 891=1,NN
 89   T(I)=TAB
      IF(NNN-(M&1))106,107,106
107   NNN=M
```

```
 106 TL1=1.-DNB(NNN)*H/(RHO1*SD(NNN)*DX1*(2.*DX1-XX1))-DNB(NNN)*H/(RHO1
    1*SD(NNN)*DX1*DX1)
     TL2=DNB(NNN)*H/(RHO1*SD(NNN)*DX1*(2.*DX1-XX1))
     TL3=DNB(NNN)*H/(RHO1*SD(NNN)*DX1**2)
     NNN=ANN&1.
     IF(NNN-(M&1))1003,1004,1003
1003 T(NNN)=T(NNN)*TL1&TAB*TL2&T(NNN&1)*TL3
     NN=NNN
     TO TO 112
1004 T(NNN)=T(NNN)*TL1&TAB*TL2&TT(2)*TL3
     TT(1)=T(NNN)
     TO TO 108
  96 NN=ANN
     MN=NN-1
     DO 79I=1,MN
  79 T(I)=TAB
     J=NN
     I=NN&1
     IF(NN-(M&1))111,71,111
  71 DX1=DX1-XX1
     TT(1)=TT(1)*(1.-(2.*DNB(M)*H/DX1&2.*CQ(1)*H/DX2)/(RHO1*SD(M)*DX1&R
    1HO2*SQ(1)*DX2))&T(M)/DX1*(2.*DNB(M)*H/(RHO1*SD(M)*DX1&RHO2*SQ(1)*D
    2X2))&TT(2)/DX2*2.*CQ(1)*H/(RHO1*SD(M)*DX1&RHO2*SQ(1)*DX2
     DX1=DX1&XX1
     GO TO 108
 111 T(NN)=T(NN)*(1.=DNB(NN)*H/(RHO1*SD(NN)*DX1**2)-DNB(J)*H/(DX1*DX1-
    1XX1)*RHO1*SD(NN)))&DNB(NN)*H*TAB/(RHO1*DX1*(DX1-XX1)*SD(NN))&T(NN&
    21)*DNB(NN)*H/(DX1**2*SD(NN)*RHO1)
 112 I=NN&1
     IF(NN-M)73,104,73
```

```
 73 DO 30J=I,M
 30 T(J)=T(J)*(1.-2.*DNB(J)*H/(RHO1*SD(J)*DX1**2))&DNB(J)*H*(T(J-1)&T(
   1J&1))/(RHO1*SD(J)*DX1**2)
104 TT(1)=TT(1)*(1.-(2.*DNB(M)*H/DX1&2.*CQ(1)*H/DX2)/(RHO1*SD(M)*DX1&R
   1HO2*SQ(1)*DX2))&T(M)DX1*(2.*DNB(M)*H/(RHO1*SD(M)*DX1&RHO2*SQ(1)*D
   2X2))&TT(2)/DX2*2.*CQ(1)*H/(RHO1*SD(M)*DX1&RHO2*SQ(1)*DX2)
108 J=2
 91 NN1=N-1
    DO 31  I=J,NN1
 31 TT(I)=TT(I)*(1.-2.*CQ(I)*H/(RHO2*SQ(I)*DX2**2))&CQ(I)*H*(TT(I-1)&T
   1T(I&1))/(RHO2*SQ(I)*DX2**2)
    NN=N
    TT(N)=TT(N)*(1.-2.*CQ(N)*H/(RHO2*SQ(N)*DX2**2)-AHC*2.*H**2/(RHO2*S
   1Q(N)*DX2))&TT(NN-1_*2.*CQ(N)*H/(RHO2*SQ(N)*DX2**2)&TIN*AHC*2.*H**2
   2/(RHO2*SQ(N)*DX1)
    WRITE(3,77)  T1,TAW,(T(I),I=1,M),(TT(I),I=1,N)
    WRITE(3,76)TF,VF,DF,TA,DE,V
    WRITE(3,11)CFFL,CFFT,TBL,TB,AHH
    WRITE(3,1117) REFF,ST1,ST2,ST3,Q1
    WRITE(3,1117) PR,VR,TR,DR
 77 FORMAT(1HO,9(2X,F10.3)
    TIN=ANN
    TIP=XX
    TI=TI&H
    IF(T1-TRIAL)36,36,39
 39 STOP
    END
```

FORTRAN SYMBOLS	MEANING
V	Free stream velocity
VF	Local free stream velocity
EM	Free stream Mach number
T(I)	Temperature at any point of first material
TW	Wall temperature
TIN	Initial temperature
TT(I)	Temperature at any point of second material
TAB	Ablating temperature
TSC	Temperature of the back surface
PR	Pressure ratio
VR	Velocity ratio
TR	Temperature ratio
DR	Density ratio
TA	Ambient temperature
TI	Total time
H	Time interval
TBO	Time for burnout
DE	Ambient density
DF	Local free stream density
VISF	Local free stream viscosity

FORTRAN SYMBOLS	MEANING
P	Prandtl number
AHH	Film co-efficient on hot surface
AHC	Film co-efficient on cold surface
REFF	Local free stream Reynolds number
CFFL	Skin friction co-efficient (laminar flow)
CFFT	Skin friction co-efficient (turbulent flow)
TIP	Number of trials
TRIAL	Total time for trial
QH	Heat flux entering
QC	Heat flux leaving
Q1	Transient heat input
AL	Distance of body station from nose
DX1	Incremental distance in first phase
DX2	Incremental distance in second phase
M	Number of points considered in first phase
N	Number of points considered in second phase
RHO1	Density of material in first phase
RHO2	Density of material in second phase

3.3 POLYNOMIAL CURVE FIT PROGRAM

The Polynomial Curve Fit Program is an adaption from the I.B.M. program library and its purpose is to simplify the input data to the main programs - 3.1 and 3.2.

In essence, the program is a solution to a general class of problems arising in engineering, which consists of matching a set of data points to a known analytic function, and relies on the method of least squares.

The method of least squares consists of choosing a suitable polynomial to represent a set of data points, by comparing the data points with an assumed curve, and adjusting the curve until the sum of the squares of deviation from the curve is a minimum.

This can be illustrated mathematically by a practical example of fitting a curve to a collection of data points, say (M_i, t_i) representing Mach number versus time, which is used in both main programs.

The program would assume that this data can be fitted with a polynomial of the form

$$M = \sum_{r=0}^{m} a_r t^r \qquad 3.3.1$$

The deviation at the ith point would be

$$\sigma_i = M_i - M = M_i - \sum_{r=0}^{n} a_r t^r \qquad 3.3.2$$

The square of the deviation would then be

$$\sigma_i^2 = M_i^2 - 2M_i \sum_{r=0}^{n} a_r t^r + \left[\sum_{r=0}^{n} a_r t^r \right]^2 \qquad 3.3.3$$

and the sum of the squares of the deviation

$$\sum_{i=1}^{m} \sigma_i^2 = \sum_{i=1}^{m} M_i^2 - 2\sum_{i=1}^{m} \left\{ M_i \sum_{r=0}^{n} a_r t_i^r \right\} + \sum_{i=1}^{m} \left\{ \sum_{r=0}^{n} a_r t_i^r \right\}^2 \qquad 3.3.4$$

Where m>n and n is the number of data points to minimise the sum of least squares. The computer differentiates 3.3.4 to give

$$\frac{\partial \sum_{i=1}^{m} \sigma_i^2}{\partial a_k} = -2 \sum_{i=1}^{m} M_i t_i^k + 2 \sum_{r=0}^{n} a_r \sum_{i=1} t^{r+k} \qquad 3.3.5$$

As k takes values from 0 to n, $n+1$ equation are generated to give the so called normal equation for the coefficients a_k. The computer then computes the sums of the various combinations of the data points, to give the polynomial coefficients for a zero to sixth order curve.

POLYNOMIAL CURVE FIT COMPUTER PROGRAM

DISK OPERATING SYSTEM/360 FORTRAN

```
      CBA CURVE FITTER - A CONVERTED VERSION OF IBM PROGRAM LIBRARY
       NO. 1260 - 07.0 .027
      DOUBLE PRECISION XCURVE,YCURVE,XMN,XRA,A,ANS,T
      DIMENSION A(7,8)
      DIMENSION ANS(7)
      DIMENSION XCURVE(30),YCURVE(30),JPOINT(30),E(20)
      READ(1,446)ITIMES
  446 FORMAT(13)
      DO 69 ICYCLE=1,ITIMES
  666 JV = 8
      WRITE(3,978)
  978 FORMAT(1H1)
      READ(1,444)(E(LUCK),LUCK=1,20)
      WRITE(3,445)(E(LUCK),LUCK=1,20)
  445 FORMAT(1HO,20A3)
      READ(1,444)(E(LUCK),LUCK-1,20)
      WRITE(3,445)(E(LUCK),LUCK=1,20)
  444 FORMAT(20A3)
      READ(1,3)MIND,INC,MAXD,XMN,XRA
    3 FORMAT(313,2F16.8)
      ARX=1.0/XRA
      MAXI = MAXD&1
      IF(JV-MAXI)7,7,8
    7 MAXI=JV-1
    8 KMIN=MIND&1
```

```
      CLEAR TOTAL BOXES
      A(1,JV)=0.0
      D=0.0
      DO 9 J=2,MAXI
      A(J,JV)=0.0
      M=J-1
      DO 9 I=M,J
    9 A(I,J)=0.0
      READ DATA AND ACCUMULATE SUMS OF POWERS
      NEXT=1
   10 READ(1.11)XCURVE(NEXT),YCURVE(NEXT),JPOINT(NEXT)
   11 FORMAT(F16.8,F16.8,I1)
      IF(JPOINT(NEXT))16,12,16
   12 D=D&1.0
      S=(XCURVE(NEXT)-XMN)*ARX
      T=1.0
      K=1
      DO 15 J=2,MAXI
      M=J-1
      DO 15 I=M,J
      IF(K-MAXI)13,13,14
   13 A(K,JV)=A(K,JV)&T*YCURVE(NEXT)
      K=K&1
   14 T=T*S
   15 A(I,J)=A(I,J)&T
      NEXT=NEXT&1
      GO TO 10
   16 WRITE(3,300)MIND,MAXD,INC,D
  300 FORMAT(1HO,17HSOLVE FOR DEGREES,12,3H TO,12,3H BY, 12,4H FOR,F4.0,
```

```
    1 7H POINTS)
      READ(1,3)IDUMMY
      A(1,1)=D
      N=(MAXI-KMIN)/INC
      MAXD = N*INC&MIND
      MAXI=MAXD&1
      SPREAD TOTALS THROUGHOUT TOP HALF OF MATRIX
      M1=MAXI-2
      DO 20 I-KMIN,M1,INC
      DO 20 J=I,MAXI,INC
      IF(J-I-2)20,19,19
   19 L=I&J
      K=L/2
      L=L-K
      A(I,J)=A(K,L)
   20 CONTINUE
      SET UP TO SOLVE EQUATIONS
      DO 42 K=KMIN,MAXI,INC
      P=1.0/A(K,K)
      A(K,K)=A(K,JV)*P
      SOLVE FOR RESIDUALS
      DO 955 JACK=1,7
  955 ANS(JACK) = 0.0
      J=K-1
      WRITE(3,27)J
   27 FORMAT(1HO,8HDEGREE =,I2)
      SOLVE FOR COEFFICIENTS
      M1=K&INC
      M=MAXI-M1
      IF(M)30,28,28
   28 DO 29 J=M1,MAXI,INC
      A(J,K)=A(K,J)
   29 A(K,J)=A(K,J)*P
```

```
30 L=1
   N=KMIN
   T=1.0
   DO 41 I=1,MAXI
   IF(N-I)31,31,40
31 N=N&INC
   IF(I-K)33,37,32
32 M1=I
33 P=A(I,K)
   IF(M)36,34,34
34 DO 35 J=M1,MAXI,INC
35 A(I,J)=A(I,J)-A(K,J)*P
36 A(I,K)=A(I,JV)-A(K,K)*P
   GO TO(38,41),L
37 L=2
38 J=I-1
   R=A(I,K)*T
   ANS(I)=R
   WRITE(3,39)J,R
39 FORMAT(1H ,10X,12,F16.8)
40 T=T*ARX
41 CONTINUE
   WRITE(2,871)ANS(7),ANS(6),ANS(5),ANS(4),ANS(3)
   WRITE(2,871)ANS(2),ANS(1)
```

```
871 FORMAT(5F16.8)
 42 JV=K
    ARX=1.0
    KMIN=MIND&1
    DO 69 K=MIND,MAXD,INC
    WRITE(3,55)K
 55 FORMAT(1HO,15HEVALUATE DEGREE,12)
    WRITE(3,462)
462 FORMAT(1H ,18X,11HINDEP. VAR.,9X,6HACTUAL,10X6HFITTED,5X,6HPCTER.)
   1 )
    M=K&1
    R=0.0
    DO 69 N=1,NEXT
    IF(JPOINT(N)69,57,69
 57 S=(XCURVE(N)-XMN)*ARX
    T=0.0
    J=M
    DO 60 I=1,M
    T=T*S
    IF(M-I-J&1)60,58,60
 58 T=T&A(J,M)
    IF(J-KMIN)60,60,59
 59 J=J-INC
 60 CONTINUE
    R=YCURVE(N)-T
    PCTER=(T-YCURVE(N))/YCURVE(N)*100.
    WRITE(3,63)XCURVE(N),YCURVE(N),T,PCTER
 63 FORMAT(1H ,15X,3F16.8,F8.3)
 69 CONTINUE
    END
```

COMPARISON OF THEORETICAL ANALYSIS AND EXPERIMENTAL RESULTS

4.0 COMPARISON OF THEORETICAL ANALYSIS AND EXPERIMENTAL RESULTS

The following sections present a comparison of theoretical and experimental results obtained from the computer programs described in sections 3.1, 3.2, 3.3 and the experiments described in sections 2.1, 2.2, 2.3 and 2.4.

Because of the dearth of theoretical and experimental data, and the unsuitability of its original form, for inclusion directly into this thesis, the theoretical and experimental data has been reduced and presented in tabular and graphical form.

4.1 COMPARISON OF THEORETICAL ANALYSIS AND EXPERIMENTAL RESULTS FOR FIN STAGNATION EXPERIMENT

This section contains a comparison of the theoretical and experimental results obtained for the fin stagnation experiment described in section 2.1.

Table 4.1.1 shows the reduced telemetry and corresponding theoretical results using computer programs 3.1 in conjunction with 3.2 and 3.3 for the Avcoat covered fin as a function of flight time. These tabulated results have been plotted in figure 4.1.1 from which it can be seen immediately that the experimental and theoretical results are in excellent agreement.

The theory predicts a noticable rise in the Avcoat-metal interface temperature about one second before any rise is noted in the experimental results. Ablation is theoretically predicted at 12.7 seconds after launch, and at this time there is an apparent reduction in change of temperature with time in the experimental plot, indicating that the Avcoat has started to ablate, reducing the rate of stagnation point heating to the Avcoat surface. The experimental curve then flattens further, indicating reduction in stagnation point

heat transfer due to ablation and the first stage booster motor thrust tail off. The corresponding theoretical curve section also indicates ablation and motor thrust tail off but the effects are not so pronounced, this is partly due to the way in which the computer was programmed to facilitate the two stage Black Brant IV flight-07 flight parameters. This will be explained later. At approximately 18 seconds, stage separation occurs, and the first stage booster motor falls away. In reality, second stage motor ignition occurs a fraction of a second later, but this coast time was undetermined in the experiment. In the theoretical analysis, second stage motor ignition was assumed immediately on stage separation. After second stage ignition the theoretical and experimental curves are in almost exact agreement for the remainder of the theoretical analysis, both peaking at about 750°F at 30 seconds.

The flattening of the theoretical and experimental curves around 25 seconds continuing until 30 seconds is due to the second stage booster motor thrust tail off. Although experimental results were obtained for the remainder of the flight, the theoretical and experimental analysis is concluded at the end of the powered flight trajectory to avoid infringement of the theoretical limitations. At 30 seconds the theoretical solution begins to diverge from the

experimental results since the mean free path of the air is becoming of the order of the experiment dimensions, indicating the gradual change from continuum to slip flow.

In conclusion, it can be seen that agreement between theory and experiment are excellent in the continuum flow regime. It appears that the use of linear forward finite difference method, instead of radial finite difference method, is adequate enough in treating thin ablative coatings of Avcoat, as would be expected. One thing which was not anticipated when writing the computer program, was the increase in stagnation point heating due to the reduction in the radius of the fin cylindrical leading edge on ablation. In view of the present correlation, it can be concluded that the effect of a slight reduction in the fin leading edge radius is negligible. This can also be explained by the fact that the shock-boundary layer interaction parameter β, which contains the radius term, is constant for Mach numbers greater than 3. Staging effects in the computer solution are not as pronounced as in the experimental results due to the manner in which the vehicle Mach number and velocity polynomial coefficients were computed from the polynomial curve fit program. The curve fit program will only fit data for which the differential is wholly positive or wholly negative. In data obtained for these curves

from a two dimensional point mass trajectory, a point of inflexion occurs during the first stage booster tail off period. To avoid difficulty with the main program which will only accept two polynomial curve fits per parameter, the curves were averaged through the point of inflexion range so that their differentials were always positive.

Table 4.1.2 shows a comparison of the experimental and theoretical results for the Insulcork-metal interface temperature as a function of time. The results from this table are plotted in figure 4.1.2. It can be seen that the results for the Insulcork are quite different from those for the Avcoat. In fact, the change of temperature with time is more indicative of a metal response to a high flux than that for an ablative material. It is thought that at approximately 7 seconds the high aerodynamic shear forces in the stagnation boundary layer removed the Insulcork prematurely from the fin, exposing the metal fin semi-cylindrical leading edge to the stagnation point heat input. This was subsequently proved by the theoretical analysis. To analyse this problem, it was decided to use the stagnation point heat transfer program and start the computation from 7 seconds. The result of this is shown plotted against the experimental results in figure 4.1.2. In view of the excellent correlation, there can be no

doubt that the Insulcork was sheared from the fin surface by the high aerodynamic shear forces.

At 7 seconds the experimental and theoretical curves rise quite sharply until about 11 seconds where there is a marked flattening effect. This is thought to be due to the thrust tail off effects of the first stage booster since this begins to occur at the same time. The experimental results remain quite constant until second stage ignition, while the theoretical curve increases slightly, this is due to the polynomial curve fit coefficients used for the input data to the main program. After second stage ignition the curves agree well till about 26 seconds when the computer solution begins to diverge from the experimental results. The reason for this is that the effect of the cork separation drastically reduced the dimensions of experiment, resulting in the mean free path being of the order of the experiment dimension* earlier, than in the case of the Avcoat fin. It can be said again that in the continuum flow regime, correlation between theory and experiment is good.

Unfortunately, the loss of Insulcork at 7 seconds on the second fin, makes the comparison of the relative merits of Insulcork and

* Leading edge radius

Avcoat, as thermal insulators an impossibility, but this is only of secondary importance. The Insulcork failure however, does reveal the extent to which thin ablative coatings of Avcoat protect stagnation points. This can be seen from inspection of figures 4.1.1 and 4.1.2. The peak experimental temperature recorded on the protected fin was 760°F while that on the unprotected fin was 1608°F, a difference of 848°F. A temperature of 760°F is quite acceptable on most external aerospace metal structures since it will not significantly reduce the structural integrity, while a temperature of 1608°F would cause large reductions in stiffness and could cause vehicle failures.

TABLE 4.1.1

THEORETICAL AND EXPERIMENTAL RESULTS
FOR
FIN STAGNATION EXPERIMENT
FLIGHT - BB IV - 07

FLIGHT TIME (SECS)	EXPERIMENTAL AVCOAT-METAL TEMPERATURE °F	THEORETICAL AVCOAT-METAL TEMPERATURE °F
0	60	60
1	60	60
2	60	60
3	60	60
4	60	62
5	60	64
6	60	64
7	60	70
8	67	99
9	113	133
10	190	181
11	252	225
12	306	263
13	329	302
14	368	340
15	383	363
16	406	402
17	422	410
18	437	439
19	452	491
20	483	519
21	568	563
22	568	602
23	630	661
24	676	710
25	722	755
26	745	763
27	760	779
28	760	783
29	745	780
30	745	780

TABLE 4.1.2

THEORETICAL AND EXPERIMENTAL RESULTS
FOR
FIN STAGNATION EXPERIMENT
FLIGHT - BB IV - 07

FLIGHT TIME SECS	EXPERIMENTAL INSULCORK-METAL TEMPERATURES °F	THEORETICAL INSULCORK-METAL TEMPERATURES °F
0	60	60
1	60	60
2	60	60
3	60	60
4	60	60
5	60	60
6	60	60
7	67	101
8	329	243
9	406	403
10	515	520
11	599	558
12	614	582
13	614	595
14	614	615
15	614	625
16	614	630
17	614	638
18	645	662
19	727	705
20	791	700
21	920	892
22	1020	981
23	1138	1100
24	1277	1220
25	1423	1342
26	1538	1465
27	1608	1540
28	1538	1620
29	1392	1620
30	1369	1597

figure 4.1.1

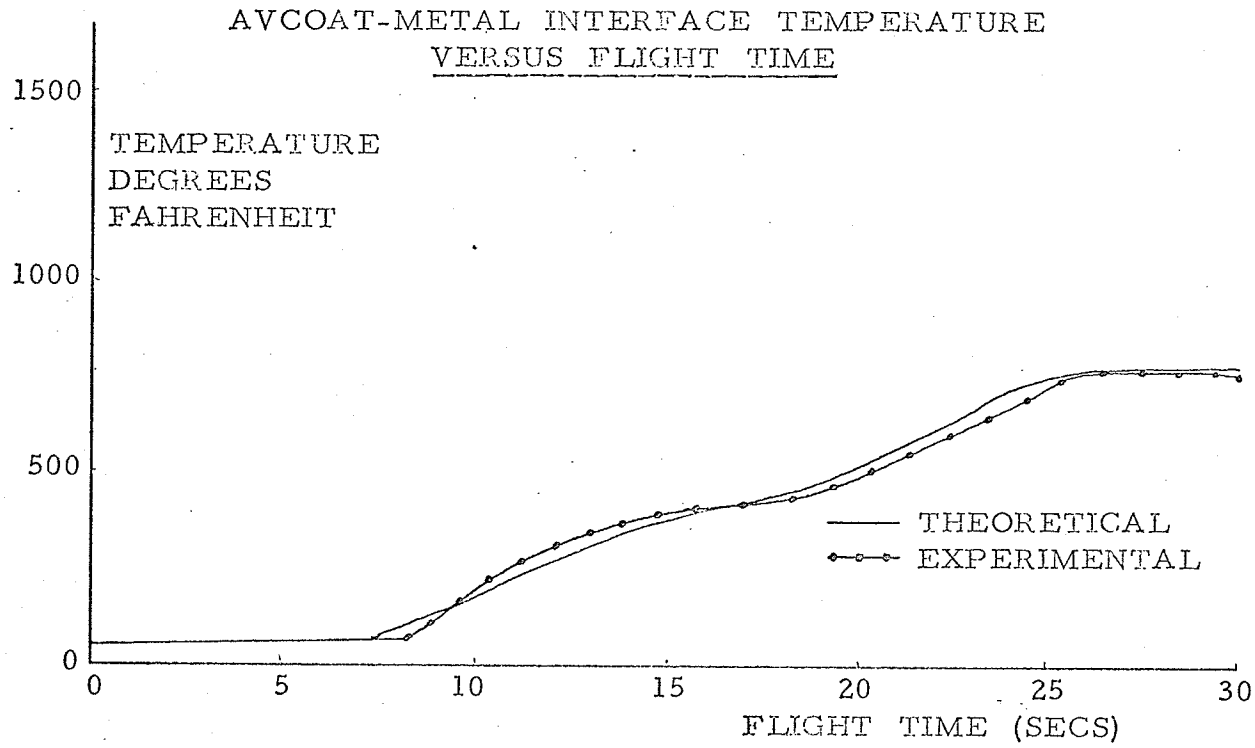

figure 4.1.2

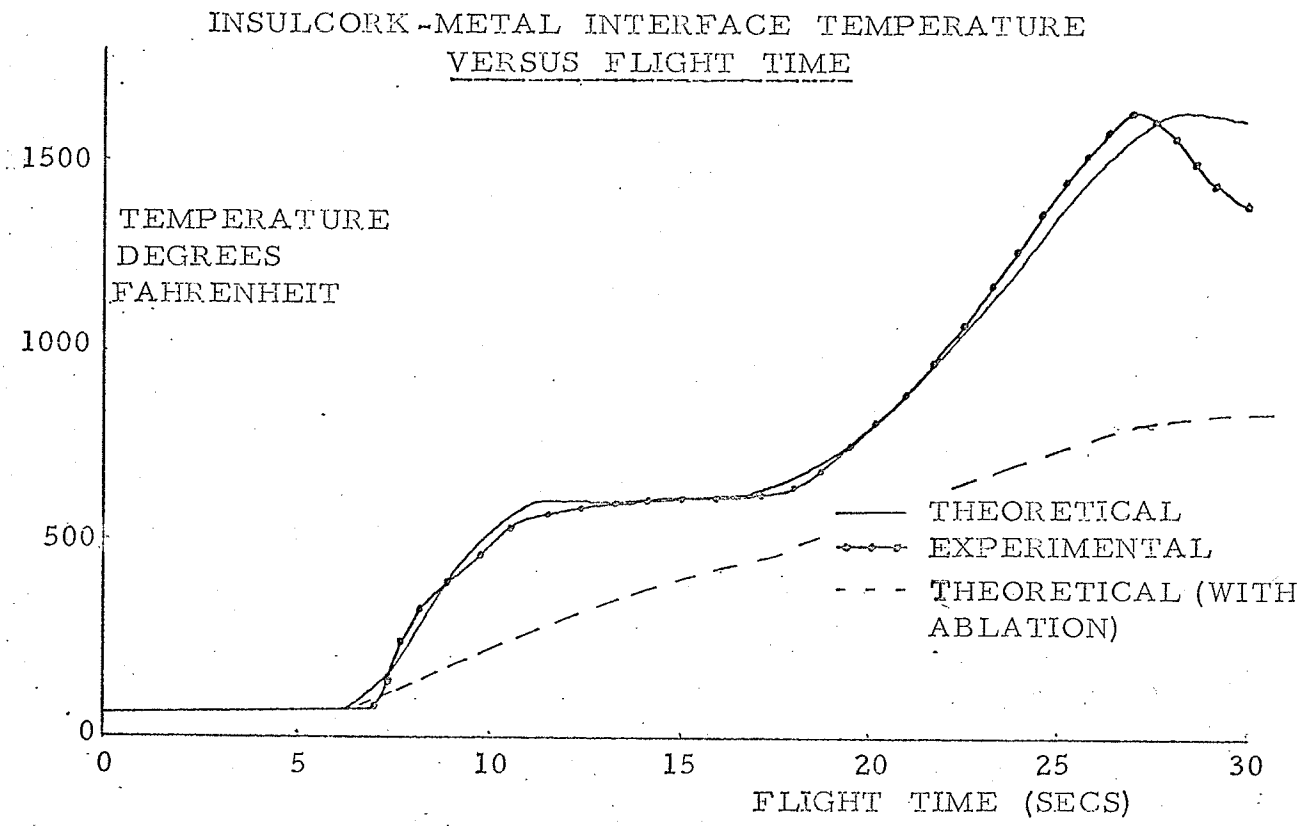

4.2 COMPARISON OF THEORETICAL ANALYSIS AND EXPERIMENTAL RESULTS FOR FIN CENTER LINE EXPERIMENT

This section gives a comparison of the theoretical and experimental results obtained for the fin center line experiment described in section 2.2.

It was decided not to do a new analysis* for the fin center line experiment, but to compare the reduced experimental results, with the theoretical results for the fin stagnation experiment. Table 4.2.1 shows the reduced telemetry and corresponding theoretical results for the Avcoat covered fin as a function of flight time. The reason that no new analysis was made, was that the theoretical trajectories of vehicles 07 and 08 were very similar, over the major portion of the powered flight. Differences do occur near burnout in the flight parameters due to the fact that 08 carried a lighter payload. This resulted in a slightly more severe thermal trajectory during the initial 25 seconds of flight, while in the continuum atmosphere.

Figure 4.2.1 shows a plot of the experimental and theoretical results of temperature versus time for Avcoat II. The experimental and theoretical curves show good overall agreement. There is no

* The theoretical results for the stagnation point were to be compared with the fin center line experimental data.

noticeable temperature rise until 8 seconds. It can be seen that the theoretical temperature lags the experimentally obtained temperature over the period 8 to 17 seconds. This is because of the more severe thermal trajectory of 0.8. After 17 seconds, the theoretical temperature leads the experimental temperature until 25 seconds, and then peaks at a temperature of 870°F while the experimental temperature peaks at 920°F, some two seconds later. This result is to be expected in view of the higher thermal trajectory. The point to be made here, however, is that it was set out to prove that heating near the stagnation point was independent of the curvilinear coordinate x. This has been done, x being 0.517 inches from the stagnation point.

Figure 4.2.2 shows a plot of the experimental and theoretical values for the Insulcork center line temperature results tabulated in table 4.2.2. Again, the Insulcork profile is more indicative of a metal thermal response to aerodynamic heating than that of an insulated metal. It is thought once again, that the high speed boundary layer stripped the protective Insulcork from the metal fin. After 7 seconds the experimental temperature rises rapidly with an initial peak of 620°F as in the first case, and clearly shows the effect of staging and first stage motor thrust tail off.

Correlation of the experimental and theoretical temperatures over the initial 15 seconds of the flight are fairly good with excellent agreement until 25 seconds, after which the theoretical and experimental results do not show good agreements. The theoretical curve tends to be quite conservative after this time and is probably due to the fact that it is a stagnation result rather than a completely new computation for the fin center line case. Nevertheless, the results shown in figure 4.2.2 show once again that aerodynamic heating near the stagnation point is independent of the curvilinear distance x.

The experimental Avcoat and Insulcork temperature profiles are remarkably similar to those obtained in the fin stagnation experiment over the initial 23 seconds of flight, as is shown in figures 4.2.3 and 4.2.4.

TABLE 4.2.1

THEORETICAL AND EXPERIMENTAL RESULTS
FOR
FIN CENTER LINE EXPERIMENT
FLIGHT - BBIV - 08

FLIGHT TIME (SECS)	EXPERIMENTAL AVCOAT - METAL TEMPERATURE °F	THEORETICAL AVCOAT - METAL TEMPERATURE °F
0	60	60
1	60	60
2	60	60
3	60	60
4	60	62
5	60	64
6	60	65
7	60	70
8	90	99
9	160	133
10	214	181
11	268	225
12	306	263
13	322	302
14	368	340
15	391	363
16	422	402
17	422	410
18	428	439
19	461	491
20	491	519
21	522	563
22	569	602
23	638	661
24	684	710
25	769	755
26	830	763
27	885	779
28	923	783
29	939	780
30	939	779

TABLE 4.2.2

THEORETICAL AND EXPERIMENTAL RESULTS
FOR
FIN CENTER LINE EXPERIMENT
FLIGHT - BBIV - 08

FLIGHT TIME (SECS)	EXPERIMENTAL INSULCORK-METAL TEMPERATURE °F	THEORETICAL INSULCORK-METAL TEMPERATURE °F
0	60	60
1	60	60
2	60	60
3	60	60
4	60	60
5	60	60
6	60	60
7	60	101
8	368	243
9	543	403
10	599	520
11	623	558
12	623	582
13	630	595
14	630	615
15	615	625
16	615	630
17	623	638
18	630	662
19	700	705
20	792	700
21	885	892
22	1008	981
23	1054	1100
24	1224	1220
25	1309	1342
26	1340	1465
27	1317	1540
28	1255	1620
29	1240	1620
30	1139	1597

figure 4.2.1

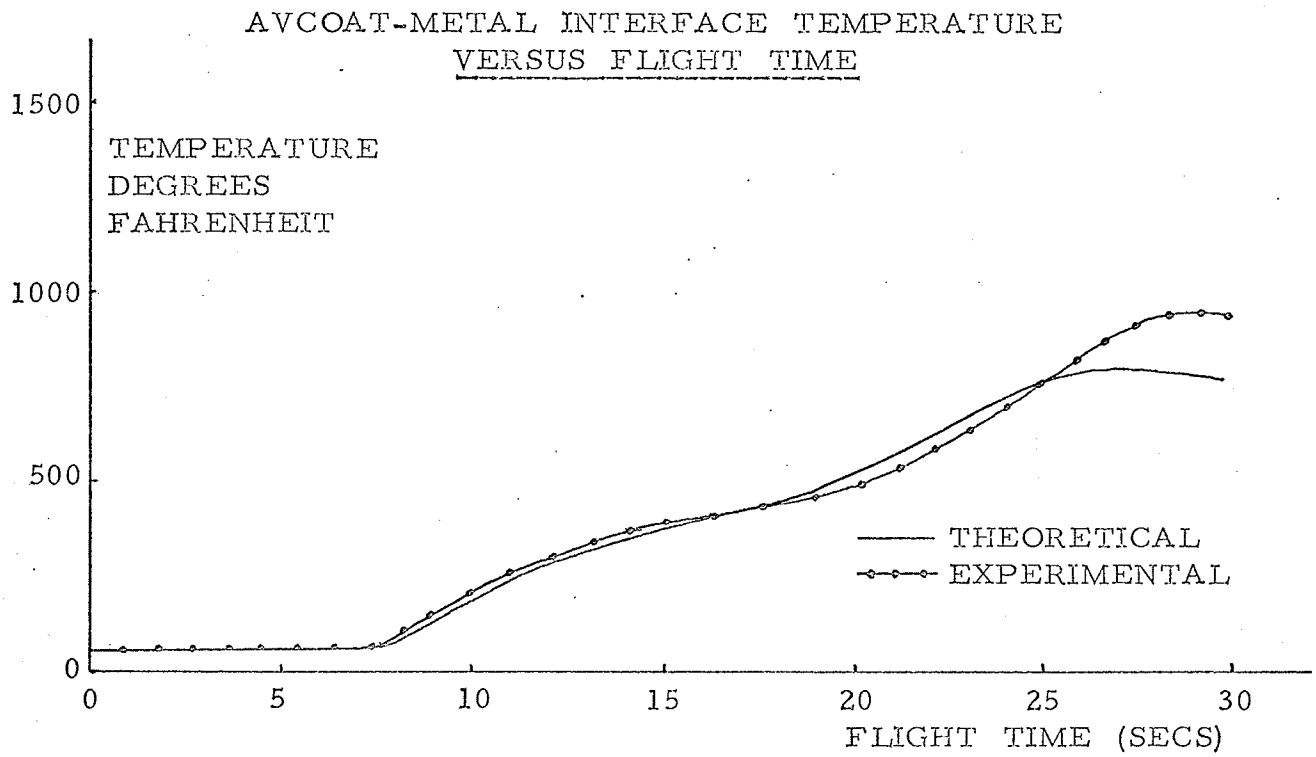

figure 4.2.2

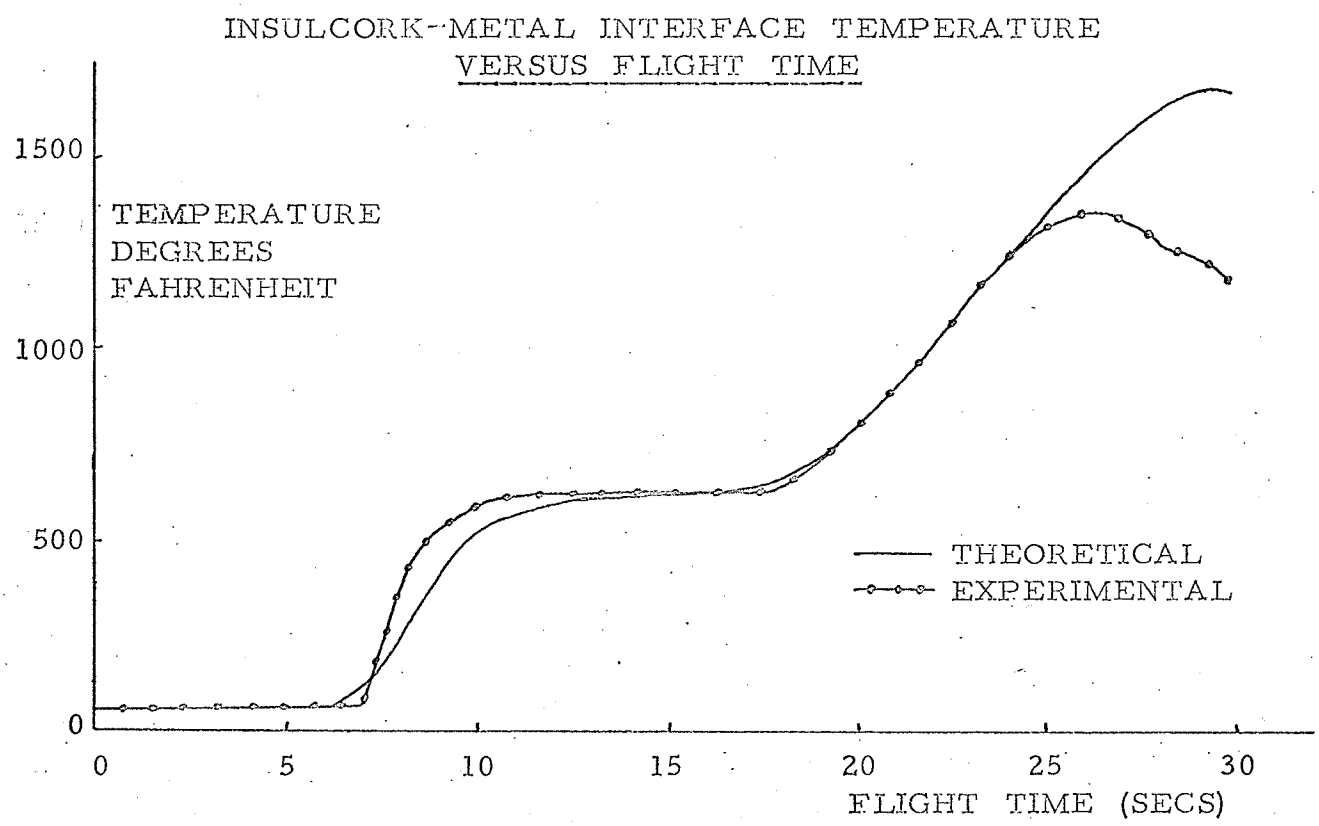

figure 4.2.3
COMPARISON OF
AVCOAT METAL INTERFACE TEMPERATURES
VERSUS FLIGHT TIME

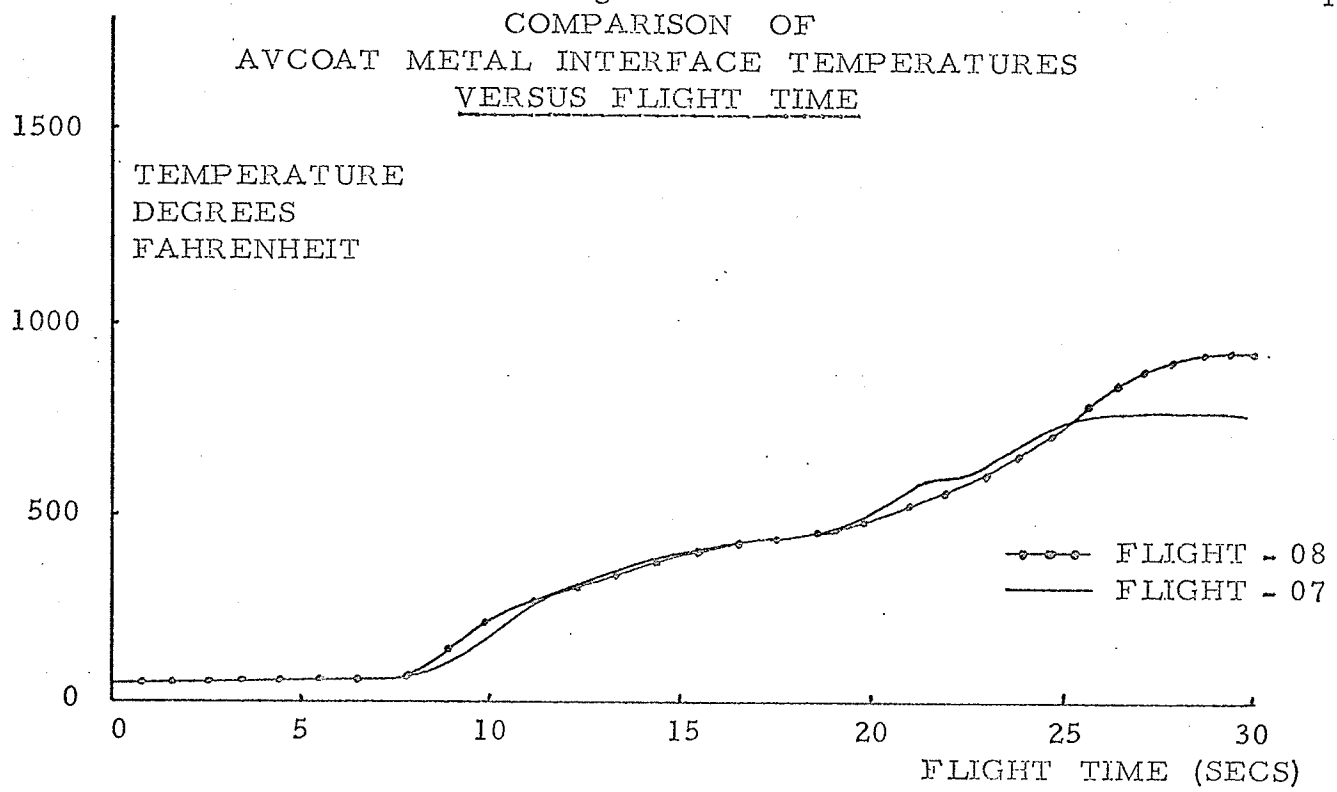

figure 4.2.4
COMPARISON OF
INSULCORK-METAL INTERFACE TEMPERATURES
VERSUS FLIGHT TIME

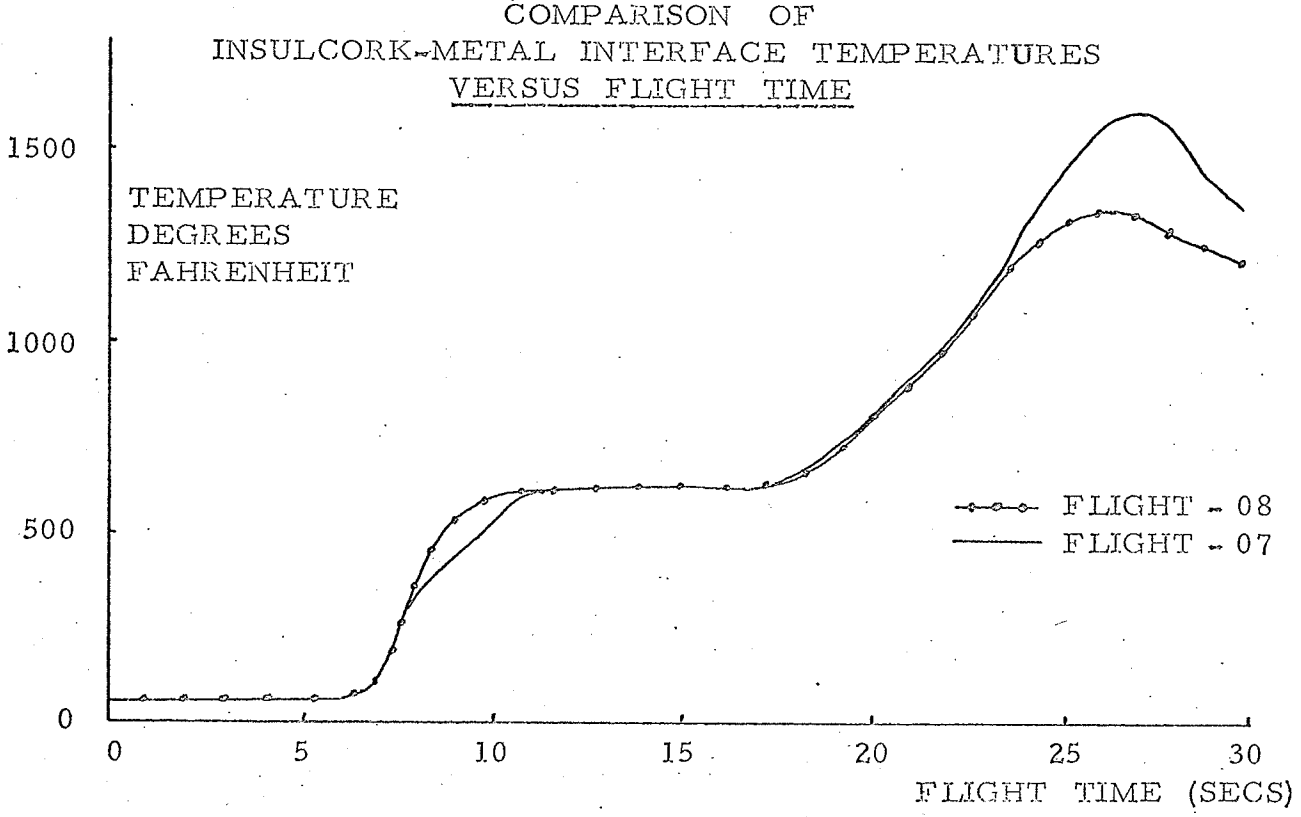

4.3 COMPARISON OF THEORETICAL ANALYSIS AND EXPERIMENTAL RESULTS FOR ABLATIVE PANEL EXPERIMENTS

In the theoretical analysis, the ablative heat transfer program was used to determine thickness of material ablated for the experimental set-up described in section 2.3. The results of the analysis are compiled in tables 4.3.1 and 4.3.2. To facilitate discussion, these results have been graphically illustrated in figures 4.3.1 through 4.3.4.

Figure 4.3.1 shows a plot from table 4.3.1 of computed heat input versus flight time during the ablation period. It can be seen that the heat input occurs as a pulse, lasting some ten seconds. At motor thrust tail-off (14.5 secs.), the vehicle acceleration drops off rapidly causing the heat input to fall. At motor burn out time (18 secs.), there is a noticeable kink in the graph, corresponding to a reduction in the heat flux due to rapid vehicle decceleration. Figure 4.3.2 and 4.3.3 show the computed thickness of Insulcork 2275 and Avcoat II ablated respectively, due to the pulse heat flux shown in figure 4.3.1. It can be seen that the ablation rate in both cases is practically linear over the ablation period. The theoretical curves also

show that the ablation rates for Insulcork and Avcoat are almost identical. This is surprising in view of the differences in the material properties, such as thermal conductivity and density. It seems that the greater density of the Avcoat compensates for its conductivity giving the same ablation rates as the less dense Insulcork, which has a lower thermal conductivity.

The broken lines on the graphs indicate the average measured thickness of materials ablated from the flight experiments described in section 2.3. It can be seen in both cases, the experimentally obtained ablated thicknesses are less than 0.002 inches greater than those obtained from theory. This difference corresponds to an accuracy of greater than 6%.

Since the panels were not instrumented for temperature measurement, no experimental temperatures were obtained. the theoretical interface temperatures plotted in figure 4.3.4 from table 4.3.2, however, indicate that the Insulcork-metal interface temperature is lower than at the Avcoat-metal interface.

From the experiment and theory in this section, it can be shown

that:

i) The ablative heat input occurs as a pulse.

ii) Ablation rates of Avcoat and Insulcork are almost identical, and are linear functions of time.

iii) Insulcork appears to be a more superior heat shield material theoretically than Avcoat from the point of view of bond line temperature.

iv) Correlation between theory and experiment is good; the difference between theoretical and measured values being less than 6%.

TABLE 4.3.1

HEAT FLUX AND THICKNESSES ABLATED
FOR ABLATIVE PANEL EXPERIMENTS

FLIGHT TIME (SECS)	HEAT FLUX DURING ABLATION (BTU/FT^2-SEC)	AVERAGE THICKNESS ABLATED (INCHES)	
		INSULCORK	AVCOAT
11	—	0.0	0.0
11.75	5.84	0.00004	0.0
12.25	6.37	0.00008	0.0004
12.5	9.15	0.0002	0.0013
13	11.85	0.0015	0.003
13.5	14.31	0.0057	0.0058
14	16.34	0.008	0.0072
14.25	17.19	0.0092	0.0086
14.5	17.37	0.0103	0.0098
15	16.01	0.0126	0.01212
15.5	15.86	0.0150	0.0144
16	14.83	0.0172	0.0165
17	11.94	0.0205	0.0211
18	9.51	0.0230	0.02274
19	6.27	0.0249	0.02472
20	3.85	0.0264	0.026
21	2.12	0.0271	0.0268
22	0.94	0.0274	0.0272
23	0.78	0.0277	0.0276
24	0.75	0.0279	0.0276

TABLE 4.3.2

INSULCORK AND AVCOAT INTERFACE TEMPERATURES FOR ABLATIVE PANEL EXPERIMENT

FLIGHT TIME (SECS)	INTERFACE TEMPERATURE* (RANKINE)	
	INSULCORK	AVCOAT
0	519	519
1	519	519
2	519	519
3	519	519
4	519	520
5	519	520
6	519	521
7	519	522
8	520	523
9	521	525
10	522	527
11	523	530
12	524	533
13	525	535
14	526	540
15	528	544
16	530	549
17	533	554
18	535	560
19	538	565
20	541	571
21	544	577
22	546	583
23	549	---
24	552	---
25	554	---
26	558	---
27	560	---
28	563	---
29	566	---
30	568	---

* Temperatures read to nearest degree.

figure 4.3.1

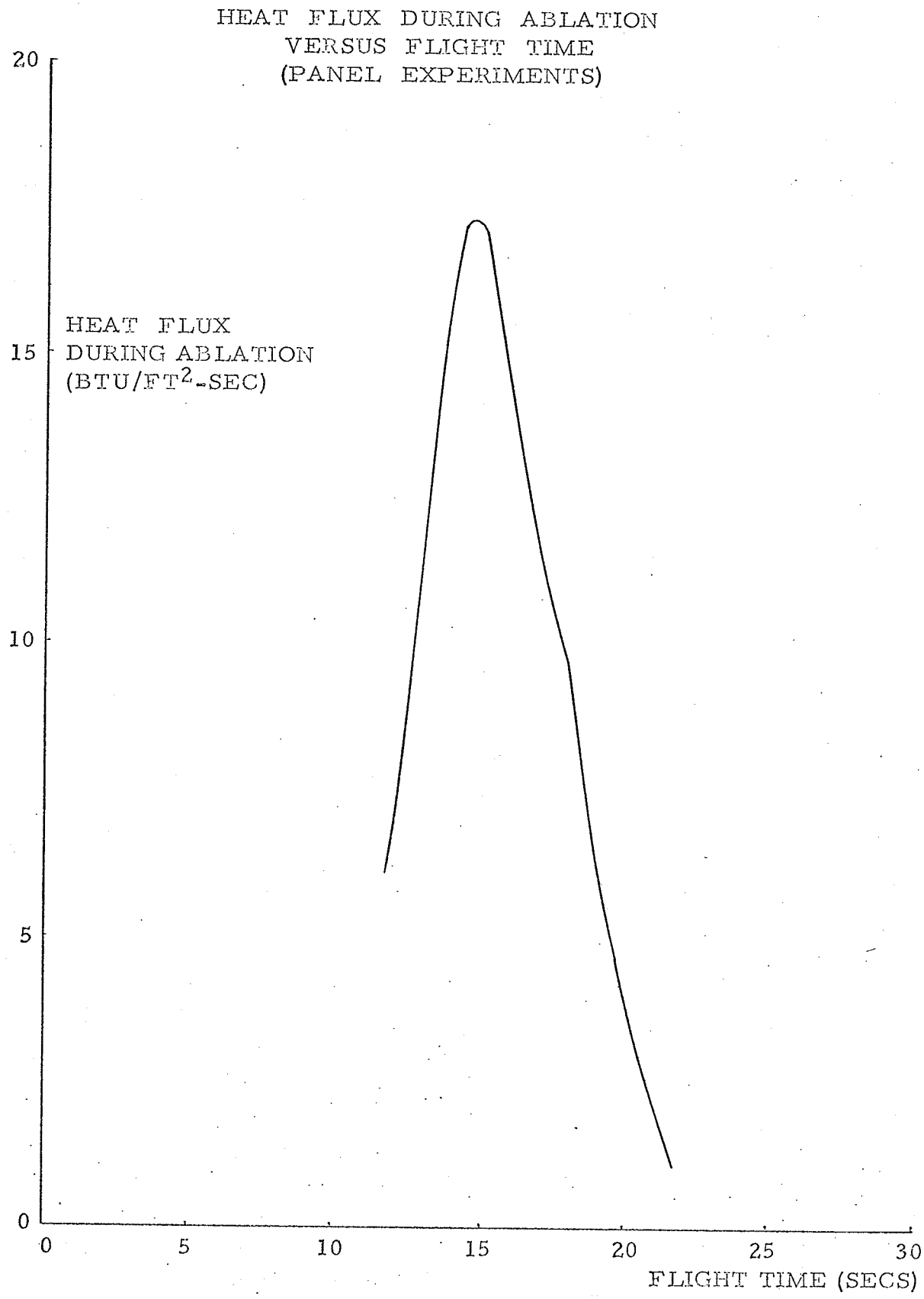
HEAT FLUX DURING ABLATION
VERSUS FLIGHT TIME
(PANEL EXPERIMENTS)
HEAT FLUX
DURING ABLATION
(BTU/FT2-SEC)
20
15
10
5
0
0
5
10
15
20
25
30
FLIGHT TIME (SECS)

figure 4.3.2

INSULCORK 2275 THICKNESS ABLATED
VERSUS FLIGHT TIME
(PANEL EXPERIMENTS)

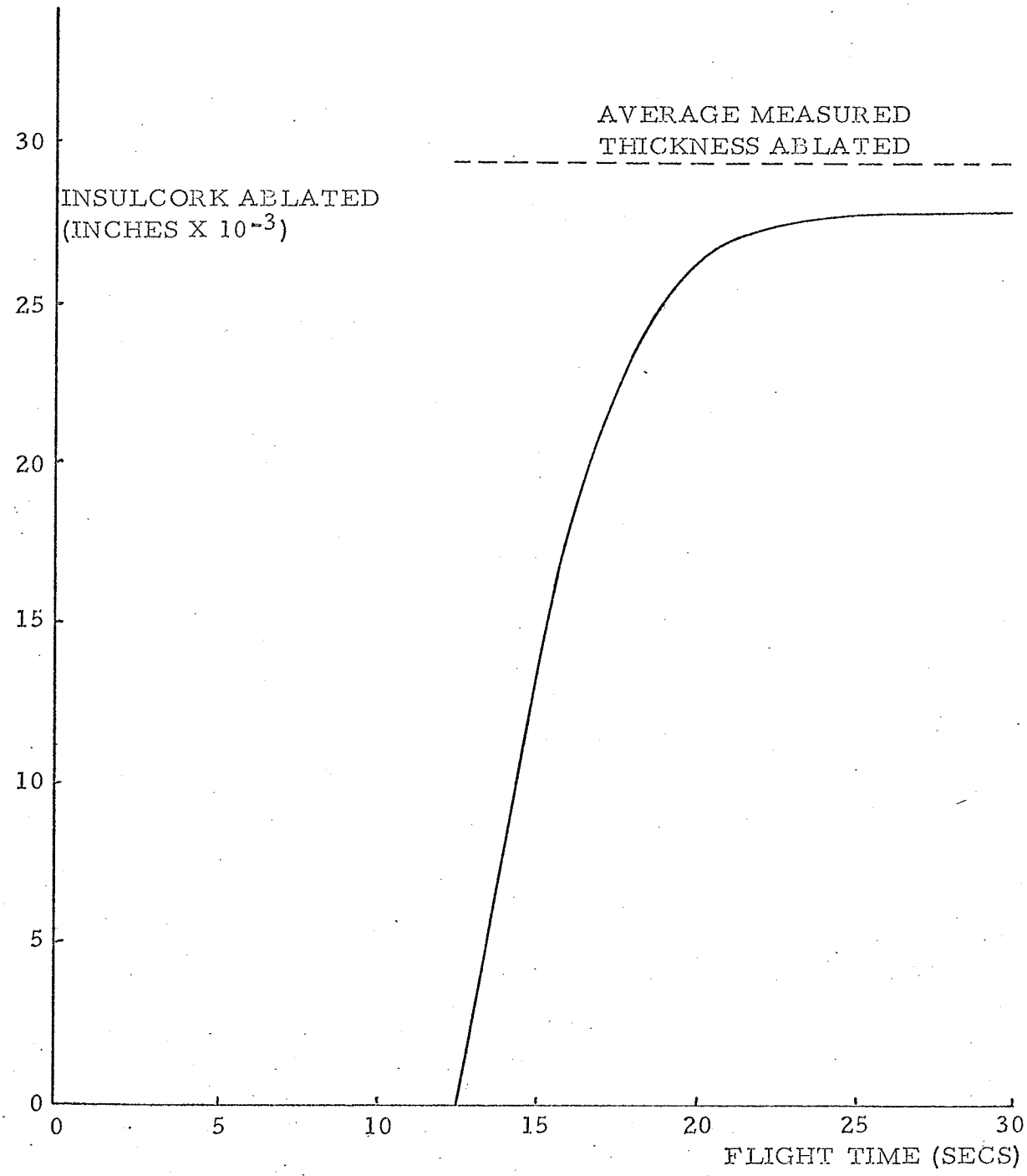

figure 4.3.3

AVCOAT II THICKNESS ABLATED
VERSUS FLIGHT TIME
(PANEL EXPERIMENTS)

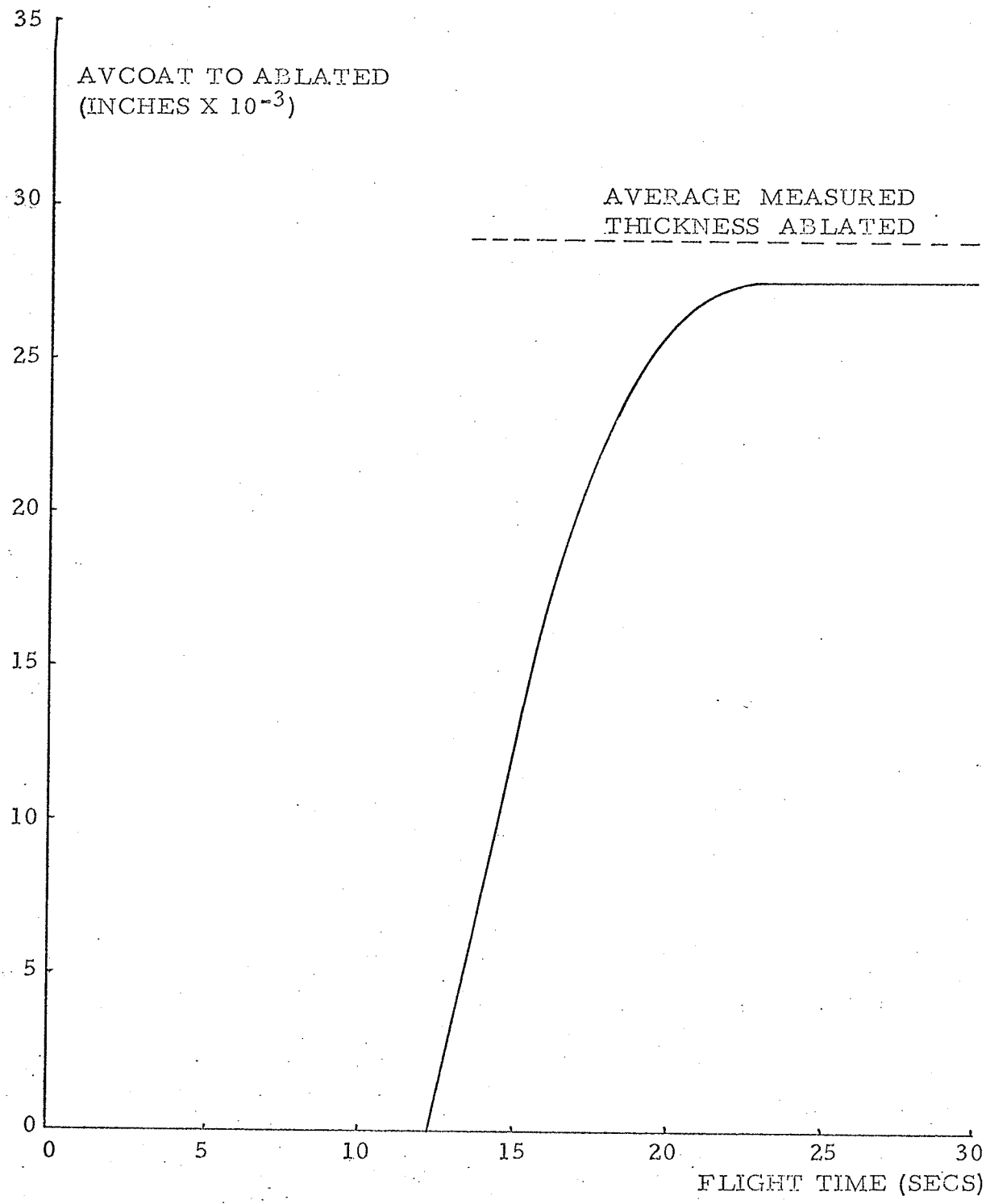

figure 4.3.4

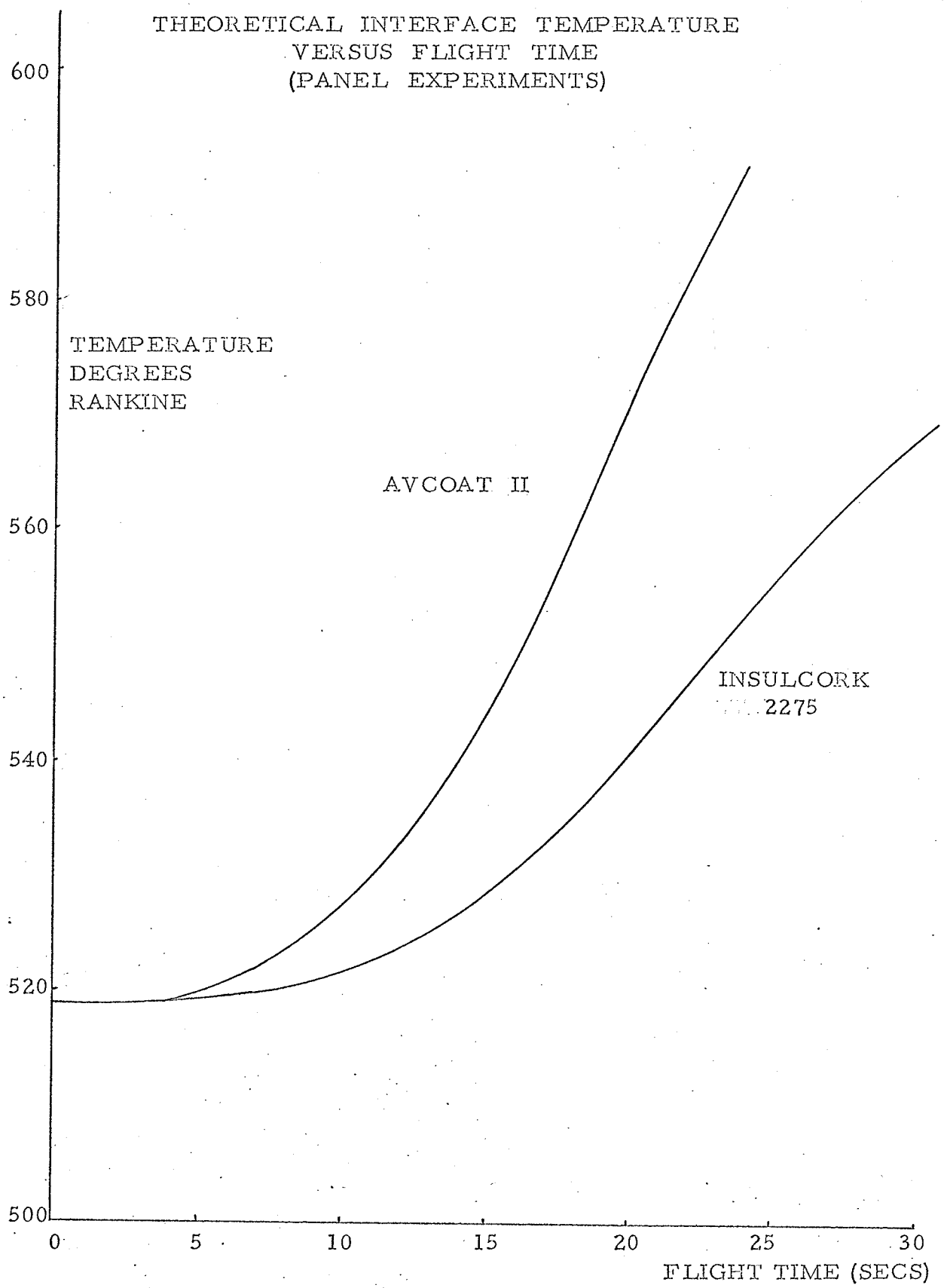
THEORETICAL INTERFACE TEMPERATURE
VERSUS FLIGHT TIME
(PANEL EXPERIMENTS)
600
580
560
540
520
500
TEMPERATURE
DEGREES
RANKINE
AVCOAT II
INSULCORK
2275
0
5
10
15
20
25
30
FLIGHT TIME (SECS)

4.4 COMPARISON OF THEORETICAL ANALYSIS AND EXPERIMENTAL RESULTS FOR FIN PLANFORM EXPERIMENTS

In this section it was intended to compare the results of the theoretical analysis with those obtained from the fin planform experiments described in section 2.4. Unfortunately, very little worthwhile experimental data was obtained from BB VA flights 119 and 120, for reasons as yet unknown. Instead, a brief discussion of a plausible reason for the experiment failures will be given, followed by the theoretical analysis, the accuracy of which will be justified by other circumstantial evidence.

As mentioned above, the reason for the experimental failures is unknown. There are, however, certain facts which point to a possible explanation for the failures. In both experiments, all fin thermocouple telemetry channels registered open circuit at approximately 13 seconds after launch, other experiment telemetry channels functioning perfectly. This indicates that the failure on both flights was due to the same reason. The author accompanied the launch team to the Churchill Rocket Range as an engineering observer and it was noted that difficulty was experienced by the vehicle technicians in threading the thermocouple lead wires

through the protective trough, shown in figure 2.4.1 of section 2.4.

Initial attempts to thread the wires on both vehicles resulted in wire breakage and the wires had to be threaded a second time. It is suggested that when the wires were successfully threaded, they were in a state of tension in the trough. It is known that shortly after thrust tail off (about 14.5 seconds), the rocket motor suffers a thermal shock due to heating from the combustion gases, elongating the motor by some 2 inches. This shock elongation could have caused the wires in tension to break and the thermocouple channels to register open circuit.

It is thought unlikely that aerodynamic shear forces, coupled with aerodynamic heating parted the trough from the motor casing, since radar did not report seeing multiple targets.

The theoretical analysis was made for a point 3.5 inches back from the fin leading edge along the mid chord line, corresponding to the location of thermocouples T3 and T4, shown in figure 2.4.1, section 2.4. The results of the analysis are compiled in tables

4.4.1 and 4.4.2.

A plot of the ablation heat input as a function of flight time from table 4.4.1 is shown in figure 4.4.1. It can be seen that the heat input occurs in the form of a pulse, having a peak value of 22.36 Btu/ft^2-sec, shortly after motor thrust tail off.

Theory shows that the heat pulse ablates approximately 0.018 inches of Avcoat material. A plot of material thickness ablated is shown in figure 4.4.2. It can be seen that the ablation rate is practically linear over the ablation period. It should be mentioned here that fins recovered from an early BB VA flight had approximately 0.038 inches of Avcoat material ablated at station 3.5 inches from the leading edge. This is over twice the figure obtained from the analysis and is due to the fact that the analysis only computes the material thickness ablated in upward flight; the recovered fins suffered ablation on the upward flight, and also during re-entry.

Figure 4.4.3 shows a plot of the transient temperature distributions, in the Avcoat material, taken from table 4.4.2. T(1) corresponds to the surface temperature, T(2) and T(3) temperatures at 0.030

and 0.060 inches below the original surface, and T(4) the temperature at the Avcoat-Aluminium bond line interface, which was 0.090 inches below the original surface. It can be seen that the Avcoat surface temperature is predicted to rise quite rapidly to the ablation temperature of 1460° Rankine at 12.5 seconds shown by the full line (1). The main reason for this rapid rise is that the Avcoat, because of its small conductivity initially confines most of the heat pulse to a surface layer, allowing very little to diffuse through to the inner structure. As time progresses the heat pulse or wave is constantly attenuated by removal of heat energy by the structure. This is shown by the shift of temperature peaks, with increasing time.

The second full line (2), indicates the laboratory determined critical temperature (800° Rankine) which must not be exceeded for fin structural integrity to be maintained. It can be seen that the bond line interface temperature T(4) is well below the critical temperature. The temperature T(3) at 0.060 inches below the original surface just exceeds the critical temperature, indicating that a fin with 0.060 inches of Avcoat insulation would be marginally unsafe.

This brings about an interesting point. Early BB VA development flights using fins with 0.060 inches of Avcoat insulation exhibited disturbing flight characteristics. These disturbances were thought to be due to a marginally unsafe fin bond line temperatures, causing the fin to warp, upsetting the vehicle aerodynamics.

The ablation program was used to predict an optimal Avcoat thickness, for the fin to withstand the BB VA thermal envelope. The thickness computed was 0.090 inches. All BB VA flights employing the fins with the optimal Avcoat thickness have been successful, giving smooth flight histories. The circumstantial evidence just given, indicates how useful the ablative theory and program can be in an actual engineering problem.

This concludes the section for comparison of theory and experiment. The next section will give a discussion of conclusions and recommendations based on the theory and its experimental verification contained in this thesis.

TABLE 4.4.1

THEORETICAL HEAT FLUX AND THICKNESS ABLATED FOR FIN PLANFORM EXPERIMENT FLIGHTS BBVA 119 AND 120

FLIGHT TIME (SECS)	HEAT FLUX DURING ABLATION (BTU/FT^2-SEC)	THICKNESS ABLATED (INCHES)
12.5	12.38	0.0004
14	21.10	0.004
15	22.36	0.006
16	20.90	0.0096
17	17.19	0.0120
18	13.94	0.0139
19	10.27	0.0155
20	7.19	0.0170
21.25	4.27	0.0175
22	3.15	0.0179
22.25	2.75	0.0180

TABLE 4.4.2.

THEORETICAL TEMPERATURE DISTRIBUTION
FOR FIN PLANFORM EXPERIMENT
BBVA FLIGHTS 119 AND 120

FLIGHT TIME (SECS)	T(1) (°R)	T(2) (°R)	T(3) (°R)	T(4) (°R)
0	519	519	519	519
1	519	519	519	519
2	526	519	519	519
3	547	522	519	519
4	584	528	520	519
5	632	534	522	519
6	692	555	525	519
7	762	576	530	519
8	846	603	537	519
9	948	637	547	519
10	1060	677	339	519
11	1202	727	574	520
12	1362	786	593	520
12.5	1460	852	615	521
14	1460	911	640	522
15	1460	966	666	523
16	1460	- *	- *	- *
17	1460	1067	718	525
18	1460	1113	744	527
19	1460	1154	769	528
20	1460	1190	792	529
21.25	1460	1226	818	531
22	1460	1243	832	533
22.5	1460	1252	841	534
24	1388	1206	856	536
25	1351	1180	858	538
26	1324	1156	856	539
27	1307	1136	852	540
28	----	1124	847	542
29	----	1123	843	543
30	----	1168	843	544

* Computer did not print.

figure 4.4.1

THEORETICAL HEAT FLUX VERSUS TIME
FOR FIN PLANFORM EXPERIMENTS
(BBVA FLIGHTS 119 AND 120)

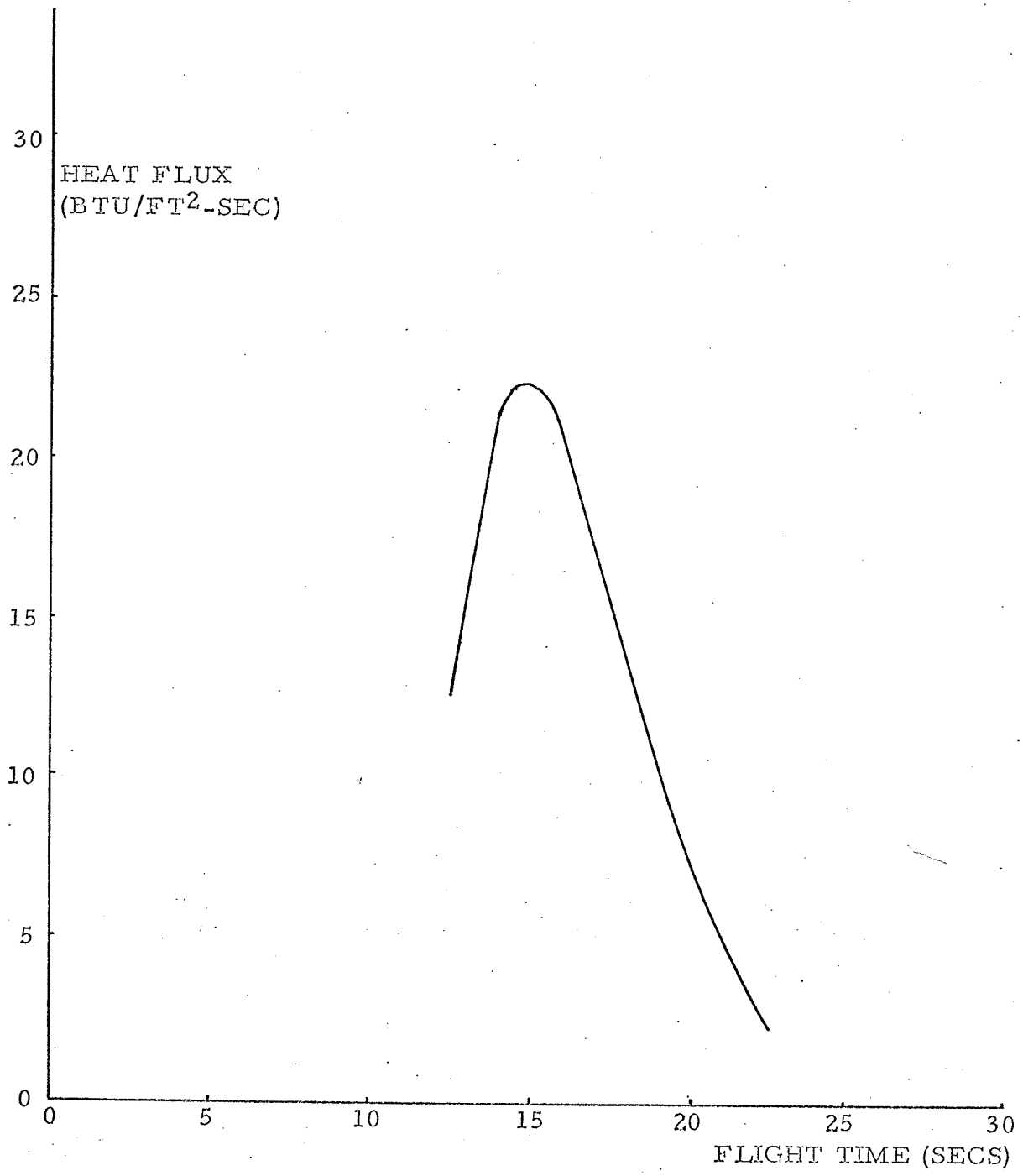

figure 4.4.2

THEORETICAL THICKNESS OF AVCOAT
ABLATED VERSUS TIME
FOR FIN PLANFORM EXPERIMENTS
(BBVA FLIGHTS 119 AND 120)

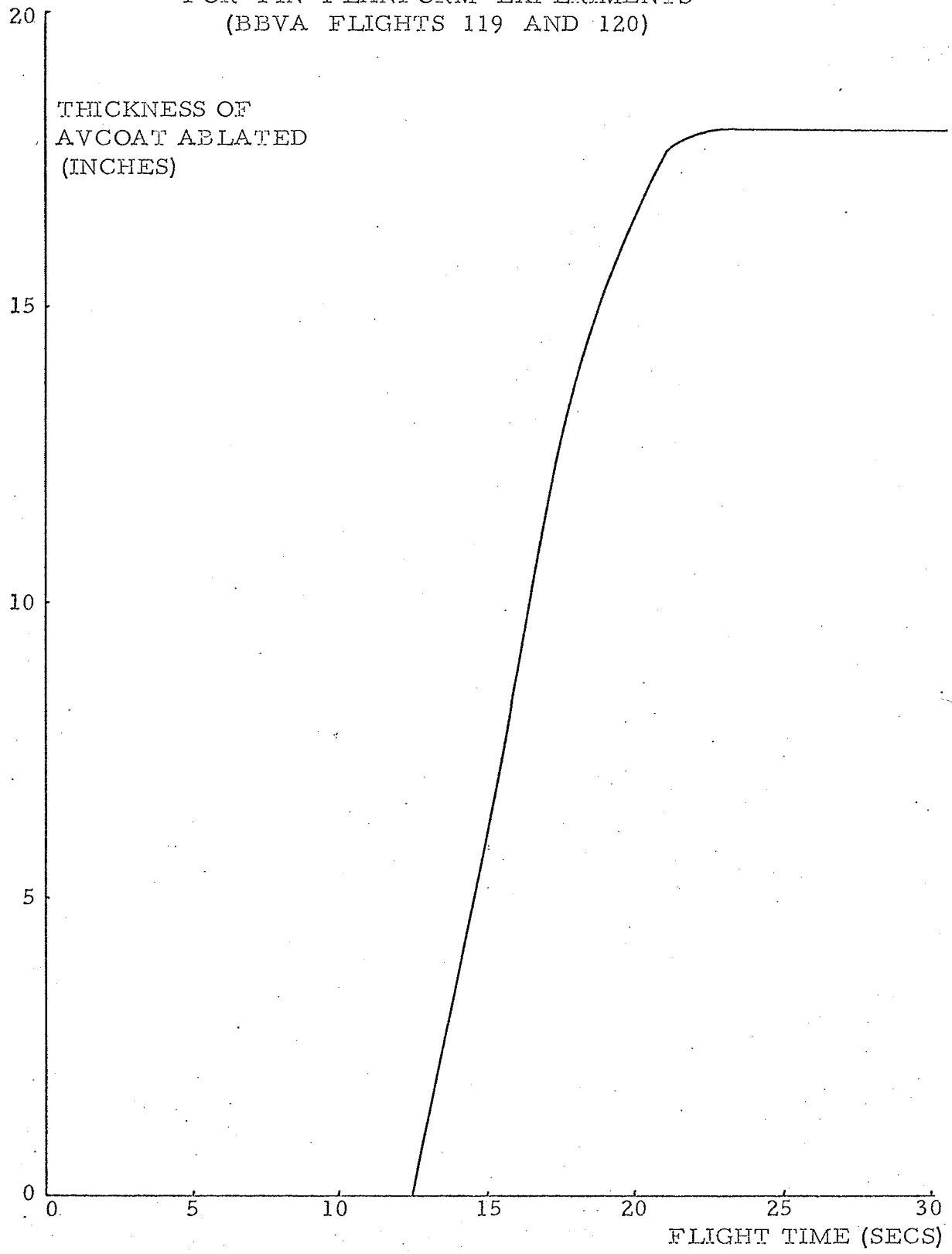

figure 4.4.3

THEORETICAL TEMPERATURE DISTRIBUTION
THROUGH FIN STRUCTURE VERSUS TIME
(BBVA FLIGHTS 119 AND 120)

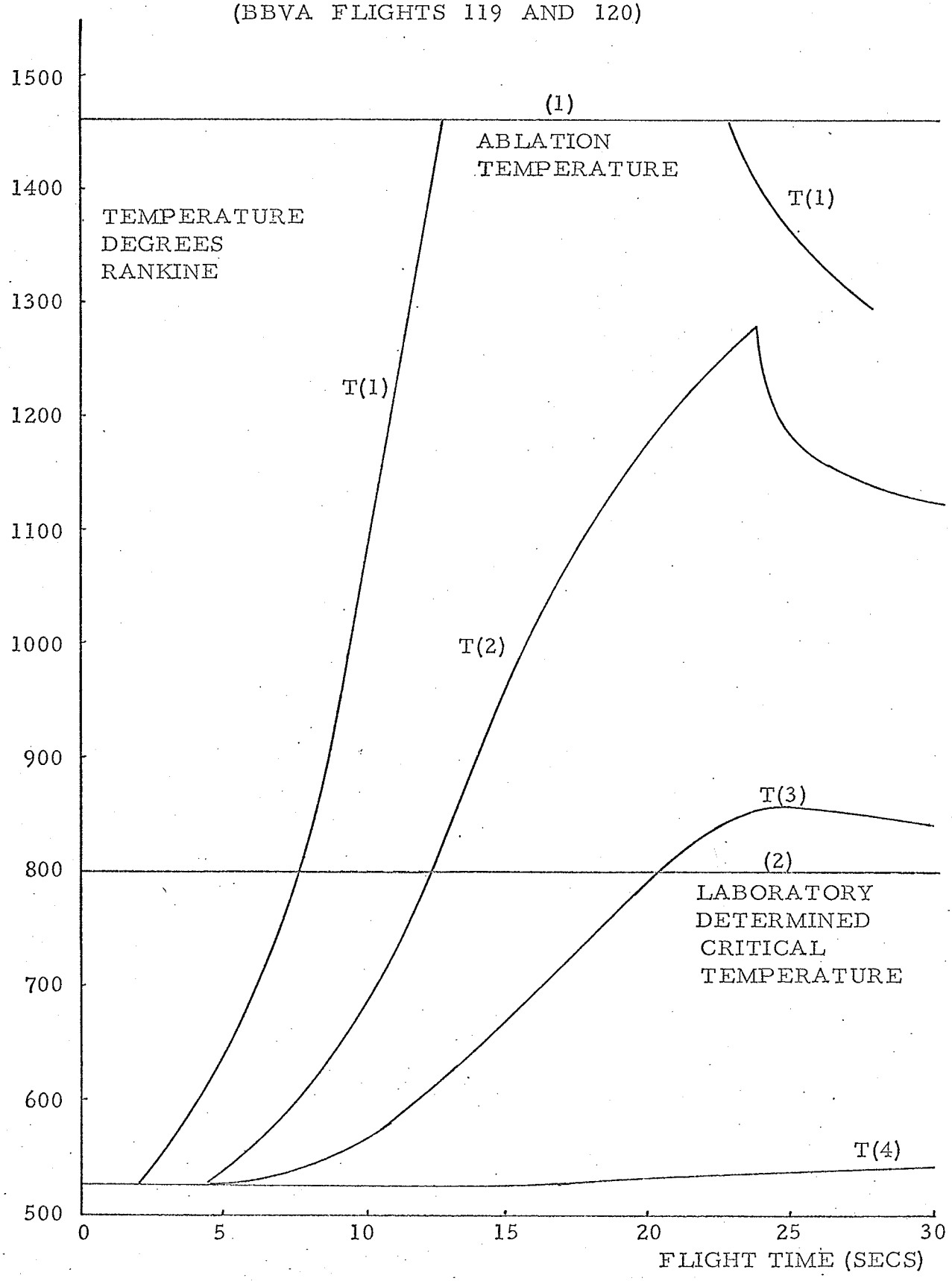

5.0 CONCLUSIONS AND RECOMMENDATIONS

The conclusions and recommendations given in the following subsections are based on the theory and experiment described in this thesis.

It is felt generally, that all initial objectives have been accomplished, the combination of theory and experiment giving sharper focus to some of the original ideas, and a better understanding of some basic heat transfer phenomena.

5.1 CONCLUSIONS

Review of the theory in section 1.0 reveals that the following general conclusions can be drawn.

a) The field equations of fluid dynamics lend themselves well to simplification and solution of high speed flow phenomena, when second order approximations for the stress tensor and heat flux vector are used.

b) Heat transfer to simple geometries, such as semi-cylinders, flat plates, and bodies with large radius of curvature, can be predicted with good accuracy by employing an adapted version of the Van Driest aerodynamic heating theory, (reference 8).

c) Heat transfer in the vicinity of the stagnation point is independent of the curvilinear coordinate distance x.

d) A satisfactory mathematical model can be formulated for ablation of subliming materials for the order of environmental flight conditions described in this thesis by assuming:

   i) The surface temperature of the material on ablation remains constant.

   ii) The heat input to the body on ablation is totally committed to the ablation process.

   iii) The ablated material is totally removed by shear forces in the high speed boundary layer. i.e.

When ablation occurs, the increase of mass flow due to diffusion and convection of ablated gaseous and solid materials, has the effect of thickening the boundary layer and changing the profile, resulting in a reduction of velocity, temperature and concentration gradients, reducing heat transfer to the wall.

e) Section 1.6 shows that the ablation procession caused by a specified transient heat flux, can be coupled with a linear finite difference method to form a simple series expression describing the ablation process.

f) The accuracy of the coupled ablation procession finite difference method is practically indistinguishable from "exact" solutions, provided the stability and β criteria are observed. This is cognizant with choosing compatible time and nodal intervals. The ablation finite difference method is admirably suited for digital programming, as indeed is theory cited in section 1.0.

Review of the experimental results with theory, reveals that:

g) Good agreement is obtained between experiment and theory

for the stub fin stagnation, and mid chord experiments described in sections 2.1 and 2.2 respectively.

h) These experiments show:

i) That heat transfer near the stagnation point is independent of the curvilinear coordinate x, thus verifying the same point made in the theory.

ii) The linear finite difference methods can be used for thin ablative coverings with good accuracy.

iii) That Avcoat is superior to Insulcork in regions of high shear flow for protection of stagnation surfaces because of its better shear resisting properties.

iv) Because of Insulcork separation from the stub fin, the extent to which Avcoat insulates, can be appreciated by comparing the recorded Avcoat bond line temperatures, and those obtained on the exposed metal fins.

i) Comparison of theory and experimental results for the ablative panel experiments described in section 4.3, shows that the theory can predict ablated material thicknesses to within an accuracy of $\pm$ 6%. It should be noted that other circumstantial

evidence which corroborates this kind of accuracy is mentioned in section 4.4.

j) The theory also indicates that Avcoat and Insulcork have approximately the same ablation rates. This is substantiated by experimental evidence because measurements of Insulcork and Avcoat degraded in the panel experiments were practically the same. The theory also shows that Insulcork is a slightly better insulator and ablative material in regions where shear forces are not critical. It was not possible to show this by the ablation experiment since no instrumentation was carried.

k) The fin planform experiment described in 2.4 yielded no worthwhile data. It is thought that wire breakage occured due to motor case expansion, causing the thermocouple sensors to register open circuit. Theoretical data, however, was generated and compared with circumstantial evidence from previous BB VA flights, and a good measure of correlation obtained.

5.2 RECOMMENDATIONS

The following recommendations are based on the general conclusions made in subsection 5.1 and should not be misconstrued as being valid for geometries or flight environments radically different than those described in this thesis.

It is recommended that:

a) Because of the restrictions placed on the theoretical analysis, theory and related computer programs should only be used for continuum supersonic flight environments.

b) Thin ablative coverings of Armstrong Insulcork should not be used as a heat shield in stagnation or high shear flow regions. Avcoat can be used with confidence.

c) In view of the failure to obtain worthwhile data from the fin planform experiments, it is recommended that future experiments of this nature have telemetry housed in the vehicle aft end.

This section concludes the thesis. Following are lists of symbols and references used, and also acknowledgements to the various people who have given time, consent, and encouragement to the author during the writing of this thesis.

6.0 SYMBOLS

a_i	i^{th} Polynomial coefficient
a_k	k^{th} Polynomial coefficient
a_r	r^{th} Polynomial coefficient
C_a	Specific heat of 1st material
C_b	Specific heat of 2nd material
C_c	Specific heat of char from ablated material
C_g	Specific heat of gas from ablated material
$\bar{C}$	Specific heat of ablated materials mixture
$\bar{C}_p$	Specific heat of air and ablated materials mixture
$C_{f\infty}$	Local free stream skin friction coefficient
$C_{h\infty}$	Stanton number for local free stream
C_p	Specific heat of air at constant pressure
$\bar{D}$	Coefficient of binary diffusivity of air and ablated materials
D	Diameter of fin semi-cylindrical leading edge
E	Internal energy of air per unit mass
F_i	External body force per unit mass in i^{th} direction
f_1	Two dimensional stagnation parameter (page 15*)
$f(\eta)$	Boundary layer function (Eq. 1.2.11)
h	Film coefficient of heat transfer (Stagnation point heating, Eq. 1.2.22a); (Non-stagnation point heating, Eq. 1.4.10)
H_{eff}	Effective heat capacity of ablative material

K	Coefficient of thermal conductivity
K_a	Coefficient of thermal conductivity 1st material
K_b	Coefficient of thermal conductivity 2nd material
k	Thermometric conductivity ($k = K/\rho c_p$)
L	Dimension of experiment (Eq. 1.1.14); Latent heat of ablation (Section 1.3)
M	Mach number
M_∞	Mach number just outside boundary layer
$\dot{m}$	Mass rate of ablation
Nu	Nusselt number
Nu_∞	Nusselt number of local free stream
Nu_w	Nusselt number at the wall
$o[x]$	Means "of order X"
p	Pressure
p_∞	Pressure just outside boundary layer
Pr	Prandtl number
Pr_∞	Prandtl number just outside boundary layer
Pr_w	Prandtl number at the wall
q	Heat flux
q_i	Heat flux vector
R	Recovery factor (fraction of local free stream dynamic-temperature rise recovered at the wall
Re_{y_∞}	Reynolds number of local free stream
Re_{y_w}	Reynolds number at the wall

R_g	Gas constant
T	Temperature
T_w	Wall temperature
T_{aw}	Adiabatic wall temperature
$T_{o\infty}$	Stagnation temperature
T_∞	Temperature just outside of boundary layer
T_{ab}	Ablation temperature (On ablation $T_1 = T_w = T_{ab}$)
T_i	Temperature in "sandwich structure" i = 1, 2...
$T(I)$	Temperature at specified depth in sandwich structure I = 1, 2...
T_b	Body temperature (Eq. 1.3.1)
t	Time
U	Velocity just outside boundary layer
U_i	Velocity in i^{th} direction
u	Velocity in boundary layer in x direction
V	Modified velocity component (Eq. 1.3.9)
V_∞	Local resultant velocity just outside boundary layer
$\bar{V}$	Velocity vector
v	Velocity in boundary layer in y direction
$\bar{v}_w$	Velocity of ablated materials at the wall
$v(Y)$	Velocity (Y greater than boundary layer thickness)
$\bar{W}$	Coefficient of mass concentration of ablated materials (It represents the ratio of mass of ablated materials to mass of ablated materials and air in unit volume)

$\overline{W}_w$	Coefficient of mass concentration of ablated materials at wall
w	Velocity in boundary layer in z direction
x	Cartesian coordinate; curvilinear coordinate (Section 1.3); depth of material ablated (Section 1.6)
x_i	Cartesian tensor coordinates $i = 1, 2, 3$.
Y	Arbitrary value outside of boundary layer
y	Cartesian coordinate; curvilinear coordinate (Section 1.3)
Z_1	Arbitrary value outside of boundary layer
z	Cartesian coordinate; transformed y coordinate (Section 1.3)
$\alpha_1(Pr)$	Stagnation function
$\alpha_2(Pr)$	Convection function (Eq. 1.4.9)
β	Stagnation velocity gradient; stability criterion (Section 1.6)
Γ	Heat absorption capacity of skin or wall
Δt	Time interval or integration interval
δ_{ij}	Kronecker delta function (unit tensor)
δ	Boundary layer thickness
δ_u	Velocity boundary layer thickness with ablation
$\delta_{u,o}$	Velocity boundary layer thickness without ablation
δ_T	Thermal boundary layer thickness with ablation
$\delta_{T,o}$	Thermal boundary layer thickness without ablation
ϵ	Emissivity

η	Gas mass fraction of ablated material (Section 1.6); dimension less coordinate (Eq. 1.2.12)
$\theta(\eta)$	Boundary layer temperature distribution function
λ	Mean free path of air in the atmosphere
μ	Coefficient of viscosity
μ_∞	Coefficient of viscosity of air just outside boundary layer
μ_w	Coefficient of viscosity at wall
ν	Kinematic viscosity
ν_∞	Kinematic viscosity just outside boundary layer
ρ	Mass density
ρ_∞	Mass density of air just outside boundary layer
ρ_w	Mass density of air at wall
$\bar{\rho}_w$	Mass density of ablated materials at wall
σ	Stefan Boltzmann constant
σ_i	i^{th} Standard deviation
τ_a	Nodal thickness of 1st material
τ_b	Nodal thickness of 2nd material
τ_{ij}	Stress tensor
ϕ	Dissipation function
Λ	Fin sweepback angle
ψ	Stream function
$\frac{\partial \bar{u}_i}{\partial x_i}$	Non-divergent symmetrical tensor (See Eq. 1.2.1)

$\frac{\partial u_i}{\partial x_i}$ Velocity gradient

7.0 REFERENCES

1. "Cork Thermal Protection Design Data for Aerospace Vehicles Ascent Flight", R. W. Hovey, T.R.W. Space Technology Laboratories, Redondo Beach California AIAA Paper 64-356, 1964.

2. "Free Flight Test Results on the Performance of Cork As a Thermal Protection Material", R.A. Graves and E. Walton, NASA T.N. D-2438, 1964.

3. "Performance of Five Ablative Materials as Coatings for Structures in Regions of Separated Flow", L.E. Clark and A.G. McLain, NASA T.N. D-3093, 1965.

4. "Tensor Calculus", J.L. Synge and A. Schild, University of Toronto Press - First Edition, 1956.

5. "The Mathematical Theory of Non-Uniform Gases", T.G. Cowling and S. Chapman, London, Cambridge University Press, 1939.

6. "Boundary Layer Theory", H. Schlichting, McGraw Hill, Toronto, Fourth Edition, 1956.

7. "Modern Developments in Fluid Dynamics - Volumes I and II", S. Goldstein, New York Dover Publications Ltd.

8. "The Problem of Aerodynamic Heating", E. R. VanDriest, Aero Engine Review, Volume 5, No. 10, October 1956, pages 26 to 41.

9. "Theory of Stagnation Point Heat Transfer in Dissociated Air", J. A. Fay and F. R. Riddell, Journal Aero Sciences, Volume 25, No. 2, February, 1958.

10. "Compressible Fluid Flow", A. H. Shapiro, Ronald Press Company, Volume 1, New York, 1953.

11. "Stagnation Point Shielding by Melting and Vaporization", L. Roberts, NASA T. R. R-10, 1959.

12. "Theoretical Study of Stagnation Point Ablation", L. Roberts, NASA T. R. R-9, 1959.

13. "Effects of Leading Edge Blunting on Local Heat Transfer and Pressure Distributions Over Flat Plates in Supersonic Flow", Marcus O. Creager, NACA T. N. 4142, 1957.

14. "Heat Transfer and Recovery Temperatures on a Sphere with Laminar Transitional and Turbulent Boundary Layers at Mach. No's 2.00 and 4.15", I.E. Beckwith and James J. Gallagher, NACA T.N. 4125, 1957.

15. "Heat Transfer and Boundary Layer Transition on Two Blunt Bodies at Mach. No. 3.12", R. Diaconis, J. Wisniewski and J.R. Jack, NACA T.N. 4099 N.S., 1957.

16. "A Theoretical Analysis of Heat Transfer in Regions of Separated Flow", D.R. Chapman, NACA T.N. 3792, 1956.

17. "Theoretical and Experimental Results using Fiberglass as an Ablative Material on the Black Brant III Nose-Cone", J.W. Richman, AIAA Sounding Rocket Vehicle Technology Specialist Conference Publication, Williamsburg, Virginia, February 27, 1967.

18. "Methods of Mathematical Physics", Volume I and II, Courant and Hilbert, John Wiley, New York, 1965.

19. "Mathematical Methods of Physics", J. Mathews and R.L. Walker, W.A. Benjamin, New York, 1956.

20. "Strength Tests for Black Brant VA Motor Trough", J. Carter, Personal file, Bristol Aerospace Limited, 1967.

21. "A Finite-Difference Heat Conduction Method Applicable During Surface Recession", R. Eppes Jr., AIAA Journal, Volume 5, No. 9, September, 1967.

8.0 ACKNOWLEDGEMENTS

The author would like to acknowledge the help and encouragement given by Bristol Aerospace Limited, especially from the Director of the Rocket and Space Division, Mr. A. W. Fia, and members of the vehicle design team.

Thanks also go to Professor R. E. Chant, Head of the Department of Mechanical Engineering, University of Manitoba, for smoothing out several administrative difficulties, Professor S. W. Greenwood, for encouragement during the writing of this thesis, and Dr. J. Tinkler for a careful checking of the final draft.